



universität  
wien

# MASTERARBEIT / MASTER'S THESIS

Titel der Masterarbeit / Title of the Master's Thesis

„Os isotopes and PGE geochemistry of target rocks and impactites from the Zhamanshin impact structure, Kazakhstan“

verfasst von / submitted by

Florian Sackl

angestrebter akademischer Grad / in partial fulfilment of the requirements for the degree of  
Master of Science (M.Sc.)

Wien, 2015

Studienkennzahl lt. Studienblatt /  
degree programme code as it appears on  
the student record sheet:

A 066 815

Studienrichtung lt. Studienblatt /  
degree programme as it appears on  
the student record sheet:

Erdwissenschaften

Betreut von / Supervisor:

Univ.-Prof. Dr. Christian Koeberl



# Erklärung zur Verfassung der Arbeit

Florian Sackl, BSc  
Althanstraße 14, 1090 Wien

Hiermit erkläre ich, dass ich diese Arbeit selbständig verfasst habe, dass ich die verwendeten Quellen und Hilfsmittel vollständig angegeben habe und dass ich die Stellen der Arbeit - einschließlich Tabellen, Karten und Abbildungen -, die anderen Werken oder dem Internet im Wortlaut oder dem Sinn nach entnommen sind, auf jeden Fall unter Angabe der Quelle als Entlehnung kenntlich gemacht habe.

---

(Ort, Datum)

---

(Unterschrift Florian Sackl, BSc)



# Danksagung

An dieser Stelle möchte ich mich bei allen Personen bedanken, die mich bei der Erstellung dieser Arbeit unterstützt haben.

Ein besonderer Dank gilt meinen Betreuern Herrn Univ.-Prof. Dr. Christian Köberl und Herrn Dr. Toni Schulz, die mit sehr viel Engagement, guten Ideen und unermüdlichem Einsatz meine Masterarbeit betreut haben und des Weiteren mir auch die Freiheit gelassen haben, die Arbeit nach eigenen Vorstellungen zu entwickeln.

Darüber hinaus möchte ich mich bei Herrn Dr. Dan Topa und Herrn Dr. Franz Brandstätter (Naturhistorisches Museum Wien) bedanken, für ihre tatkräftige Unterstützung bei den Mikrosondenuntersuchungen.

Ebenfalls bedanken möchte ich mich bei meinem guten Freund Herrn Dr. Henning Wallner, der mir stets mit seinem kompetenten Rat zur Seite gestanden hat.

Großer Dank gebührt auch meinen Eltern Christine und Manfred, welche mir dieses Studium ermöglicht haben.

Meiner Verlobten Patricia danke ich von ganzem Herzen für ihre unermüdliche Unterstützung, ihre Liebe und Motivation.



# Abstract

The 1 Ma, 14-km-diameter, Zhamanshin impact structure, situated in a semi-arid region of Kazakhstan, has a heterogeneous suite of target rocks, including basement Silurian quartzites, Devonian shales and rare middle Paleozoic ultramafic dikes, Carboniferous volcanoclastic rocks of andesitic composition, Cretaceous sandstones, shales, marls, and limestones, as well as Cenozoic clays. The center of the crater is filled with lake sediments and loess. There are a variety of impact glasses (zhamanshinites) and tektite-like objects (irghizites), both subclassified into Si-poor ( $\sim 54$  wt%  $\text{SiO}_2$ ) and Si-rich ( $\sim 74$  wt%  $\text{SiO}_2$ ) varieties. One drill core and four surface target rocks, as well as five impactite samples (two irghizites and three zhamanshinites), were analyzed in this study for their petrography, geochemical composition (including highly siderophile element contents), as well as Sr, Nd, and Os isotopic compositions in order to study the relationship between target rocks and impactites and to search for a possible meteoritic components within the irghizites and zhamanshinites.

Impact glasses from the Zhamanshin impact structure appear as chunky black rocks with pitted surfaces and bubbles (zhamanshinites) or as aerodynamically-shaped splash forms with either a lustrous or dull surface (irghizites). Both kinds of impact glasses have been investigated by electron microprobe analysis and are found to be homogeneous in their major element composition. Strontium and neodymium isotopic data obtained during this study for impactites are in the range of literature data.

Based on the Re/Os ratios, a general bimodal trend can be observed between impactites (zhamanshinites and irghizites) and most target rocks. Impactites in general show lower Re/Os ratios than the investigated target rocks.

Even though the concentrations of selected highly siderophile elements (Re, Os, Ir, and Pt) and the corresponding interelement patterns of most analyzed impactites are comparable to those of the target rocks (which, on average, mirror the trend defined by the upper continental crust), one of the analyzed (Si-rich) irghizites and one of the analyzed (Si-rich) zhamanshinites exhibit highly siderophile element concentrations up to two orders of magnitude higher and a less fractionated and nearer to chondritic interelement pattern compared to the upper continental crust. The irghizite sample also shows the most unradiogenic  $^{187}\text{Os}/^{188}\text{Os}$  isotope ratio of all analyzed samples. Interpreted in terms of a meteoritic component, and after excluding a possible contamination with one of the rare examples of ultramafic target rocks that occur in the Zhamanshin area (which could simulate such an extraterrestrial signal), the presence of about 0.1% of a chondritic component within this irghizite and this zhamanshinite is postulated.





# Kurzfassung

Die Gesteine der in Kasachstan gelegenen Zhamanshin-Impaktstruktur, mit einem Durchmesser von 14 km und einem Alter von etwa 1 Millionen Jahre, weisen eine sehr variable Zusammensetzung auf und bestehen aus silurischen Quarziten, devonischen Sedimentiten und mittelpaläozoischen ultramafischen Dykes, sowie kretazischen und palaeogenen Sand- und Tonsteinen. Der Krater ist mit fluviatilen Sedimenten und Loess aufgefüllt. Des Weiteren befinden sich im Bereich des Zhamanshin Kraters zwei verschiedene Arten von Impaktgläsern: die Zhamanshinite und die tektitaehnlchen Irghizite. Diese lassen sich jeweils in silikatreiche ( $\sim 74$  wt%  $\text{SiO}_2$ ) und silikatarmer ( $\sim 54$  wt%  $\text{SiO}_2$ ) Varietäten subklassifizieren.

Im Rahmen dieser Arbeit wurden eine Bohrkernprobe, sowie vier Oberflächengesteine und fünf Impaktite (zwei Irghizite und drei Zhamanshinite) im Hinblick auf ihre Petrographie, ihre geochemische Zusammensetzung (inklusive der Konzentration hochsiderophiler Elemente) und ihrer Sr, Nd, sowie Os Isotopenzusammensetzung untersucht, um Zusammenhänge zwischen Kratergesteinen und Impaktiten zu studieren und mögliche meteoritische Komponenten in den Zhamanshiniten und Irghiziten zu identifizieren.

Die Impaktgläser in der Zhamanshinregion sind schwarze, blockige Gesteine mit einer rauhen Oberfläche und zahlreichen Bläschen (Zhamanshinite) oder aerodynamisch tropfenförmige Gebilde mit glänzender oder matter Oberfläche (Irghizite). Sowohl Zhamanshinite als auch Irghizite wurden mittels einer Elektronenstrahl-Mikrosonde auf ihren Hauptelementchemismus untersucht und dieser wurde als homogen befunden. Die im Zuge dieser Arbeit gewonnenen Sr-Nd Daten der Impaktgläser decken sich gut mit den bekannten Werten aus der Literatur.

Während die Konzentrationen an hochsiderophilen Elementen (Re, Os, Ir und Pt) und die entsprechenden Interelementverhältnisse der meisten hier analysierten Impaktite vergleichbar sind mit denjenigen der hier untersuchten Bohrkern und Oberflächengesteine (welche ihrerseits den Trend der oberen kontinentalen Kruste widerspiegeln), weist einer der hier analysierten (silikatreichen) Irghizite und einer der analysierten (silikatreichen) Zhamanshinite eine um bis zu zwei Größenordnungen höhere Konzentration an diesen Elementen auf (und ein weniger fraktioniertes und chondritähnlicheres Interelementmuster). Dieser Irghizit hat ebenfalls das unradiogenste  $^{187}\text{Os}/^{188}\text{Os}$  Isotopenverhältnis aller hier analysierten Gesteine. Im Sinne einer meteoritischen Kontamination interpretiert und nach Ausschluss einer möglichen Kontamination mit einer der im Kratergebiet seltenen ultramafischen Lithologien (welche ein extraterrestrisches Signal vortäuschen könnten), können etwa 0.1% einer CI chondritischen Kontamination in diesem Irghiziten sowie im Zhamanshiniten postuliert werden.



# Contents

<b>1</b>	<b>Introduction</b>	<b>1</b>
1.1	Thesis objectives . . . . .	1
1.2	Impact cratering . . . . .	1
1.2.1	Types of impact craters . . . . .	3
1.2.2	The impact cratering process . . . . .	4
1.2.3	Impactites . . . . .	4
1.3	Geochemistry of impact structures . . . . .	7
1.3.1	Chromium, Ni, and Co . . . . .	7
1.3.2	Rhenium and Platinum Group Element abundances . . . . .	7
1.3.3	The Os isotopic system . . . . .	8
1.3.4	The Cr isotopic system . . . . .	8
1.3.5	The Sr-Nd isotopic system . . . . .	9
1.4	The Zhamanshin impact structure . . . . .	10
1.4.1	Geological setting . . . . .	10
1.4.2	Impact breccias . . . . .	11
1.4.3	Impact glasses . . . . .	12
<b>2</b>	<b>Samples and Methods</b>	<b>13</b>
2.1	Samples . . . . .	13
2.1.1	Target rock samples . . . . .	13
2.1.2	Impactite samples . . . . .	14
2.2	Methods . . . . .	17
2.2.1	Optical microscopy . . . . .	17
2.2.2	Electron Probe Micro Analysis (EPMA) . . . . .	17
2.2.3	Wet chemistry . . . . .	17
2.2.4	Mass spectrometry . . . . .	18
2.2.5	Standard Os solution for N-TIMS measurements . . . . .	19
2.2.6	International standard reference materials . . . . .	19
<b>3</b>	<b>Results</b>	<b>21</b>
3.1	Petrography of target rocks and impactites . . . . .	21
3.1.1	Target rocks . . . . .	21
3.1.2	Impactites . . . . .	22

3.2	Major element compositions . . . . .	22
3.3	Rhenium and platinum group element concentrations . . . . .	24
3.4	Osmium isotope systematics . . . . .	27
3.5	Strontium-neodymium isotope systematics . . . . .	31
<b>4</b>	<b>Discussion</b>	<b>35</b>
4.1	The Re-Os concentration bimodality . . . . .	35
4.2	Identification of a meteoritic component in zhamanshinites and irghizites . . .	37
4.2.1	Evidences from major elements compositions . . . . .	37
4.2.2	Evidence from highly siderophile elements . . . . .	39
4.2.3	Evidence from Os isotopes . . . . .	41
4.3	Strontium-neodymium isotopic composition . . . . .	45
4.4	Meteoritic components in impactites - a comparison of selected case studies . .	48
<b>5</b>	<b>Summary and Conclusions</b>	<b>49</b>
	<b>Bibliography</b>	<b>51</b>
	<b>List of Tables</b>	<b>57</b>
	<b>List of Figures</b>	<b>59</b>
<b>A</b>	<b>Sample images</b>	<b>63</b>
<b>B</b>	<b>Chemical Composition of Samples</b>	<b>71</b>
<b>C</b>	<b>EPMA data</b>	<b>73</b>

# Introduction

## 1.1 Thesis objectives

The scope of this master thesis is a geochemical analysis of target rocks and impactites (zhamanshinites and irghizites) from the Zhamanshin impact structure (Kazakhstan). The main objectives of this work are a study of the geochemical relationship between target rocks and impactites and the search for a possible meteoritic components in the here analyzed impact glasses. This is done by (i) detailed petrographic inspections including ion microprobe investigations, especially of the here analyzed impact glasses, (ii) isotope dilution generated concentration data of several highly siderophile elements, (iii) high-precision Os isotope composition measurements, and (iv) Sr and Nd isotope systematics. Besides contributing to a so far sparse dataset on highly siderophile element concentrations and Os isotope signatures of rocks from this area, this study aims to contribute to our knowledge about the mechanisms that lead to the incorporation of meteoritic components in impactites, especially in the unique Zhamanshin structure, where two different types of impact glasses can be found.

## 1.2 Impact cratering

Impact craters are one of the most common landforms on objects with solid surfaces in the Solar System. Except on Earth, where active geologic and atmospheric processes obscure the impact record, impact structures are very common geomorphological features on solid planetary bodies including asteroids and icy moons. There have been ~190 impact structures reported on Earth and for ~45 of them meteoritic components have been identified (Earth impact database, 2015; Koeberl, 2014; Osinski and Pierazzo, 2012). Due to erosion, tectonic and volcanic activities terrestrial impact structures continually disappear, making the Earth's impact crater record incomplete. Dating impact structures is challenging, leading to large uncertainties in age information. Despite the fact that the oldest known impact

structure dates to about 2020 Ma before present, there are only few structures older than 700 Ma (Bailer-Jones, 2011). Generally the temporal distribution of known terrestrial impact structures is strongly biased towards younger ages with ~60% being younger than 200 Ma (see Fig. 1.1) (Grieve and Shoemaker, 1994; Jourdan et al., 2009; Earth impact database, 2015).

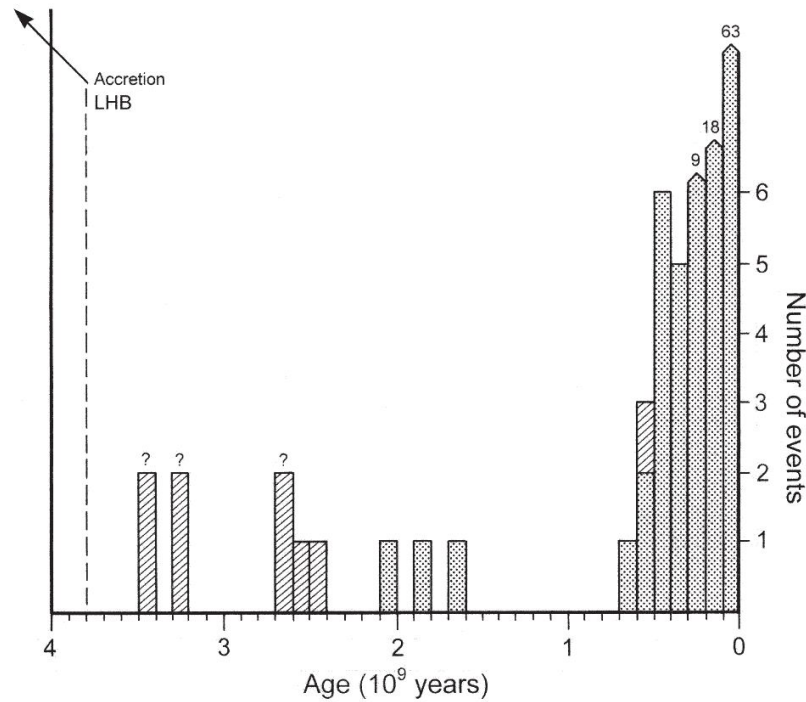


**Figure 1.1:** Histogram of ages of known terrestrial impact structures. Note that the scale is by far exceeded within the past 300 Ma. The dot-pattern indicates impact structures, whereas the hatched pattern signifies ejecta and/or spherule layers (from Koeberl, 2006).

Contrary, the Moon displays ample evidence for a "late heavy bombardement" around 3.9-3.8 Ga, which, due to its larger gravitational cross section, must have occurred to an even larger extent on Earth. However, no such witnesses can be found on Earth, besides some evidences in the form of Archean ejecta layers (marked in Fig. 1 with hatched patterns). The oldest of these ejecta layers (consisting of ballistically transported and quickly solidified melt droplets, called spherules), found in the Baberton Greenstone Belt in South Africa and the Pilbara Craton in Western Australia, are suspected to mark the tail end of the late heavy bombardement (e.g., Ryder, 1990; Ryder et al., 2000). This heavy bombardement must have destroyed and massively reshaped the surface of the Early Earth also by mixing juvenile crust back into the mantle (Koeberl, 2006). Beside the recycling of juvenile crust severe environmental changes would have occurred on Earth if the "late heavy bombardment" really happened. The impact events and the corresponding vapor plumes may

have affected the Archean atmosphere and influenced the evolution of life on Earth (e.g., Krull-Davatzes et al., 2010).

### 1.2.1 Types of impact craters

The previously mentioned erosive geological processes make it necessary to differentiate between impact 'crater' and impact 'structure'. An impact 'crater' is the result of the impact event whereas an impact 'structure' is what is observed today after modification. Morphologically two kinds of craters can be distinguished on Earth (i) simple craters, which are bowl-shaped depressions with diameters of up to 4 km or (ii) complex crater which are larger and have a central peak or central ring of hills (see Fig. 1.2; e.g., Koeberl, 2014, and references therein). The transition from simple to complex craters does not solely depend on the projectile size but also on the kind of target rocks. For sedimentary rocks, smaller diameters ( $\sim 2$  km) are observed compared to crystalline rocks ( $\sim 4$  km) (e.g., Grieve, 1987). Larger structures, so-called multi-ring basins, can be observed on other planets (Melosh, 1989).

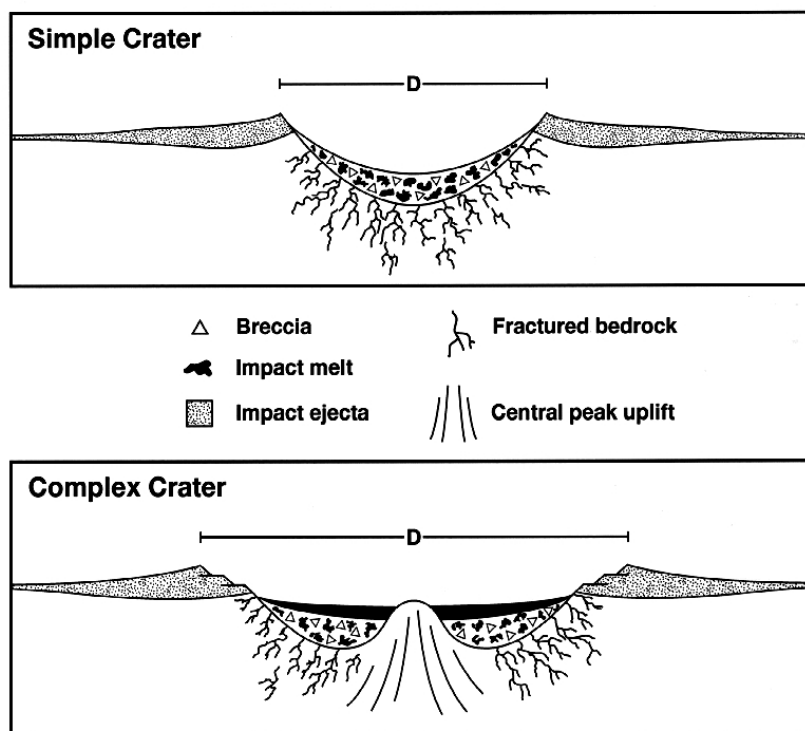


**Figure 1.2:** Schematic cross section of the two main crater types (from Koeberl, 2014)

## **1.2.2 The impact cratering process**

The formation of an impact crater is a very rapid geological process that takes place in a few seconds to some minutes, whereas it can last up to some hours for the ejecta to be deposited (Melosh, 1989). The impact cratering process itself consists of three main stages which are (i) contact and compression, (ii) excavation and (iii) modification. The first stage starts when the projectile (asteroid or comet) hits the target. A large amount of kinetic energy gets transferred from the projectile to its target. From the boundary between the compressed and uncompressed target material shock waves propagate into the lithosphere and back into the target. The shock pressures reach hundreds of GPa and by far exceed the yield strength of the projectile which results in partial or complete vaporization of the projectile. Thus, as a result of shock compression, the target material is shock metamorphosed, melted, or vaporized. In the second stage (excavation) the impact crater is opened. The projectile, having been melted or vaporized, takes no place in the excavation process. Complex interactions between the surface and the shock wave cause the target material to be displaced. The hemispherical shock wave and its rarefactions lead to tensional stress exceeding the strength of the target rocks. Rocks are fractured and the generation of a so-called 'transient cavity' takes place from which material gets ejected ballistically or is displaced within. The opening of the transient cavity stops when the energy of the shock waves is too low to displace material beyond the cavity rim. Immediately after the excavation stage the modification stage begins. Craters with diameters less than 2 km to 4 km experience only little modification during the modification stage. The result is a bowl-shaped crater the size of the transient cavity (simple crater). Craters with a larger diameter are modified by gravitation which forces the transient cavity rim to collapse and a central uplift is formed (complex crater; see Osinski and Pierazzo, 2012, and references therein).

## **1.2.3 Impactites**

Stöffler and Grieve (2007) published a detailed classification of impactites that is widely used in the scientific community today. The term "impactite" is used for any rock affected by a hypervelocity impact event. Impactites can be roughly classified in (i) proximal impactites, which are deposited within a distance of less than 2.5 crater diameters, whereas those found at greater distances are (ii) distal impactites.

Other criteria than the distance to the parent crater are the degree of shock metamorphism, the texture, and the lithological components. In the case of proximal impactites it can be distinguished between shocked target rocks, lithic impact breccias, suevites, and melt rocks. Tektites, microtektites, and air-fall beds, among others, can be assigned to the distal impactites.

### **Shocked target rocks**

The term shocked target rock is used for rocks formed within or close to the crater, excluding all rocks that were brecciated or that were completely molten during the impact event. They



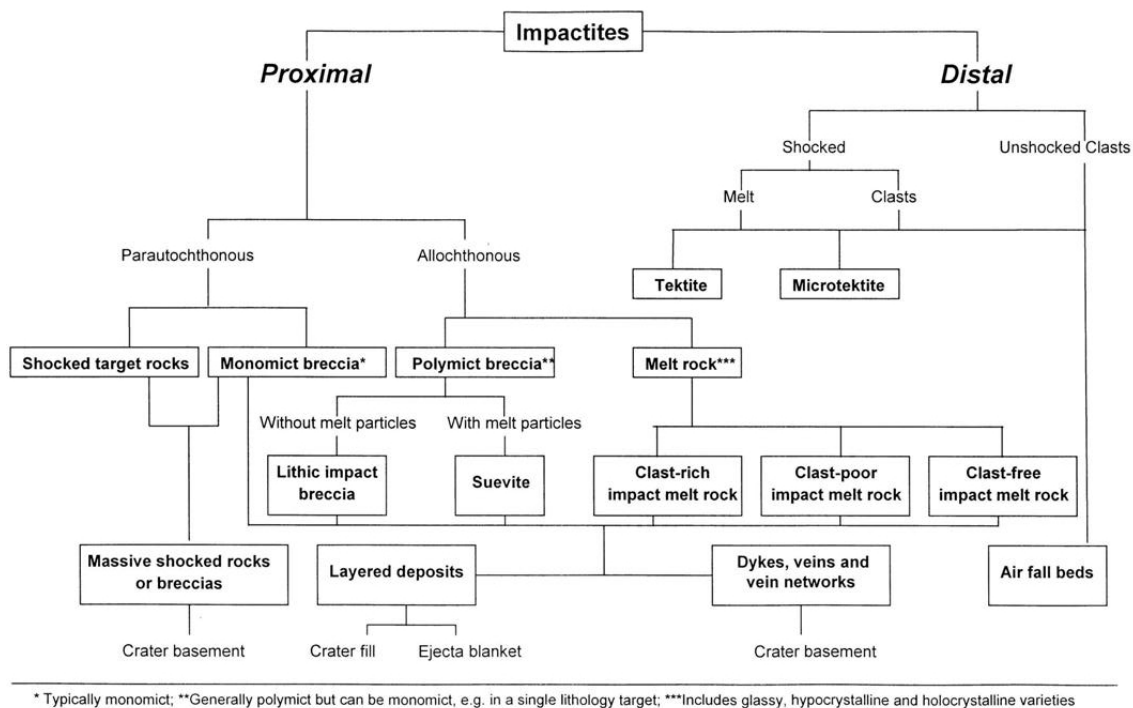


**Figure 1.3:** Classification of impactites from single impacts according to geological setting, composition, texture and degree of shock metamorphism (from Stöffler and Grieve, 2007)

can be further classified by the stage of metamorphism, the texture, and mineral content (Stöffler and Grieve, 2007).

### Impact breccias

Impact breccias are classified by their components which can be (i) remnants of target rocks and/or (ii) melts. Monomict breccias are found in the crater floor and consist of brecciated target rock and exhibit weak or no shock metamorphism. Lithic impact breccias are polymict consisting of shocked or unshocked minerals and lithic clasts embedded in a clastic matrix but without impact melt particles. Suevite or polymict impact breccias are made up by shocked or unshocked minerals, lithic clasts, monomict breccias, and glassy impact melt particles embedded in an either clastic or melt matrix (Stöffler and Grieve, 2007).

### Impact melt rocks

Impact melt rocks are crystalline, semihyaline or hyaline rocks containing variable amounts of clastic components with or without shock metamorphism. They can be classified as clast-rich, clast-poor, and clast-free varieties (Stöffler and Grieve, 2007).

## Tektites and microtektites

Tektites are glasses that in some cases are aerodynamically shaped and were formed from melt ejected ballistically from the impact crater (Stöffler and Grieve, 2007). In general they are homogeneous, contain abundant lechatelierite (amorphous silica glass) and occur in geographically extended strewn fields but not directly in or around the impact crater. Tektites commonly contain little water and seem to originate from the upper most target rock layer. Sizes range from sub-millimeter (microtektites, which are commonly found in pelagic sediments) to centimeter (Montanari and Koeberl, 2006). On Earth four large tektite strewn fields are known (see Fig. 1.4) which are the Central European tektites originated from the Nördlinger Ries, the Ivory Coast tektites from the Bosumtwi crater, the North American tektites from Chesapeake Bay impact structure and the Australasian strewn field for which yet no source crater was identified so far (e.g., Koeberl, 2014, and references therein).

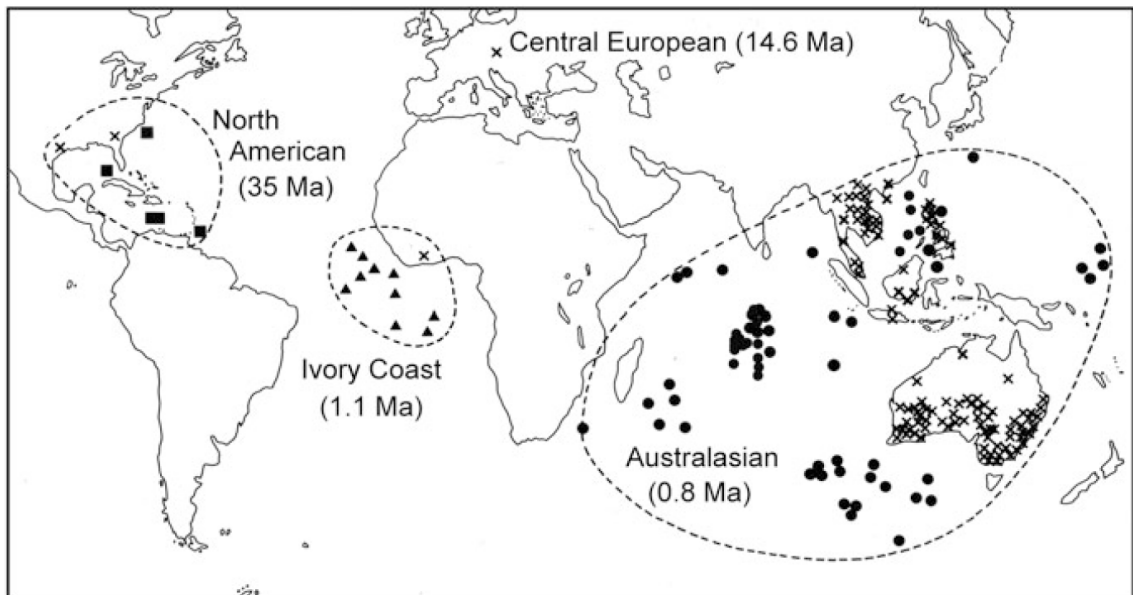


**Figure 1.4:** Map showing the four tektite strewn fields on Earth. Formation ages of the tektites are shown in parentheses (from Glass and Simonson, 2012).

## Airfall beds

Airfall beds are made up from impactoclastic, pelitic material containing shocked or unshocked minerals and melt particles, which were ejected ballistically at the formation of the impact crater. This material can be transported over long distances in the atmosphere and, therefore, cover large areas up to a global scale (Stöffler and Grieve, 2007).

## 1.3 Geochemistry of impact structures

Besides mineralogical evidences for the identification of an impact event, like planar deformation features, shatter cones or shocked minerals (e.g., coesite and stishovite) which can only form during the high pressures and temperatures which occur during an impact event, geochemical tools allow the identification of meteoritic fingerprints in impactites.

Since projectiles are rarely found at impact structures geochemical tools are important to detect geochemical traces of the projectile in impact rocks. As the meteoritic projectile vaporizes at the beginning of the cratering process, small quantities of the projectile vapor can be mixed with vapor and melt from target rocks before forming the impactites. These very minor meteoritic traces lead to slight chemical changes in the composition of impact related rocks. For the identification of meteoritic components in impactites, elements with high abundances in meteorites and low abundances in the upper continental crust (in which most impact sites are located) are used. These minor admixtures also lead to changes in the isotopic composition (meteorites are more unradiogenic compared to the rocks from the upper continental crust), which can be used to identify meteoritic components. The best candidates to fulfill this requirement are highly siderophile elements such as the platinum group elements (PGE) and Re, as well as corresponding Cr, Co, and Ni contents and interelement ratios. However, elevated concentrations of these elements in impactites and near chondritic interelement ratios not necessarily indicate a meteoritic component because they can also be attributed to basic or ultrabasic contaminations (requiring careful petrographic and isotopic inspection in order to exclude them (e.g., Koeberl, 1998; Koeberl et al., 2012; Koeberl and Schulz, 2015)).

### 1.3.1 Chromium, Ni, and Co

The elements Cr, Ni, and Co have often been used for suggesting the possible presence of meteoritic components (e.g., Palme et al., 1978; Shukolyukov and Lugmair, 1998). In addition, the interelement ratios of these elements were used for discrimination between impactor types. Typically the ratios of Ni/Cr and Co/Cr in addition to the Cr abundance can help to distinguish iron from chondritic projectiles (e.g., Koeberl et al., 2002).

### 1.3.2 Rhenium and Platinum Group Element abundances

As mentioned previously, the Platinum Group Elements (PGE) and Re abundances and their interelement ratios can be used for the identification of an meteoritic component in impactites and are probably the most valuable for such an undertaking. In meteorites (except achondrites, which have undergone magmatic differentiation) these highly siderophile elements are present in high abundances, while they are depleted in the fractionated terrestrial upper continental crust. Due to the mixing of small amounts of the projectile (having significantly higher abundances of PGEs and Re) with target material these elements can occur in detectable higher amounts in impactites compared to the average crust. Also the interelement ratios differ from that of crustal rocks and, to a lesser extent, mantle melts. Considering a target with low PGE abundances, meteoritic components down to 0.1 wt% can

be detected (e.g., Lee et al., 2006). Elevated concentrations of PGEs, if interpreted in terms of a meteoritic contamination, can be indicative for chondritic or iron projectiles, whereas the identification of an achondritic projectile is more difficult due to lower PGE abundances. However, it is important to sample all possible target rocks to determine the so-called indigenous component, which is the contribution of the target to the impact-melt rocks PGE signature (e.g. Koeberl et al., 2012 and references therein). For example, McDonald et al. (2001) suggested and Maier et al. (2006) confirmed that the projectile of the Morokweng impact structure is a L or LL chondrite by comparing PGE interelement ratios in melt rocks with that from possible impactor materials.

### 1.3.3 The Os isotopic system

The osmium isotopic system is based on the formation of  $^{187}\text{Os}$  from  $^{187}\text{Re}$  by  $\beta^-$  decay with a half-life of  $42.3 \pm 1.3$  Ga (Smoliar et al., 1996). Based on the fact that Re is less compatible than Os during melting events the  $^{187}\text{Os}/^{188}\text{Os}$  and the Re/Os elemental ratios in typical crustal rocks are generally higher than those in the mantle, ultrabasic rocks and also all chondritic and iron meteorites (achondritic meteorites are products of planetary melting processes and their Re/Os ratios, thus, differ to a lesser extent from those in terrestrial crustal rocks). As a result, the radiogenic ingrowth of  $^{187}\text{Os}$  due to the decay of  $^{187}\text{Re}$  is higher in crustal rocks compared to all other mentioned lithologies. This effect is all the more pronounced the older the crustal target material is.  $^{187}\text{Os}/^{188}\text{Os}$  ratios can, therefore, be used to evaluate whether or not a chondritic component is present in impactites. In the absence of any basic contamination and supported by Re/Os elemental ratios, an unradiogenic Os isotope composition in impactites compared to a significantly more radiogenic crustal target could indicate such a component (e.g., Koeberl and Shirey, 1993; Koeberl et al., 1996; Koeberl and Shirey, 1996; Koeberl and Shirey, 1997; Koeberl et al., 1998). With the Re-Os isotope tool even very minor proportions of a meteoritic component, on the order of  $>0.1\%$ , can be identified, as they lead to a significant shift in the Os isotope signature (see Fig. 1.5) (e.g., Koeberl, 2014, and references therein). A weakness of the Os isotopic system in cosmochemistry is the fact that it is not usable for identification of the projectile type (Koeberl, 2002).

### 1.3.4 The Cr isotopic system

Another method for detecting a meteoritic component is the Cr isotopic system, based on the relative abundance of  $^{53}\text{Cr}$ , the daughter isotope of  $^{53}\text{Mn}$ . In contrast to meteorites terrestrial rocks do not show any variation of the  $^{53}\text{Cr}/^{52}\text{Cr}$  ratios (Shukolyukov et al., 2000; Koeberl, 2002). Shukolyukov and Lugmair (1998) identified a carbonaceous chondritic impactor in samples from the K-Pg boundary, which was later found to be CM2 chondrite by Trinquier et al. (2006), with the help of the Cr isotopic method. Another application of Cr isotopes was the proof of an evidence of a carbonaceous chondritic impactor by Shukolyukov et al. (2000) for the event(s) responsible for the generation of the Barberton spherules found by Lowe and Byerly (1986).

The above mentioned tools make a detection of meteoritic components in impactites rather

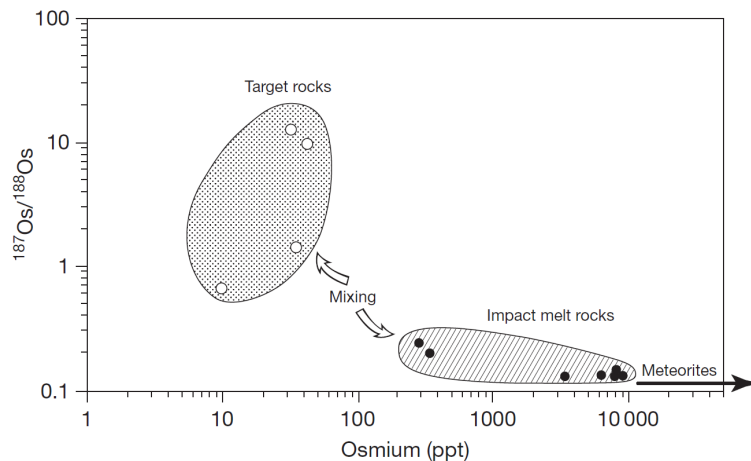


**Figure 1.5:** Osmium isotopic ratios vs. Os content showing the mixing relationship between a meteoritic and target rock endmember. Compositions of melt rocks plot along the hyperbolic mixing line, indicating extraterrestrial admixture (from Koeberl, 2014).

straightforward. This is not true for impactites derived from basic target materials or that have formed from target rocks that are dominated by felsic lithologies but are occasionally interbedded with ultrabasic rocks. A pure basaltic target is rare (one of the few examples is the Lonar crater, India) and a felsic crustal environment containing minor ultrabasics is much more common. Therefore, for a search of an extraterrestrial component in impactites it is crucial to rule out ultrabasic contaminants in impactites. However, significantly larger amounts of an ultrabasic contaminant would be needed to generate the same isotopic or elemental abundance signal in an impactite that a meteoritic component would produce. The Sr-Nd isotope system is a reliable tool to identify basic admixtures in impactites and is explained in the next section.

### 1.3.5 The Sr-Nd isotopic system

The isotopic decay-systems  $^{87}\text{Rb} - ^{87}\text{Sr}$  (based on the  $\beta^-$ -decay of  $^{87}\text{Rb}$  to  $^{87}\text{Sr}$  with a corresponding half-life of 48.8 Ga; Steiger and Jäger, 1977) and  $^{147}\text{Sm} - ^{143}\text{Nd}$  (based on the  $\alpha$ -decay of  $^{147}\text{Sm}$  to  $^{143}\text{Nd}$  with a corresponding half-life of 106 Ga; Lugmair and Marti, 1978) behave complementary due to the different compatibilities of the respective parent and daughter isotopes. While Rb preferentially partitions into the melt due to its greater incompatibility compared to Sr during partial silicate melting, Sm is more compatible compared to Nd. This results in a significantly higher radiogenic ingrowth of  $^{87}\text{Sr}$  (and corresponding unradiogenic  $^{143}\text{Nd}$  signatures) in crustal rocks compared to basic lithologies, which tend to exhibit lower Rb concentrations, a less radiogenic  $^{87}\text{Sr}$  signature and elevated  $^{143}\text{Nd}$  values. Thus, from the coupled Sr-Nd isotopic signature of impactites it can be determined if their precursor material was a crustal rock or from the deep crust or mantle and whether or not basic or ultrabasic contaminations are present in impactites. In addition the

Rb-Sr and Sm-Nd isotopic systems are important tools to help identify the source crater of tektites. (e.g., Koeberl, 2014).

After this brief introduction of the basic tools that can be applied for the identification of meteoritic components in impactites (and which, in part, will be applied in this study), a brief description of the impact structure on which this master's thesis is focused, is given below.

## 1.4 The Zhamanshin impact structure

The Zhamanshin impact structure, with a diameter of  $\sim 14$  km, is centered at  $48^{\circ}22'N$ ,  $60^{\circ}58'E$  in a semi-desert plain in Kazakhstan with topographic levels of 150 m to 300 m. The complex structure, which has a northwest-southeast symmetry axis, includes an inner ring, a circular depression  $\sim 6$  km diameter and 100 m to 150 m in depth, and was formed in flat-lying Paleogene sediments overlying Paleozoic and mesozoic metamorphic rocks. (McHone et al., 2002; Burba and Meshcherskaya, 1993; Bouška et al., 1981).

The structure was first recognized in 1939 by Vakhromev and Yashin who noticed inverse stratification of Paleozoic and Cenozoic deposits. Piliya (1960) is the first who mentions glasses, slags and pumice like materials around the structure (both cited by Boiko et al., 1991). Kostik and Piliya (1973) consider the glasses of the Zhamanshin area to be of volcanic origin (e.g., Florensky, 1977 and references therein). The impact origin of the structure was discovered by Florensky in 1975 due to the presence of lechatelierite, shock metamorphism and impact related rocks (Florensky et al., 1977). The age of the impact structure was determined by laser-fusion  $^{40}\text{Ar}/^{39}\text{Ar}$  ages to  $\sim 870$  ka (Deino et al., 1990). Slightly higher fission track ages of  $\sim 1.08$  Ma were obtained by Storzer and Koeberl (1989).

### 1.4.1 Geological setting

The region north of the Aral Sea is a hilly semi-desert in which relatively undisturbed Neogene deposits are exposed. These are underlain by Cretaceous rocks, and, at depths of 100 m to 150 m, by Paleozoic basement rocks. The Paleozoic basement consist of lower Paleozoic metamorphic shales and middle Paleozoic volcanoclastic sediments. Two ultrabasic intrusions in the basement, which also cut the crater area, were traced by geophysical methods (Florensky and Dabizha, 1980).

In the area of the Zhamanshin impact structure Mesozoic-Cenozoic bedrocks outcrop. The Cretaceous rocks are represented by (i) Cenomanian sandstones (thickness 30 m), (ii) dark-gray Turonian shales, and (iii) light-gray Maastrichtian marls and limestones with crinoids and bivalves (thickness 20 m).

The Paleogene deposits are build up (from bottom to top, thickness given in brackets) by (i) greenish-gray and cinnamon-brown pelitic shales of the Middle Eocene (145 m), (ii) gray quartz sands and clays of the Upper Eocene (15 m), and (iii) gray and greenish-gray clays of the Upper Eocene to Lower Oligocene (45 m). These Paleogene deposits form the Zhamanshin structure's inner ring and are most often overlain by Paleozoic rocks, glass, and cinder-like formations. Above this the Paleogene stratigraphic sequence continuous

with (iv) the sands and sandstones of the Middle Oligocene (15 m) which cover the surfaces of the elevation of the outer ring and in some places, on the highest areas of the outer ring, remnants of (v) brown and gray sandstones and gritstones of the Upper Oligocene (~5 m) are found (see Fig. 1.6). The structure's central basin, which nowadays forms a gently eastward inclined flat plain, is filled with Neogene lake sediments and loess (Florensky, 1977).

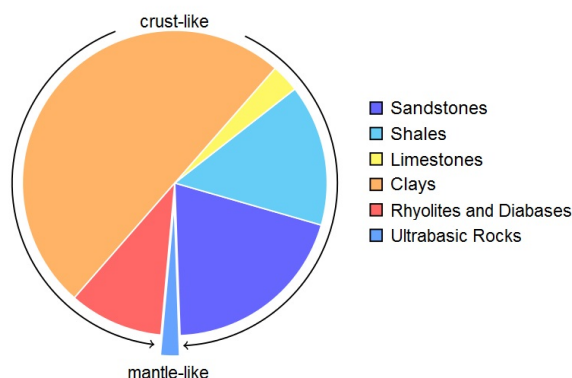


**Figure 1.6:** Approximated abundance of target rock lithologies in the Zhamanshin area. The calculation is based on target rock major element analyses from Izokh et al. (1993).

## 1.4.2 Impact breccias

The walls of the sporadically interrupted ring of the structure are made up from a body of loose, friable shattered rocks. This allogenic breccia exhibit a variable composition in different locations. Beside shattered Mesozoic-Cenozoic deposits up to 10% Paleozoic angular rock fragments, with no signs of rounding, are found. Due to the lack of massive rocks shatter cones were not found. The petrographic composition of the Paleozoic rocks is inconsistent around the crater.

On the structure's southwestern and northern edges predominantly dark-gray, thin-bedded variegated quartzitic-phyllitic and quartzitic-sericitic schists belonging to the Lower Cambrian occur. Also metamorphic fragments of actinolite-epidote bearing schist and serpentinized dunites were found to be fragments of Cambrian deposits.

On the eastern and southeastern edges of the structure fragments of andesites and andesite-basalts predominate along with the presence of pebbles of schists and limestones with Late Carboniferous faunas (Florensky, 1977).

The depression of the structure is filled up with an autochthonous breccia consisting of debris of various types of Paleozoic rocks, Mesozoic sedimentary rocks cemented by argillaceous material including also fragments of impact glass (Florensky, 1977; Florensky and Dabizha, 1980).

### 1.4.3 Impact glasses

Impact glasses are irregularly scattered on the surface and occur mainly along the outer margin of the structure. The two types of impact glasses that occur at Zhamanshin are irghizites and zhamanshinites. Zhamanshinites are compact or porous, opaque, greenish-black glassy or re-crystallized bodies up to 50 cm in size and can be subdivided from their silica content (ranging from 39 to 88 wt%) in high-silica (70 - 88 wt%), intermediate (52 - 57 wt%) and low-silica ( $\sim 40$  wt%) varieties (e.g., Koeberl and Fredriksson, 1986). A special variety are blue zhamanshinites, which were found only in one location within the crater and show blue and brown-gray layers. The blue coloring originates from small spherical silicate glass inclusions due to Rayleigh scattering of light (Mizera et al., 2012; Vetvicka et al., 2010; Zolensky and Koeberl, 1991).

Irghizites are dark, lustrous, and homogeneous glasses, usually with a size of 1–3 cm and various shapes (drops, flat drops, small rods, and often irregularly rope-wise twisted fragments). They contain lechatelierite particles and vesicles. Some specimens have small spherules fused to the surface. Irghizites are acidic glasses with high-silica contents ( $\sim 74$  wt%  $\text{SiO}_2$ ), but also si-poor glasses with a very low Ni content have been described (Mizera et al., 2012; Koeberl and Fredriksson, 1986). Mizera et al. (2012) suggests that a classification by size and morphology of irghizite samples should be the primary criterion, not their chemical composition. Ackerman et al. (2015) mentioned basic ( $\sim 54$  wt%  $\text{SiO}_2$ ) splash-forms with rather uniform tear-drop shapes or their fragments which he names "basic splash-forms" and which are referred to as "basic irghizites" by Florensky and Dabizha (1980). Figure 1.7 shows photographs of one zhamanshinite and two irghizites. Zhamanshinites are found at distances of up to 6 km from the crater especially in the northern and north-western parts whereas irghizites are found in the southeastern part of the Zhamanshin depression dispersed over an area of  $\sim 2$  km (Bouška et al., 1981).

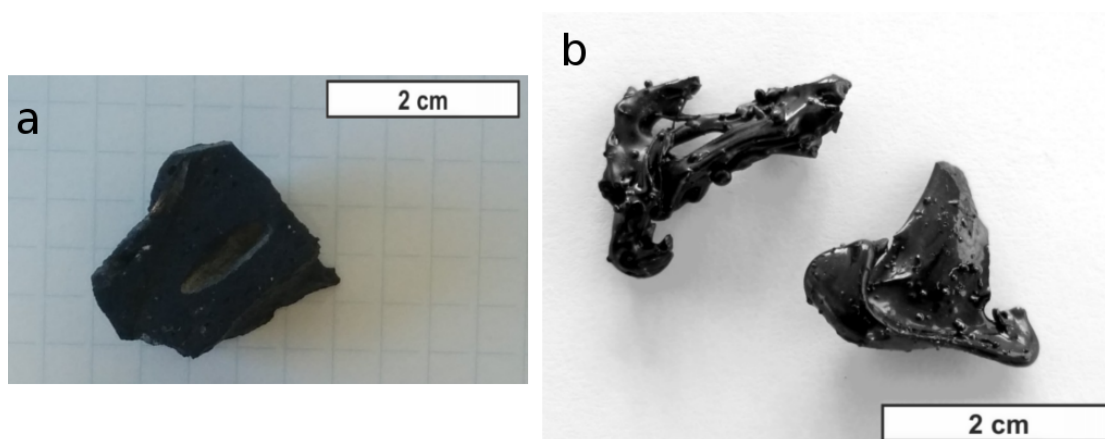


**Figure 1.7:** a) Zhamanshinite (photo by author) b) Irghizites (Figure from Ackerman et al., 2015).



# Samples and Methods

## 2.1 Samples

Five target rocks and five impactites (three zhamanshinites and two irghizites) from the Zhamanshin impact structure were made available by Christian Koeberl from his collection at the University Vienna and were analyzed in this study. Four target rock samples (DB-6, DB9, Zh-2DBI, and Zh-55/5) were collected from the crater rim, whereas target rock sample ZSK-8 was sampled at 50 m depth within the core of borehole no. 100, which was drilled at the center of the impact structure (Abate et al., 1998).

The here analyzed target rocks were selected in order to get a representative collection of the different lithologies from the Zhamanshin impact structure and its vicinity (see section 1.4.1 for details). The here analyzed impactites encompass three zhamanshinites (Zh-6014, Zh-62/3b and Zh-30a) as well as two irghizites (IRG-2015/1 and Irgh-2) which were sampled in the crater rim area.

Photomicrographs of all samples are shown in Figures 2.1–2.2. Images of all samples and backscattered electron (BSE) images of the impactites can be found in the appendix A. A petrographic summary and petrographic details is provided in section 3.1.1 (see also table 3.1).

### 2.1.1 Target rock samples

Target rock samples analyzed in this study have been selected with the attempt to represent the different lithologies in the Zhamanshin area. Therefore, also one of the rare ultrabasic rocks that occurs in the Zhamanshin area was included (sample Zh-55/5 with a SiO<sub>2</sub> content of 40.29 wt.%; see table 4.1 and table B.1 for further geochemical data). Figure 1.6 illustrates the approximated proportions of such ultrabasic lithologies in comparison to the more and crust-like target lithologies described in the Zhamanshin area. The crust-like target rock samples analyzed in this study (SiO<sub>2</sub> contents ranging from 45.11 wt.% to 58.96 wt.%).

**Target rocks collected from the crater rim:** DB-6 and DB-9 are shales which exhibit a common mineralogy and texture. In the hand specimen these samples appear as grayish layered rocks, predominantly consisting of plagioclase and biotit which contain hypidiomorphic to granular quartz and quartz veins. Muscovite and chlorite are found as secondary minerals. Zh-2DBI is an andesite appearing grayish and fine grained in the hand specimen. It consists of hypidiomorphic plagioclase, pyroxene, amphibole, clays and quartz embedded in an aphyric to sub-aphyric groundmass. Also minor glass and phenocrysts of plagioclase are found. Zh-55 is a fine-grained ultrabasic rock appearing black to greenish in hand specimen. The rock predominantly consist of antigorite and chlorite as well as clinopyroxene. Several larger grains were identified as olivine and numerous crosscutting veins of chlorite suggest that this rock has undergone extensive physical and chemical alterations.

**Target rock from the drill core:** ZSK-8, which was collected from a depth of 50 m in a drill-core, is a highly weathered claystone. The sample appears grayish in hand specimen and no grains can be determined. Under the microscope it appears brownish-black regardless if viewed in plane or polarized light. There is organic matter with densely packed peloids and also abundant glauconite. No lamination or gradation is observed in the thin section.

### 2.1.2 Impactite samples

**Zhamanshinites:** Zhamanshinites analyzed in this study encompass samples Zh-6014, Zh-62/3b, and Zh-30a, all of them sampled in the crater rim area. The zhamanshinites are chunky black rocks with pitted surfaces and bubbles and in some cases weathering (for example sample Zh-30a, see microphotograph in Fig. 2.2) can be observed.

In thin section under the microscope all samples, except Zh-62/3b, which appears black, are transparent. Vesicles of different size were found in all samples. From BSE images in all zhamanshinite samples fluid structures and schlieren can be found. In sample Zh-62/3b also fine grains which exhibit more or less the same chemical composition as the surrounding matrix were found an also finshaped crossing features which were interpreted to originate from pressure dissolution.

**Irghizites:** Irghizites analyzed in this study encompass samples IRG-2015/1 and Irgh-2, all of them sampled in the crater rim area. Both irghizites appear as aerodynamically shaped splash forms with either a lustrous or dull surface. In contrast to the zhamanshinites, no bubble cavities can be observed on the irghizites in the macroscopic view.

The biggest bubbles in thin sections were found in sample IRG-2015 with diameters of up to 1.2 mm. This sample also shows an additional brown glass phase under transmitted light. In BSE images schlieren are also observed in the two irghizites.

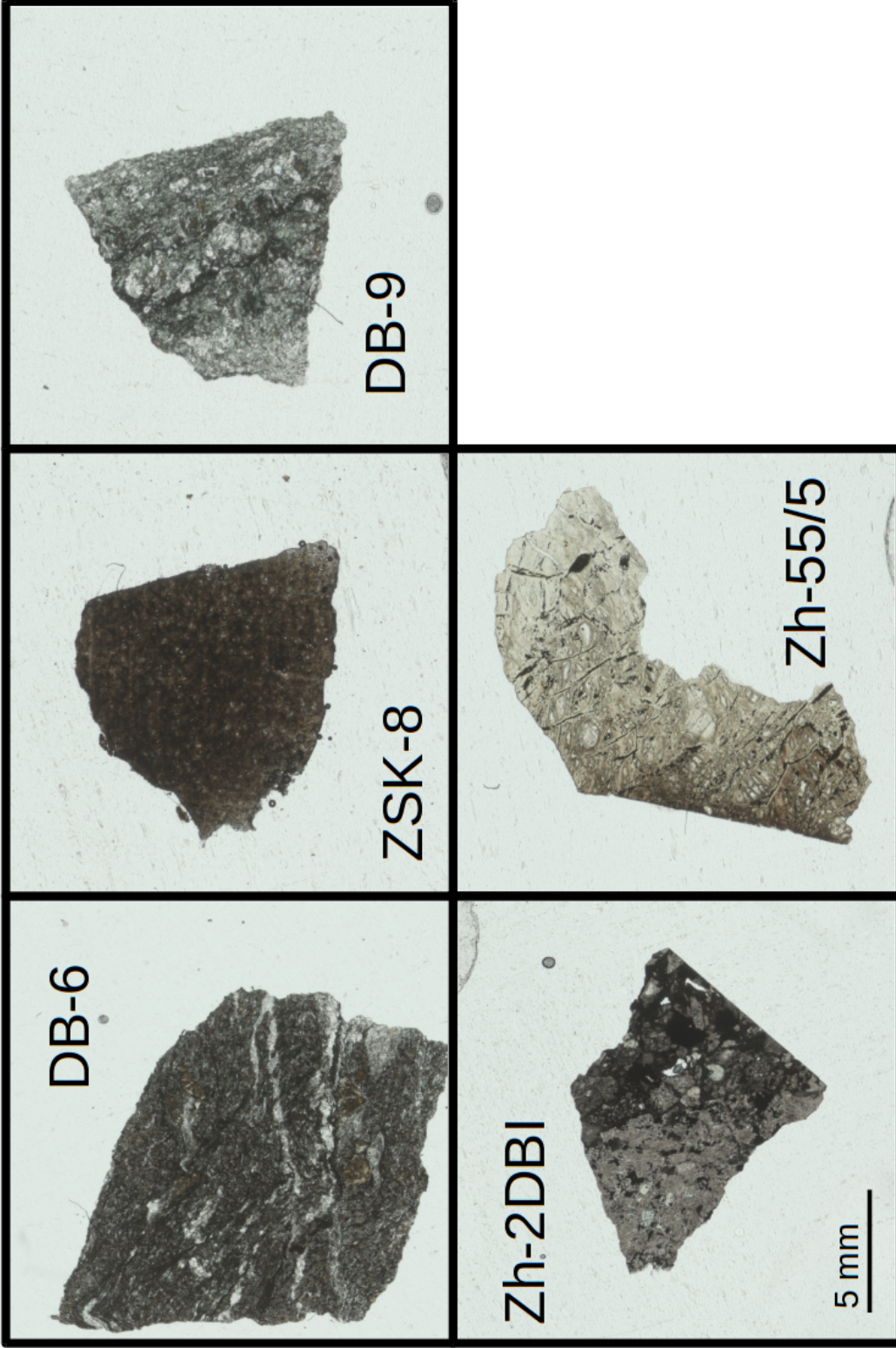


**Figure 2.1:** Photomicrographs of thin sections for target rocks samples. DB6, and DB-9 are shales. ZSK-8 is a claystone. Zh-2DBI is a andesite. Zh-55/5 is an ultrabasic rock. Scale applies to all images.

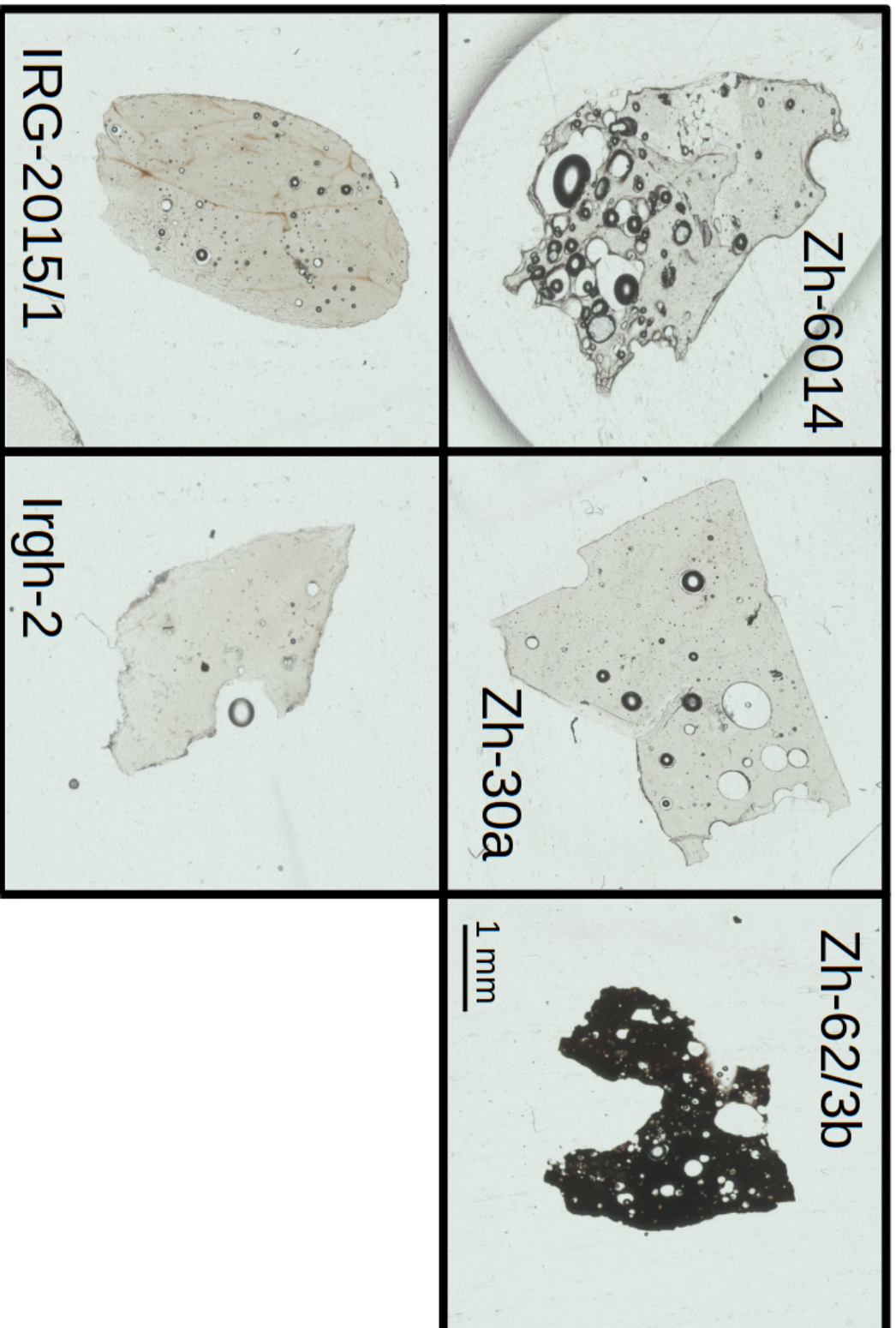


**Figure 2.2:** Photomicrographs of thin sections for impactite samples. Zh-6014, Zh-30a, and Zh-62/3b are zhamanshinites. IRG-2015/1, and Irgh-2 are irghizites. Scale applies to all images.

## 2.2 Methods

### 2.2.1 Optical microscopy

The thin sections of target rocks and impactites were examined by transmitted light microscopy, using a Leica DM2500 P petrographic microscope. Photographies of thin sections were obtained using a high-resolution scanner or a digital single-lens reflex camera Nikon D70 mounted on the petrographic microscope.

### 2.2.2 Electron Probe Micro Analysis (EPMA)

Carbon-coated polished thin sections were made from all impactite samples and viewed with an electron microscope in secondary and in backscattered electrons. For measurements carried out to test the homogeneity and composition of the impact glasses a JXA-8530F field emission electron microprobe at the Natural History Museum in Vienna was used. The major and trace element composition were obtained at 15 kV accelerating voltage and 20 nA beam current with a defocused electron beam of 10  $\mu\text{m}$  by wavelength-dispersive spectrometry (WDS-EPMA). The used standards, spectrometer crystals and counting times (peak and background) for calibration and measurements are given in Table 2.1.

**Table 2.1:** Standard materials, used crystal, measuring times, and detection limits of EPMA analysis performed during this study with a Jeol JXA-8530F field emission electron microprobe.

Element	Crystal	Standard	Counting time [s]		detection limit [ppm]
			peak	back-ground	
Si	TAP	Glass/Olivine	10	5	86
Al	TAP	Jadeite	10	5	51
Cr	LIF	Glass	25	8	84
Ti	LIF	TiO <sub>2</sub>	10	5	29
K	PETH	Glass	10	5	36
Ca	PETH	Wollastonite	10	5	46
P	PETH	Apatite	25	8	50
Fe	LIFH	Troilite	10	5	96
Mn	LIFH	Tephroite	10	5	91
Ni	LIFH	NiO	25	8	100
Na	TAP	Jadeite	10	5	45
Mg	TAP	Olivine	10	5	44

### 2.2.3 Wet chemistry

The entire sample material was cleaned in an ultrasonic bath prior to being broken to smaller chunks in an agate mill. Chunks of about 1 g of target rock samples and  $\sim 0.7$  g of impactite

samples were then powdered in an agate mill. About 0.5 g of the so obtained homogeneous sample powder was then spiked with a mixed tracer composed of  $^{185}\text{Re}$ ,  $^{190}\text{Os}$ ,  $^{191}\text{Ir}$ , and  $^{194}\text{Pt}$  and digested in 7 ml inverse aqua regia (5+2) and treated at 270 °C and 130 bar in an Anton-Paar high pressure asher (HPA) for 12 hours. During this leaching procedure, the platinum-group elements and Re partition into the liquid-phase, from which Os was extracted after the HPA treatment using a liquid extraction procedure as described in Cohen and Waters (1996). Osmium was then further purified using a  $\text{H}_2\text{SO}_4/\text{H}_2\text{CrO}_4$  microdistillation technique (Birck et al., 1997). After Os extraction, the aqua regia fraction containing all other HSEs, as well as the undissolved sample (usually containing some unleached Re), was dried down and redissolved in conc. HF in closed teflon beakers at 120 °C over night. After drying down and converting to chloride form by multiple redissolution steps using 6 M HCl, group separation of the HSEs via anion exchange columns, filled with 1 ml AG1x8 (200-400 mesh) resin, was undertaken. The samples were loaded in 1M HCl and elements were eluted using concentrated  $\text{HNO}_3$  (Rehkämper and Halliday, 1997; Coggon et al., 2013).

For the Sr and Nd isotopic analysis, about 50 mg of the sample were digested in an ultra-pure mixture of HF :  $\text{HNO}_3$  (4:1) for 2 weeks at 100 – 120 °C on a hotplate. After acid evaporation and multiple redissolution of the residue using conc. and 6 N HCl, clear solutions for all samples were obtained. Extraction of Sr and the Rare Earth Elements (REE) was performed using AG 50W-X8 (200-400 mesh, Bio-Rad) resin and 2.5 N and 4.0 N HCl as eluants. Neodymium was separated from the REE group using teflon-coated HdEHP and 0.24 M HCl as eluants.

#### 2.2.4 Mass spectrometry

Osmium isotope ratio measurements were carried out at the Department of Lithospheric Research at the University of Vienna, Austria. All Os isotope analyses were performed using a ThermoFinnigan Triton Thermal Ionization Mass Spectrometer operating in negative mode. Osmium was loaded as a bromide on single Pt ribbon filaments covered with a saturated  $\text{Na}(\text{OH})/\text{Ba}(\text{OH})_2$  solution as an activator (Luguet et al., 2008). The runs were performed with an oxygen bleed in order to raise ionization yields. Osmium was measured as  $\text{OsO}_3^-$  ions, via a peak hopping measurement sequence using the Triton SEM detector. Oxygen corrections were performed using  $^{17}\text{O}/^{16}\text{O}$  of 0.0003866 and  $^{17}\text{O}/^{16}\text{O}$  of 0.00203406 (see Acken et al., 2011, and references therein). Isobaric interferences attributable to Pt-oxide were not observed. Correction for isobaric interferences of  $^{187}\text{Re}$  on  $^{187}\text{Os}$  and mass fractionation (using  $^{192}\text{Os}/^{188}\text{Os} = 3.083$ ; Brandon et al., 2005) were conducted offline. The Os total procedural blank was  $\sim 0.5$  pg ( $n = 2$ ) contributing to less than 1% to the measured Os concentration of all samples.

Rhenium and PGEs were measured using a Thermo Element ICP-MS in single collector mode at the Steinmann Institute at University Bonn, Germany. Instrumental drift was monitored with a 1 ppb in-house multi-element HSE standard solution, measured at the beginning, middle and end of the analytical session. Mass bias was corrected relative to this standard solution, using ratios of 0.5986 for  $^{185}\text{Re}/^{187}\text{Re}$ , 0.5957 for  $^{191}\text{Ir}/^{193}\text{Ir}$  and 0.2117 for  $^{198}\text{Pt}/^{195}\text{Pt}$  and corrections were insignificant for all samples. Additionally, isobaric interferences caused by Hf on Ir and Pt were monitored and corrected for offline. In order to

do so, Hf-doped 1 ppb HSE solutions were run at the beginning, middle, and end of each analytical session, in order to determine the oxide production. Rhenium, Ir, and Pt were measured with a cyclonic borosilicate glass spray chamber. Total blanks for this study ( $n = 3$ ) were 3 – 4 pg for Re, 0.5 – 3 pg for Ir and 20 – 60 pg for Pt. Due to the low HSE contents of the analyzed samples, blank corrections, except for Pt, were applied in all cases where blank contributions exceeded 1%.

Strontium and Neodymium isotope ratio measurements were carried out at the Department of Lithospheric Research at the University of Vienna, Austria. All analyses were performed using a ThermoFinnigan Triton Thermal Ionization Mass Spectrometer operating in positive mode. Strontium and Nd pure element fractions were evaporated using a Re double filament assembly and run in static mode. A mean  $^{87}\text{Sr}/^{86}\text{Sr}$  ratio of  $0.710284 \pm 0.000004$  ( $n=3$ ) was determined for the NBS987 and a mean ratio of  $0.511846 \pm 0.000004$  ( $n=2$ ) for the La Jolla international Nd standard. Mass fractionation was corrected using  $^{88}\text{Sr}/^{86}\text{Sr} = 8.3752$ , and  $^{146}\text{Nd}/^{144}\text{Nd} = 0.7219$ , respectively. Errors quoted represent  $2\sigma$  errors of the mean. Maximum total procedural blanks were  $< 1$  ng for Sr and  $\sim 50$  pg for Nd, and were taken as negligible.

### 2.2.5 Standard Os solution for N-TIMS measurements

Repeated N-TIMS measurements ( $n=3$ ) of 10 pg loads of a DROsS (Durham Romil Osmium Standard) solution were performed using the electron multiplier at signal intensities that were typically achieved during the sample runs ( $\sim 10,000$  to  $\sim 100,000$  counts on mass 240 ( $^{192}\text{OsO}_3^-$ )). The DROsS measurements yield an average of  $0.16088 \pm 56$  for  $^{187}\text{Os}/^{188}\text{Os}$ ,  $1.2167 \pm 40$  for  $^{189}\text{Os}/^{188}\text{Os}$  and  $1.9782 \pm 80$  for  $^{190}\text{Os}/^{188}\text{Os}$  ratios (errors refer to the last two digits). These values agree within the  $2\sigma$  uncertainty of the average values reported by Luguët et al. (2008) obtained for much larger Os loads of DROsS. The long-term external reproducibilities are  $\pm 0.4\%$  for  $^{187}\text{Os}/^{188}\text{Os}$ ,  $\pm 0.2\%$  for  $^{189}\text{Os}/^{188}\text{Os}$  and  $\pm 0.3\%$  for  $^{190}\text{Os}/^{188}\text{Os}$ . See Table 2.2 for details.

### 2.2.6 International standard reference materials

To quantify the precision and accuracy of the Os and HSE chemistry and analytical procedures, replicate analyses of international reference materials were performed. For Os, the reference materials analysed were chosen to show an extremely different range of concentrations, e.g. from  $< 100$  ppt Os in TDB-1 (Diorite, CANMET, international standard material) to  $> 1000$  ppt Os in OKUM (Komatiite, IAG-certified ultrabasic rock reference material, Meisel et al., 2001; Meisel and Moser, 2004a; Meisel and Moser, 2004b; Savard et al., 2010; Ishikawa et al., 2014; Meisel et al., 2013; Koeberl et al., 1996). Averages and relative standard variations (% RSD) of element concentrations for Re and PGEs for these two materials are reported in Tables 2.3 & 2.4 and are indistinguishable from the literature values within  $2\sigma$  uncertainty (see caption to table 2.3 for details). In addition,  $^{187}\text{Os}/^{188}\text{Os}$  ratios for OKUM and TDB-1 are also reported in Table 2.3. While  $^{187}\text{Os}/^{188}\text{Os}$  literature data for OKUM are in excellent agreement with our here presented data (see Table 2.3), TDB-1 exhibits linear correlations between  $^{187}\text{Os}/^{188}\text{Os}$  and  $^{187}\text{Re}/^{188}\text{Os}$  ratios, reflecting significant

**Table 2.2:** Osmium isotope compositions for DROsS Os reference materials. Low sensitivity measurements in this study were performed in peak jumping mode using an electron multiplier in negative modus using the Triton Thermo Scientific TIMS at the University Vienna. Typical intensities for mass 240 ( $^{192}\text{OsO}_3$ ) ranged between  $\sim 10.000$  and  $\sim 100.000$  counts. Literature values are listed for comparison and represent high-precision measurements performed in multi-collector mode.

Reference material	$^{186}\text{Os}/^{188}\text{Os}$	$^{187}\text{Os}/^{188}\text{Os}$	$^{189}\text{Os}/^{188}\text{Os}$	$^{190}\text{Os}/^{188}\text{Os}$
DROsS				
measured	$0.12053 \pm 49$	$0.16088 \pm 56$	$1.2167 \pm 40$	$1.9782 \pm 80$
literature <sup>1</sup>	$0.119929 \pm 6$	$0.160924 \pm 4$	$1.219705 \pm 15$	$1.983803 \pm 15$

<sup>1</sup>Luguet et al., 2008

**Table 2.3:** Concentrations (in  $\text{ngg}^{-1}$ ) and relative standard deviations (RSD) for two standard reference materials.

Reference material	Ir	RSD	Pt	RSD	Re	RSD	Os	RSD
TDB								
measured	62	6%	4.99	5%	0.76	5%	98	5%
expected <sup>1,2,3,6</sup>	77	22%	5.02	7%	0.74	7%	112	10%
OKUM								
measured	0.7	4%	11.1	9%	0.4	8%	0.92	5%
expected <sup>4,5,6</sup>	0.99	7%	11.0	6%	0.4	50%	0.98	33%

<sup>1</sup>Meisel et al., 2001; <sup>2</sup>Meisel and Moser, 2004a; <sup>3</sup>Meisel and Moser, 2004b; <sup>4</sup>Savard et al., 2010; <sup>5</sup>Ishikawa et al., 2014; <sup>6</sup>Meisel et al., 2013; <sup>7</sup>Koeberl et al., 1996.

**Table 2.4:** Os isotopic composition for standard reference materials.

Reference material	$^{187}\text{Os}/^{188}\text{Os}$			
	TDB	OKUM	MUH-1	BG-168
measured	0.615 (6)	0.27 (1)	0.130 (9)	0.665 (12)
expected <sup>1-7</sup>	0.53-1.39	0.27 (2)	0.127 (1)	0.668 (20)

<sup>1</sup>Meisel et al., 2001; <sup>2</sup>Meisel and Moser, 2004a; <sup>3</sup>Meisel and Moser, 2004b; <sup>4</sup>Savard et al., 2010; <sup>5</sup>Ishikawa et al., 2014; <sup>6</sup>Meisel et al., 2013; <sup>7</sup>Koeberl et al., 1996.

sample heterogeneity (see Ishikawa et al., 2014 for details). However, our  $^{187}\text{Os}/^{188}\text{Os}$  and  $^{187}\text{Re}/^{188}\text{Os}$  data for  $\sim 0.5$  g TDB-1 replicates match the trend defined by the High Pressure Asher data from the literature (see Ishikawa et al., 2014), which were obtained using various digestions techniques (e.g., Ishikawa et al., 2014), reflecting the suitability of our isotope data.



# Results

## 3.1 Petrography of target rocks and impactites

### 3.1.1 Target rocks

Target rock samples analyzed in this study have been selected with the attempt to represent the different lithologies in the Zhamanshin area. Therefore, also one of the rare ultrabasic rocks that occur in the Zhamanshin area was included (sample Zh-55/5 with a SiO<sub>2</sub> content of 40.29 wt.%; see table 4.2 and appendix A.1 for further geochemical data). Figure 1.6 illustrates the approximated proportions of such ultrabasic lithologies in comparison to the more felsic target lithologies described in the Zhamanshin area. Contrary, all other target rock samples analyzed in this study represent more felsic and (upper continental) crust-like lithologies of the Zhamanshin area (SiO<sub>2</sub> contents ranging from 45.11 wt.% to 58.96 wt.%).

DB-6 and DB-9 are shales which exhibit a common mineralogy and texture. In the hand specimen these samples appear as grayish layered rocks, predominantly consisting of plagioclase and biotite which contain hypidiomorphic to granular quartz and quartz veins. Muscovite and chlorite occur as secondary minerals.

Zh-2DBI is an andesite appearing grayish and fine grained in the hand specimen. It consists of hypidiomorphic plagioclase, pyroxene, amphibole, clays, and quartz embedded in an aphyric to sub-aphyric groundmass. Also minor glass and phenocrysts of plagioclase are present.

ZSK-8, which was collected from a borehole at a depth of 50 m, is a highly weathered claystone. The sample appears grayish in hand specimen and no grains can be discerned. Under the microscope it appears brownish-black regardless if viewed in plane or polarized light. There is organic matter with densely packed peloids and also abundant glauconite. No lamination or gradation is observed in the thin section.

Zh-55 is a fine-grained ultrabasic rock appearing black to greenish in hand specimen. The rock consist predominantly of antigorite, chlorite, and clinopyroxene. Several larger

grains were identified as olivine and numerous crosscutting veins of chlorite suggest that this rock has undergone extensive physical and chemical alteration.

### 3.1.2 Impactites

**Zhamanshinites:** The zhamanshinites are chunky black rocks with pitted surfaces and bubbles and in some cases corrosion (for example sample Zh-30a, see microphotograph) can be observed. Under the microscope all samples, except Zh-62/3b, which is black, are transparent. Vesicles of different size were found in all samples. From BSE images in all zhamanshinite samples fluid structures and schlieren can be noticed. In sample Zh-62/3b also fine grains which exhibit more or less the same chemical composition as the surrounding matrix were found and also finshaped crossing features are interpreted to have originated from pressure dissolution.

**Irghizites:** Both irghizites are aerodynamically shaped splash forms with either a lustrous or dull surface. In contrast to the zhamanshinites no bubble cavities can be observed on the irghizites in the macroscopic view but under the microscope big bubbles in the thin sections were found in Sample IRG-2015 with diameters up to 1.2 mm. IRG-2015/1 also shows an additional brown glass phase under transmitted light. In back scattered electron (BSE) images, schlieren are also observed on the two irghizites and in Irgh-2 the same finshaped crossing features as in Zh-62/3b were observed (see BSE images).

Table 3.1 summarizes the observed petrographical features in target rocks and impactites.

## 3.2 Major element compositions

The results of the major element determinations for five impactites (Zhamanshinites: samples Zh-6014, Zh-62/3b and Zh-30a; Irghizites: samples IRG-2015/1 and Irgh-2) are given in Table 3.4 and plotted in Fig. 3.2. The data were obtained by WDS-EPMA and represent averages of at least 16 single measurements scattered over each thin section. The multiple analyses also serve as an indicator for the internal homogeneity of the analyzed zhamanshinites and irghizites. All impactites, except the zhamanshinite sample Zh-62/3b, exhibit a good homogeneity as can be seen from tables C.1–C.5 in the appendix. Koeberl and Fredriksson (1986) also observe an overall better homogeneity in irghizites than in zhamanshinites.

Table 3.2 lists the elemental ranges for zhamanshinites and irghizites from the literature. Our values for irghizites and zhamanshinites fit well into the range reported in the literature, except for an unusually low value for Ni in irghizite sample Irgh-2 (~100 ppm). This value may represent an analytical artefact, as irghizites are known to exhibit on average by orders of magnitude higher Ni contents compared to zhamanshinites (25-126 ppm in zhamanshinites and 1075-1720 ppm in irghizites; see Koeberl and Fredriksson, 1986, and references therein).

**Table 3.1:** Petrographic description of target rocks and impactites.

Sample Name	Location	Petrographic Description
DB-6	crater rim	Shale (hypidiomorphic to granular quartz, plagioclase, biotite, porphyritic texture, frequent quartz veins, secondary mineralizations suspected to be muscovite)
DB-9	crater rim	Shale (like DB6, with additional chlorite and orthopyroxene)
Zh-2DBI	crater rim	Andesite (highly altered breccia, containing abundant quartz, chlorite, and plagioclase)
ZSK-8	borehole No. 100	Claystone (highly weathered, fine grained, minor quartz, brownish color resulting from organics, abundant glauconite)
Zh-55/5	crater rim	Ultrabasic rock (ophiolitic texture, highly serpentinized, abundant antigorite and chlorite, accessory phases suspected to be ilmenite)
Zh-30a	crater rim	Zhamanshinite (transparent glass containing few bubbles up to 200 $\mu\text{m}$ in diameter, some exhibiting dark rims)
Zh-62/3b	crater rim	Si-rich zhamanshinite (opaque glass containing frequent bubbles of 1-50 $\mu\text{m}$ )
Zh-6014	crater rim	Si-rich zhamanshinite (transparent glass containing inhomogeneously distributed bubbles, some up to 250 $\mu\text{m}$ , exhibiting dark rims and corroded interior)
IRG-2015/1	crater rim	Irghizite (transparent glass with few bubbles of not more than 10 $\mu\text{m}$ in diameter, glass patches are separated by fractures and schlieren of sometimes pale-reddish color)
Irgh-2	crater rim	Irghizite (very homogeneous glass with rare bubbles of not more than 5 $\mu\text{m}$ in diameter and black interior)

**Table 3.2:** Range of major element compositions of zhamanshinites and irghizites from the literature (Koeberl and Fredriksson, 1986; Izokh et al., 1993). Values are in wt%.

	Zhamanshinites		Irghizites	
	high silica	low silica	high silica	low silica
SiO <sub>2</sub>	62.9 - 88.1	49.94 - 60.57	70.0 - 79.4	52.4 - 56.7
TiO <sub>2</sub>	0.23 - 1.10	0.6 - 1.36	0.69 - 0.99	0.73 - 1.09
Al <sub>2</sub> O <sub>3</sub>	4.80 - 21.2	16.19 - 20.62	9.45 - 13.6	18.8 - 21.8
Fe <sub>2</sub> O <sub>3</sub>	1.98 - 8.05	0.5 - 8.98	4.24 - 6.81	0.86 - 8.75
MgO	0.34 - 1.16	2.04 - 4.9	2.16 - 3.76	1.82 - 3.12
CaO	0.55 - 2.16	4.75 - 10.65	1.75 - 2.85	5.56 - 9.87
Na <sub>2</sub> O	0.57 - 1.84	2.29 - 5.74	0.85 - 1.22	2.91 - 4.45
K <sub>2</sub> O	0.10 - 3.07	0.54 - 2.47	1.58 - 2.14	1.06 - 1.75

However, even though zhamanshinite samples Zh-6014 and Zh-30a can be classified as high-Si zhamanshinites, sample Zh-62/3b is an intermediate silica zhamanshinite. The irghizite sample IRG-2015/1 is a high silica variety and the sample Irgh-2 can be classified as basic splash-form or basic irghizite. According to the here presented major element chemistry, our samples represent typical zhamanshinites and Irghizites. The similarity between the here presented and the literature data for impact glasses (zhamanshinites) and tektite-like objects (irghizites) are (together with a selection of also analysed target rocks and literature data for target rocks) shown in the ternary plot in Fig. 3.1.

The Ni and Cr abundance measurements via JXA-8530F field emission electron microprobe of irghizite sample Irgh-2 suffers from an unsteady distribution of these elements throughout the thin-section (accumulation in aggregates) and might not represent the real concentration (this is also reflected by its low Ni concentration of ~100 ppm, which would represent the lowest Ni concentration measured in an irghizite so far, whereas the Ni concentration of sample IRG-2015/1 -with ~1580 ppm- fits perfectly in the literature trend; see section 4.2.1).

### 3.3 Rhenium and platinum group element concentrations

The concentrations of platinum group elements (PGEs) and Re, collectively termed highly siderophile elements (HSEs), of five target rocks (two shales DB-6 and DB-9, one claystone ZSK-8, one volcanic breccia Zh-2DBI, and one ultrabasic rock Zh-55/5) and five impact glasses (two tektite-like irghizites IRG-2015/1 and Irgh-2 and three zhamanshinites Zh-6014, Zh-30a and Zh-62/3b) are summarized in Table 3.3.

The more felsic target rocks (SiO<sub>2</sub> range from 45.11 to 58.96 wt%, encompassing all target rocks analyzed in this study except the ultrabasic sample Zh-55/5) vary for Os from ~7 to ~75 ppt, for Ir from ~7 to ~19 ppt, for Pt from ~68 to ~427 ppt, and for Re from ~14 to ~1209 ppt. These values mirror the trend defined by the upper continental crust, which exhibits ~31 ppt Os, ~22 ppt Ir, ~510 ppt Pt and ~198 ppt for Re (Peucker-Ehrenbrink

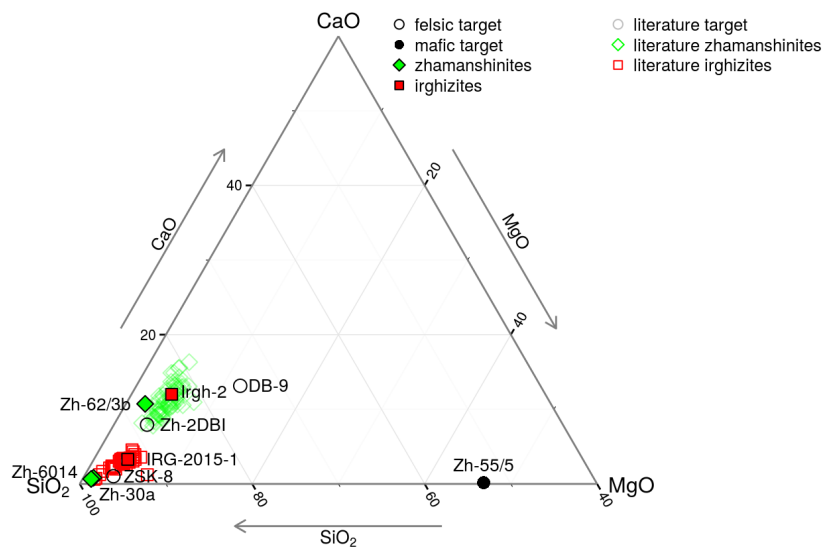


**Figure 3.1:** Ternary plot of the relative abundances of SiO<sub>2</sub>, CaO, and MgO, showing the trend defined by literature data for zhamanshinites and irghizites. Also shown are the impactite samples analyzed in this work, which in plot the fields defined by the literature data. Literature data from Izokh et al. (1993).

and Jahn, 2001). This similarity is expected due to the wide variety of lithologies present in the Zhamansin area and selected for this study. However, although representing a minor lithology in the Zhamanshin area, one ultrabasic target rock was also selected for analysis (sample Zh-55/5). This sample exhibits orders of magnitude higher PGE abundances (~2.4 ppb Os, ~1.6 ppb Ir and ~10 ppb Pt) and a similar Re concentration (~48 ppt) compared to the crust-like target samples presented above. No PGE data are available from the literature for comparison with the results presented here.

The two zhamanshinite samples Zh-62/3b and Zh-30a (the former belonging to the intermediate silica-, the latter to the high silica zhamanshinite subtypes) range in Os content from ~4 to ~15 ppt, for Ir from ~3 to ~5 ppt, for Pt from ~96 to ~386 ppt and from ~18 to ~80 ppt for Re (except for Re mirroring the range defined by the crust-like target rocks). Notably, the zhamanshinite Zh-60/4 (high silica type) has orders of magnitude higher Os (~0.97 ppb) and Ir (~0.16 ppb), a lower Pt concentration (~132 ppt) and a similar Re concentration (~15 ppt). Again, no PGE data for zhamanshinites are available from the literature for comparison.

The irghizite samples analyzed in this study also call for a separate discussion of their PGE and Re concentrations. While irghizite Irgh-2 (low silica type) exhibits overall low PGE concentrations of ~20 ppt for Os, ~1.4 ppt for Ir and ~190 ppt for Pt as well as ~127 ppt for Re (except for Re mirroring the range defined by the crust-like target rocks), irghizite sample

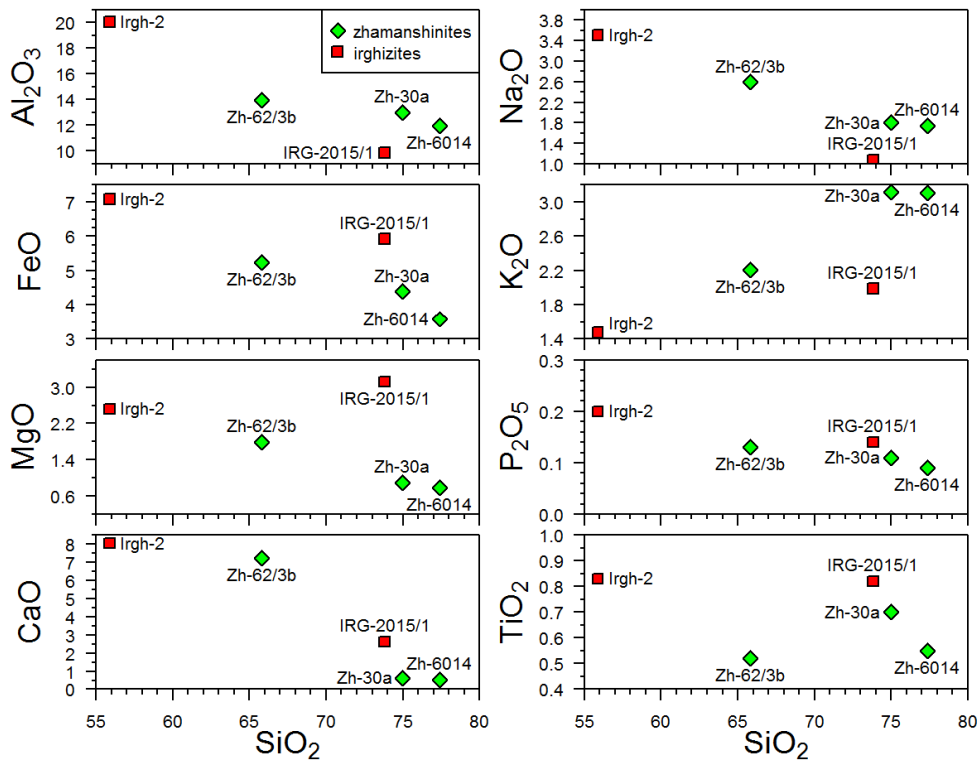


**Figure 3.2:** Harker diagrams for major elements in impactite samples analyzed in this work. Values are in wt-%.

IRG-2015/1 (high silica type) shows elevated PGE concentrations of  $\sim 0.59$  ppb Os,  $\sim 0.58$  ppb Ir,  $\sim 8.8$  ppb for Pt and a similar Re concentration ( $\sim 319$  ppt). The only available literature PGE dataset for irghizites reports abundances ranging between  $\sim 1$  to  $\sim 140$  ppt for Os,  $\sim 10$  to  $\sim 1680$  ppt for Ir, and between  $\sim 120$  to  $\sim 6870$  ppt for Pt (Ackerman et al., 2015 and Jonášová et al., 2015; see also Table 3.6). The most enriched of these samples were interpreted by these authors as potentially resulting from meteoritic admixture (see section 4.2.2 for further discussion). However, whereas the lower range of the literature values presented above is comparable to the concentrations in the low-silica Irghizite Irgh-2, the here analyzed high-silica irghizite IRG-2015/1 is comparable or even higher compared to the highest reported literature data. The highest PGE abundances reported here and in the literature for zhamanshinites and irghizites, although orders of magnitude higher compared to the dominant (crust-like) lithologies in the Zhamanshin area, are still lower than the values reported for the ultrabasic target rock sample Zh-55/5 (representing one of the rare basic dykes occurring in the area). Attributing elevated PGE contents in impactites from the Zhamanshin impact structure to extraterrestrial admixtures (as mentioned by Jonášová et al., 2015 and Ackerman et al., 2015) is, thus, premature without careful examination of potential ultrabasic contaminations in the suspected impactites (see chapter 4.2.1 for a detailed discussion).

Notably, Re concentrations are significantly lower in all of the here analyzed impactites (zhamanshinites and irghizites) compared to the felsic target rocks. Even though zhamanshinites have the lowest contents, ranging between  $\sim 15$  and  $\sim 80$  ppt Re, irghizites range from  $\sim 127$  to 319 ppt Re. These values are much lower compared to most target rocks, which exhibit values up to  $\sim 1200$  ppt Re (see Table 3.5). This bimodality in Re concentrations between the impactites and the target rocks is even more significant when taking the Re/Os ratios into account (see Table 3.5), which range from  $\sim 0.02$  to  $\sim 5.3$  for zhamanshinites, from  $\sim 0.6$  to  $\sim 6.4$  for irghizites (the lowest ratios represented by the most PGE enriched zhamanshinites and irghizites) and from  $\sim 2$  to  $\sim 151$  for the upper crust-like target rocks (the ultrabasic sample Zh-55/5 exhibits a value of  $\sim 0.02$ ). The "Re and Os concentration dichotomy" is also shown, along with other interelement correlations, in Fig 3.3 (see also Table 3.5 for a summary of the PGE interelement ratios). Those impact glasses, exhibiting the highest PGE concentrations (IRG-2015/1 and Zh-60/4) also show the lowest Re/Os ratios (0.55 and 0.016, respectively). The ultrabasic sample Zh-55/5 plots within the trend for impact glasses. There are no such correlations in the Ir vs. Os, Pt vs. Ir and Pt vs. Os plots (see Fig. 3.3).

### 3.4 Osmium isotope systematics

Present-day (measured) and initial (back-calculated) isotope ratios for five target rocks and four impact glasses (two irghizites and two zhamanshinites) are listed in Table 3.7. The ratio for sample Zh-6014 could not be measured due to high mass interferences with Re

**Table 3.3:** Rhenium and platinum-group element concentrations for target rocks and impact glasses (irghizites and zhamanshinites), measured via isotope dilution. Errors for element concentrations are  $< 5\%$  ( $2\sigma$  RSD).

Target Rocks				
Sample Name	Re [ppt]	Os [ppt]	Ir [ppt]	Pt [ppt]
DB-6	1208.5	8	11	68
DB-9	13.6	7	11.2	113.8
ZSK-8	1193	75	19.4	427
Zh-2DBI	453.9	8.3	7.1	286.32
Zh-55/5	47.6	2406	1583.6	9883
Impactites				
Sample Name	Re [ppt]	Os [ppt]	Ir [ppt]	Pt [ppt]
Zh-6014	15.3	966	160	132
Zh-62/3b	79.4	15	3.4	385.5
Zh-30a	17.8	4	4.5	96.4
IRG-2015/1	318.9	585	582.5	8814.8
Irgh-2	127.3	20	1.35	191

**Table 3.4:** Major Element composition obtained by WDS-EPMA analysis. Averages from tables C.1–C.5 in the appendix. Concentrations in wt-%. Detection limits and  $2\sigma$ -errors see Table 2.1

Sample Name	SiO <sub>2</sub>	Al <sub>2</sub> O <sub>3</sub>	Cr <sub>2</sub> O <sub>3</sub>	TiO <sub>2</sub>	K <sub>2</sub> O	CaO	FeO	MnO	Na <sub>2</sub> O	MgO	P <sub>2</sub> O <sub>5</sub>	NiO	Total	# A.
Zh-6014	77.38	11.94	0.01	0.55	3.11	0.52	3.58	0.09	1.74	0.78	0.09	0.01	99.8	19
Zh-62/3b	65.81	13.99	0.01	0.52	2.21	7.23	5.24	0.12	2.59	1.79	0.13	0.01	99.64	17
Zh-30a	74.99	13.02	0.03	0.7	3.12	0.63	4.38	0.1	1.8	0.9	0.11	0.01	99.79	16
IRG-2015/1	73.82	9.86	0.06	0.82	1.99	2.62	5.93	0.1	1.08	3.12	0.14	0.2	99.75	18
Irgh-2	55.87	20.05	0.02	0.83	1.48	8.05	7.08	0.14	3.51	2.52	0.2	0.01	99.75	21

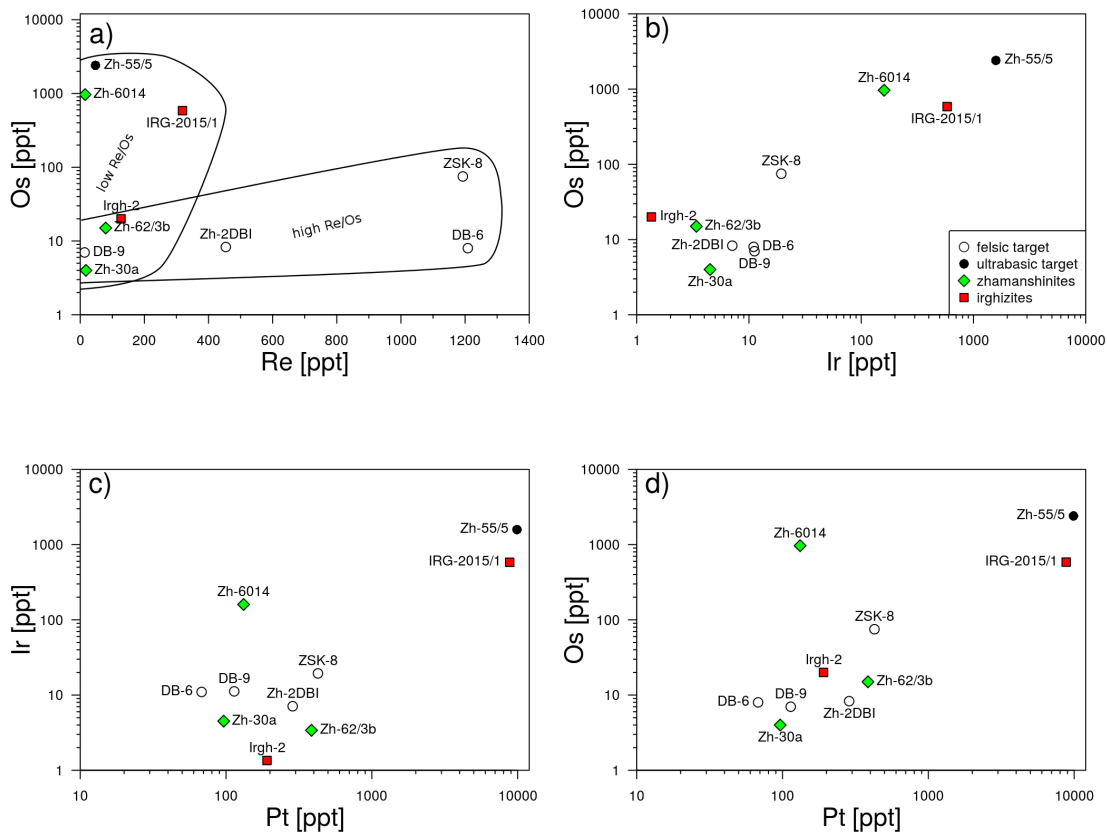
**Table 3.5:** Concentration of HSEs (in ppt) and CI chondrite-normalized values for selected element ratios in target rocks and impactites. Errors for element concentrations are  $< 5\%$ . of HSEs in CI chondrites used are from Horan et al. (2003).

Sample Name	Re/Os	Pt/Ir	Os/Ir	Re/Ir	Target Rocks						
					Re/Pt	(Re/Os) <sub>n</sub>	(Pt/Ir) <sub>n</sub>	(Os/Ir) <sub>n</sub>	(Re/Ir) <sub>n</sub>	(Re/Pt) <sub>n</sub>	
DB-6	151	6.18	0.72	109	17.8	1948	3.17	0.7	1233.7	389.6	
DB-9	1.94	10.16	0.63	1.21	0.12	25	5.2	0.61	13.6	2.62	
ZSK-8	15.9	22	3.86	61.5	2.79	205	11.27	3.75	690.5	61.3	
Zh-2DBI	54.7	40.3	1.17	63.9	1.59	705	20.66	1.13	717.9	34.8	
Zh-55/5	0.019	6.24	1.52	0.03	0.005	0.26	3.2	1.47	0.34	0.11	

Sample Name	Re/Os	Pt/Ir	Os/Ir	Re/Ir	Impactites						
					Re/Pt	(Re/Os) <sub>n</sub>	(Pt/Ir) <sub>n</sub>	(Os/Ir) <sub>n</sub>	(Re/Ir) <sub>n</sub>	(Re/Pt) <sub>n</sub>	
Zh-6014	0.016	0.83	6	0.09	0.12	0.2	0.42	5.85	1.07	2.54	
Zh-62/3b	5.29	113	4.41	23.4	0.2	68.3	58.07	4.28	262.2	4.52	
Zh-30a	4.45	21.4	0.89	3.95	0.18	57.4	10.97	0.86	44.42	4.05	
IRG-2015/1	0.55	15.1	1	0.55	0.04	7	7.75	0.97	6.15	0.79	
Irgh-2	6.37	141	14.8	94.3	0.67	82	72.47	14.36	1058.9	14.6	





**Figure 3.3:** Selected interelement plots of platinum-group element (PGE) and rhenium abundances. Errors are smaller than symbol sizes.

observed during measurement. Similar mass interferences have not been monitored in any of the other measurements. Comparable to the PGE concentrations, measured  $^{187}\text{Os}/^{188}\text{Os}$  isotope ratios of the more felsic target rocks (samples DB-6, DB-9, ZSK-8 and Zh-2DBI, ranging from  $\sim 0.7$  to  $\sim 5.2$ ) are radiogenic and scatter around the average value for the upper continental crust ( $\sim 1.05$ ; Peucker-Ehrenbrink and Jahn, 2001), again justifying the collective term "crust-like target rocks" for these samples. Only the ultrabasic target sample Zh-55/5 exhibits a mantle-like and near chondritic value of  $\sim 0.19$ .

Impact glasses show on average lower ratios ( $1.99 \pm 1.50$ ), with irghizites ranging from  $\sim 0.31$  to  $\sim 0.96$  and zhamanshinites from  $\sim 0.39$  to  $\sim 2.8$ . Irghizite sample IRG-2015/1, which has the highest PGE contents of all analyzed impactites also exhibits the most unradiogenic  $^{187}\text{Os}/^{188}\text{Os}$  isotope ratio ( $\sim 0.313$ ).  $^{187}\text{Re}/^{188}\text{Os}$  ratios vary in crust-like target rocks from  $\sim 14$  to  $\sim 1207$ , averaging at 2.7 and for impactites from  $\sim 2.7$  to  $\sim 34$ , averaging at 1.1 (sample IRG-2015/1 has the lowest ratio), again reflecting the overall lower Re/Os

**Table 3.6:** Platinum-group element abundances for irghizites reported in Ackerman et al. (2015) and Jonášová et al. (2015). All values were estimated from HSE pattern plots. Samples IR-7 and IR-13 were interpreted to exhibit a meteoritic admixture.

	Irghizites						
	Re [ppt]	Os [ppt]	Ir [ppt]	Pt [ppt]	Co [ppm]	Ni [ppm]	Cr [ppm]
Low Os	~3-120	~1-16	~10-1680	~120-6870	~4-25	~2-450	~4-85
IR-7	~10	~130	~1680	~4900	~4	~45	~20
IR-13	~25	~150	~330	~1100	~5	~10	~6

**Table 3.7:** Isotopic composition in target rocks and impactites (zhmanshinites and irghizites; this study). Initial ( $^{187}\text{Os}/^{188}\text{Os}$ ) ratios were calculated with a decay constant from Smoliar et al. (1996) and the age of the cratering event from Deino et al. (1990).

Target Rocks					
Sample Name	$^{187}\text{Os}/^{188}\text{Os}$		$^{187}\text{Re}/^{188}\text{Os}$		$(^{187}\text{Os}/^{188}\text{Os})_{(T_0)}$
DB-6	5.241	(37)	1207.343	5.223	(37)
DB-9	4.015	(8)	14.023	4.015	(8)
ZSK-8	0.6633	(24)	81.1205	0.662	(24)
Zh-2DBI	0.826	(9)	284.512	0.822	(9)
Zh-55/5	0.1936	(34)	0.095	0.193	(34)
Impactites					
Sample Name	$^{187}\text{Os}/^{188}\text{Os}$		$^{187}\text{Re}/^{188}\text{Os}$		$(^{187}\text{Os}/^{188}\text{Os})_{(T_0)}$
Zh-6014	-		-	-	
Zh-62/3b	2.794	(45)	34.122	2.794	(45)
Zh-30a	0.393	(19)	21.934	0.393	(19)
IRG-2015/1	0.31293	(78)	2.6594	0.313	(78)
Irgh-2	0.956	(12)	33.637	0.956	(12)

ratios in impactites compared to crust-like target rocks (for a comparison of  $^{187}\text{Re}/^{188}\text{Os}$  ratios and  $^{187}\text{Os}/^{188}\text{Os}$  ratios between the different lithologies see also Figure 3.4). The ultrabasic sample Zh-55/5, however, exhibits the lowest ratio of  $\sim 0.1$ . Initial (back-calculated)  $^{187}\text{Os}/^{188}\text{Os}$  isotope ratios were calculated relative to the age of the Zhamanshin impact event at  $\sim 0.87$  Ma and are shown in Table 3.7. The resulting initial values are nearly indistinguishable from the respective present day values. Variations in present-day (as well as back-calculated)  $^{187}\text{Os}/^{188}\text{Os}$  ratios roughly correlate with  $^{187}\text{Re}/^{188}\text{Os}$  ratios, without showing an isochronous relationship. This is, however, not surprising due to the variety of target lithologies (with varying ages) analyzed. Interestingly, those impactites which belong to the low-silica type (irghizite sample Irgh-2) or intermediate silica type (zhmanshinite sample Zh-62/3b) exhibit the most radiogenic (highest)  $^{187}\text{Os}/^{188}\text{Os}$  ratios of all analyzed impactites ( $\sim 0.96$  and  $\sim 2.80$ , respectively).

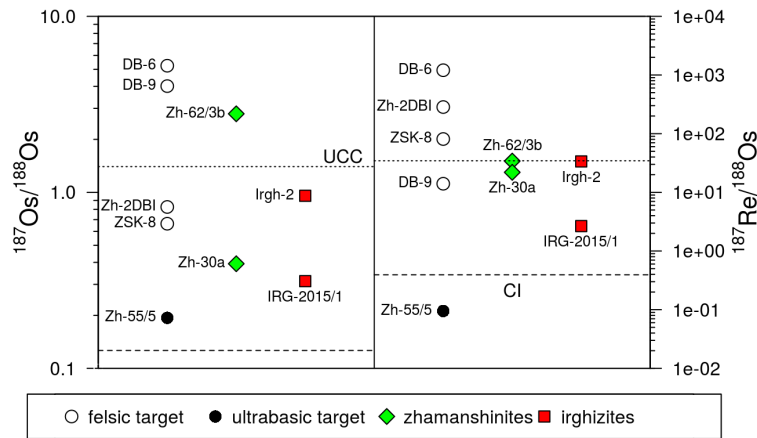


**Figure 3.4:** Isotope ratios measured in target rocks (subdivided into felsic or crust-like target rocks and basic target rocks, as represented by sample Zh-55/5) and impactites (subdivided into zhamanshinites and irghizites) of the Zhamanshin impact structure. The dotted line represents the average of the upper continental crust (UCC; ratios from Peucker-Ehrenbrink and Jahn, 2001). The dashed line represents the CI chondritic ratios from Shirey and Walker (1998). Errors are smaller than symbol sizes.

### 3.5 Strontium-neodymium isotope systematics

One felsic and one ultrabasic target rock and five impactites were measured for their Sr and Nd isotopic compositions. Results from this measurements together with selected literature data (Abate et al., 1998; Ostermann et al., 1996; Shaw and Wasserburg, 1982) for Sr-Nd isotope ratios and Sr and Nd concentrations, are given in Table 3.8 and plotted in Fig. 3.5.

Isotope ratios for target rocks measured in this study (including the ultrabasic sample Zh-55/5) mirror the huge spread as defined by available literature data for target rocks from the Zhamanshin area.

Two of the three investigated zhamanshinite samples (Zh-6014 and Zh-30a) plot exactly in the trend defined by the literature zhamanshinite data with  $^{87}\text{Sr}/^{86}\text{Sr}$  ratios of 0.715767 and 0.71585 and corresponding  $^{143}\text{Nd}/^{144}\text{Nd}$  ratios of 0.512407 and 0.512432, respectively. The third investigated zhamanshinite (Zh-62/3b) exhibits a  $^{87}\text{Sr}/^{86}\text{Sr}$  ratio of 0.704946 and a  $^{143}\text{Nd}/^{144}\text{Nd}$  ratio of 0.512703 and plots off the trend defined by the other zhamanshinites. Interestingly, zhamanshinite sample Zh-62/3b belongs to the intermediate silica type zhamanshinites, whereas all other zhamanshinites shown in Fig. 3.5 belong to the high-silica type (see Table 3.4 for a summary of the  $\text{SiO}_2$  contents of all impactites).

Irghizites analyzed in this study perfectly fit into the apparent Sr and Nd isotope dichotomy between high- and low- silica types. Whereas irghizite sample Irgh-2 ( $\text{SiO}_2$  content

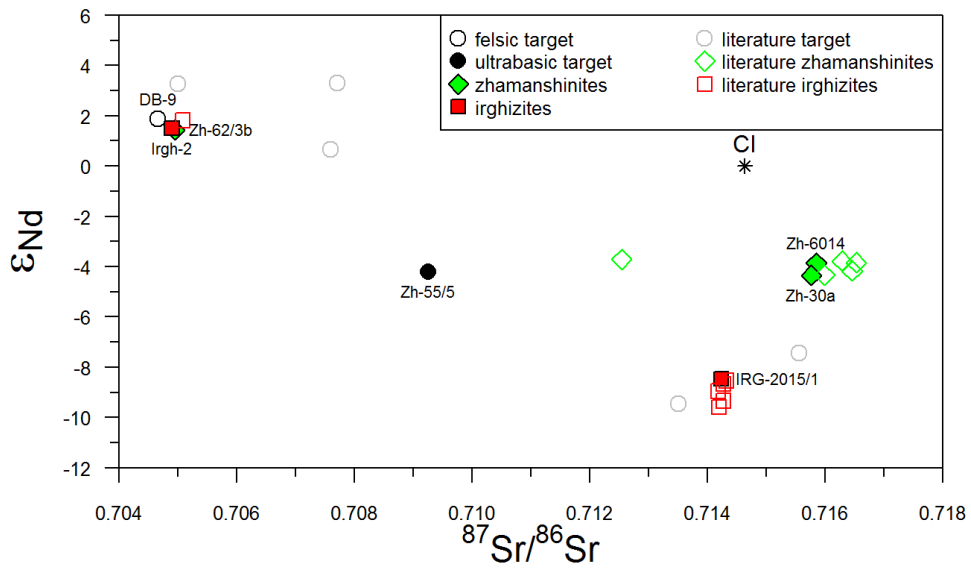


**Figure 3.5:**  $\epsilon_{\text{Nd}}$  vs  $^{87}\text{Sr}/^{86}\text{Sr}$  plot for comparison with literature data. Literature data from Abate et al. (1998), Ostermann et al. (1996), and Shaw and Wasserburg (1982) (see Tab. 3.8). Errors are smaller than symbol sizes.

of 55.87 wt.%; see Table 3.4) plot within the low silica subtype trend (defined by only one available Sr-Nd isotope literature value for a low silica irghizite), irghizite sample IRG-2015/1 (with a  $^{87}\text{Sr}/^{86}\text{Sr}$  ratio of 0.714241, a  $^{143}\text{Nd}/^{144}\text{Nd}$  ratio of 0.512196 and a  $\text{SiO}_2$  content of 73.82 wt.%; see Table 3.8) perfectly matches the trend for high silica irghizites as defined by five literature values from Shaw and Wasserburg (1982) and Ostermann et al. (1996) (Fig. 3.5).

**Table 3.8:** Strontium-Nd isotope compositions and concentrations in target rocks and impactites (zhamanshinites and irghizites) from the Zhamanshin impact structure. Concentrations for SiO<sub>2</sub> are mentioned for comparison in wt.%, Sr and Nd in ppm. References: bold: this study; a: Abate et al. (1998); b: Shaw and Wasserburg (1982); c: Ostermann et al. (1996).

Target Rocks									
Sample	Nd	<sup>143</sup> Nd/ <sup>144</sup> Nd	$\epsilon_{\text{Nd}}$	Sr	<sup>87</sup> Sr/ <sup>86</sup> Sr	SiO <sub>2</sub>	Ref.		
DB-9		<b>0.512 726</b>	<b>(4)</b>	<b>1.87</b>	410.9	<b>0.704 656</b>	<b>(13)</b>	45.11	a
Zh-55/5	0.49	<b>0.512 415</b>	<b>(40)</b>	<b>-4.19</b>	9.83	<b>0.709 253</b>	<b>(7)</b>	40.29	a
ZSK-1	24.73	0.512 248	(15)	-7.45	99.46	0.715 56	(2)	56.07	a
ZSK-8	31.36	0.512 145	(44)	-9.46	173.5	0.713 51	(2)	58.96	a
DB-6	17.83	0.512 799	(35)	3.30	139.6	0.707 707	(22)		b
DB-7					28.7	0.716 389	(16)	88.4	b
Zh-2DBI	15.292	0.512 797	(45)	3.26	673.9	0.705 003	(25)	55.9	a
Zh-5DBI	5.205	0.512 664	(109)	0.66	36.71	0.707 59	(6)	55.3	a
Zh-5DB3	0.5806	0.512 18	(40)	-8.78	712.6				a
Irghizites									
Sample	Nd	<sup>143</sup> Nd/ <sup>144</sup> Nd	$\epsilon_{\text{Nd}}$	Sr	<sup>87</sup> Sr/ <sup>86</sup> Sr	SiO <sub>2</sub>	Ref.		
IRG-2015/1		<b>0.512 196</b>	<b>(4)</b>	<b>-8.62</b>		<b>0.714 241</b>	<b>(5)</b>	<b>73.82</b>	
Irgh-2		<b>0.512 708</b>	<b>(4)</b>	<b>1.36</b>		<b>0.704 899</b>	<b>(4)</b>	<b>55.87</b>	
GpIV #12	14	0.512 731	(33)	1.81	777.5	0.705 08	(11)	54.27	b
GpIII 3-1	17.5	0.512 200	(29)	-8.54	142.2	0.714 32	(6)	75.11	b
GpIII 3-6	18.2	0.512 159	(26)	-9.34	143.7	0.714 27	(5)	74.46	b
Irgh-gb	17.61	0.512 186	(9)	-8.82	141.2	0.714 273	(25)		c
Irgh-I	17.48	0.512 171	(9)	-9.10	141.3	0.714 189	(21)	74.5	c
Irgh-II	18.27	0.512 138	(14)	-9.75	144.7	0.714 193	(21)	75.5	c
Zhamanshinites									
Sample	Nd	<sup>143</sup> Nd/ <sup>144</sup> Nd	$\epsilon_{\text{Nd}}$	Sr	<sup>87</sup> Sr/ <sup>86</sup> Sr	SiO <sub>2</sub>	Ref.		
Zh-6014		<b>0.512 432</b>	<b>(3)</b>	<b>-4.02</b>	112.6	<b>0.715 850</b>	<b>(4)</b>	<b>77.38</b>	a
Zh-62/3b	13.66	<b>0.512 703</b>	<b>(8)</b>	<b>1.27</b>		<b>0.704 946</b>	<b>(4)</b>	<b>65.81</b>	a
Zh-30a		<b>0.512 407</b>	<b>(4)</b>	<b>-4.50</b>		<b>0.715 767</b>	<b>(4)</b>	<b>74.99</b>	
Zh-1	23.77	0.512 416	(11)	-4.33	99.8	0.716 457	(27)	80.0	c
Zh-15	25.71	0.512 408	(11)	-4.49	105.6	0.715 994	(25)	78.1	c
Zh-49	19.87	0.512 433	(10)	-4.00	100.4	0.716 527	(21)		c
Zh-54	25.25	0.512 436	(10)	-3.94	104.7	0.716 288	(25)	79.15	c
Zh-158	46.09	0.512 440	(18)	-3.86	75.66	0.712 543	(27)		c



# Discussion

Any attempt to identify an extraterrestrial component based on Re-Os isotopes and Re and PGE concentrations in impactites from the Zhamanshin crater (zhamanshinite samples Zh-6014, Zh-62/3b, and Zh-30a and irghizite samples IRG-2015/1 and Irgh-2) are hampered by the fact that the impactor's PGE composition and its Re-Os isotope signature is more similar to an ultrabasic than a granitic target (see also introductory chapter). As mentioned in previous sections (see 1.4.1), the lithologies of the Zhamanshin crater and its vicinity are dominated by crust-like lithologies with SiO<sub>2</sub> contents ranging from 45.1 to 59.0 wt.% (see 1.6). The investigated ultrabasic target rock represents only a minor component of the target lithologies, but its possible contribution to the PGE concentration and Re-Os isotope budget of the impactites has to be explicitly ruled out before making any conclusions regarding a meteoritic admixture. This discussion has to focus on the zhamanshinite sample Zh-30a and the irghizite sample IRG-2015/1, which, according to their (in comparison to all other analyzed impactites) elevated PGE concentrations and unradiogenic <sup>187</sup>Os/<sup>188</sup>Os ratios (see Tables 3.3 and 3.7), represent the only candidates for a suspected extraterrestrial admixture. In order to exclude any ultrabasic contributions in these impactites, we introduce a variety of tools, including (i) evidence from major element compositions, (ii) Os isotopic signatures, (iii) normalized PGE abundance patterns and, (iv) Sr-Nd isotopic signatures. However, it might be helpful to first discuss the possibility of an impact-related process that affected the impactites in general, regardless of the presence of a suspected meteoritic admixture.

## 4.1 The Re-Os concentration bimodality

In Figure 3.3a the Os concentration is plotted against the Re concentration of all measured samples. As already mentioned in section 3.3 a general bimodal trend can be observed between impactites (zhamanshinites and irghizites) and crust-like target rocks. While Re/Os ratios range from ~1.94 to ~151 for the crust-like lithologies (dominating in the Zhamanshin area), those in impactites range from ~0.02 to ~6.37. This dichotomy between these

lithologies can neither be easily explained in terms of a coincidental concentration distribution, nor can this trend be plausibly explained by a contamination with or derivation of all the analyzed impactites from the sparse ultrabasic components that are observed in the Zhamanshin area (which also exhibit impactite-like or even lower Re/Os ratios; Fig. 3.3a). A general derivation from or contamination with ultrabasic components of all the impactites, is possible but, as revealed by numerous irghizite and zhamanshinite analyses reported in the literature, as well as by our own data (see Table 3.4), contents up to ~78 wt.% in irghizites and 88 wt.% in zhamanshinites (e.g., Izokh et al., 1993) makes any significant contribution of a basic or basic precursor material for these impactites improbable. Although unlikely, it is the task of the following chapters to establish more elaborated tools (based on major elements as well as Sr and Nd isotopic compositions) in order to rule out such a ultrabasic impactite-precursor or basic impactite-contaminant on a quantitative basis.

Other possibilities that might explain the apparent Re-Os concentration bimodality include hydrothermal activity or cryptic metasomatism, accompanied by selective Re loss or gain (e.g., Day et al., 2008).

However, impactites analyzed in this study belong to two different types of impact glasses (zhamanshinites and irghizites), which are widely distributed around the crater rim and within the Zhamanshin area with probably varying precursor materials, making a common hydrothermal or cryptometasomatic disturbance very unlikely. In addition, no evidences for hydrothermal overprint of rocks in the Zhamanshin area is reported in the literature.

It is, instead, much more reasonable to assume selective Re-loss in all impactites during the impact event. This process could easily explain the on average lower Re contents in impactites and their lower Re/Os ratios. Such degassing of volatile Re-oxides was already described as a mechanism that tends to deplete Re in specific types of lavas (e.g., Lassiter, 2003) and was also mentioned as a possible process in impact related mechanism (e.g., Koeberl and Shirey, 1993).

The low Re/Os ratios for the two impactites that contain a suspected meteoritic admixture (zhamanshinite sample Zh-30a with a Re/Os ratio of 4.45 and irghizite sample IRG-2015/1 with a Re/Os ratio 0.55) could be explained to result from an extraterrestrial component as very low amounts of a chondritic contaminant significantly enhance the Os concentrations in the impactites, thereby lowering their Re/Os ratios (such an admixture is most likely for sample IRG-2015/1 as this sample exhibits the highest Re concentration of all impactites, which evidences that for this sample the, so far postulated, Os addition due to meteoritic admixture dictates the Re/Os budget instead of Re-loss alone).

Rhenium-Os concentrations and their bimodal distributions between the crust-like target materials and the impactites, thus, serve as a geochemical fingerprint of the impact event in the Zhamanshin structure.



## 4.2 Identification of a meteoritic component in zhamanshinites and irghizites

### 4.2.1 Evidences from major elements compositions

The comparison between literature data for zhamanshinites and irghizites in table 3.2 already revealed that the here analyzed impactite specimen are typical members of their classes without any noticeable deviations from the typical major element compositional range defined by previous analyses (except for Ni, see discussion below).

As mentioned in the introductory chapter, Cr, Co, and Ni contents and their interelement ratios provide the only viable major-element based tool for a possible identification of meteoritic components in impactites. A brief discussion about their abundances in the here analyzed samples is, thus, required.

#### Chromium, Co, and Ni abundances

It is long known that irghizites have elevated Ni concentrations in comparison to zhamanshinites and other tektites (e.g., Koeberl and Fredriksson, 1986). Nickel concentrations in zhamanshinites typically vary between  $\sim 10$  to  $\sim 100$  ppm, whereas irghizites exhibit concentrations typically varying between  $\sim 1000$  to  $\sim 1800$  ppm (see Koeberl and Fredriksson, 1986, and references therein). No correlation exist between the Ni content within zhamanshinites or irghizites and their respective high silica and low silica subtypes. However, differences in Co and Cr concentrations between zhamanshinites and irghizites are, although existent, more inconspicuous. The Cr and Co contents in zhamanshinites typically vary from  $\sim 60$  to  $\sim 90$  ppm and  $\sim 10$  to  $\sim 20$  ppm, respectively, whereas irghizites show slightly higher values ranging from  $\sim 170$  to  $\sim 260$  ppm for Cr and from  $\sim 70$  to  $\sim 100$  ppm for Co. Recently published data from Ackerman et al. (2015) and Jonášová et al. (2015) extent the ranges mentioned above for irghizites to 2100 ppm Ni, 115 ppm Co, and up to 410 ppm Cr in their samples (see also Table 3.6). The interpretation of the high abundances of these elements in irghizites as resulting from a meteoritic contamination (if at all, only chondrites could account for these enrichments, as Cr and Co delivery from irons or achondrites can be regarded as negligible) is difficult to substantiate on the ground of these elements alone as the possibility of incorporation of basic material in Irghizites must be considered (which could easily alter the Ni, Cr, and Co budget).

The impactites analyzed in the present study contain about 80 ppm Ni and between  $\sim 70$  to  $\sim 200$  ppm Cr for Zhamanshinites, whereas Irghizite sample IRG-2015/1 exhibit  $\sim 1570$  ppm Ni and  $\sim 410$  ppm Cr. These values are spot on with the general trends mentioned above.

The crust-like target rocks analyzed in this study (DB-6, DB-9, ZSK-8, Zh-2DBI) contain from  $\sim 18$  to  $\sim 103$  ppm for Ni and from  $\sim 40$  to  $\sim 259$  for Cr, values that are comparable to the zhamanshinites and orders of magnitude below the elevated concentrations in irghizites. Contrary, the ultrabasic sample Zh-55/5 has a value of  $\sim 2320$  ppm Ni and  $\sim 3340$  ppm Cr (values from Abate et al., 1998). Any ultrabasic component in the impactites analyzed in this study could, therefore, easily simulate a meteoritic component or obscure an existing

one (or, in more general words, would alter the preexisting Ni and Cr budget). However, a significant ultrabasic component in any of the impactites is unlikely, as all of them are in line with the more or less uniform Ni and Cr literature trends for zhamanshinites and irghizites. The presence of an ultrabasic component in our impactites would, therefore, require that all zhamanshinites and irghizites ever analyzed are also affected by such an admixture.

Tables 4.1 and 4.2 show calculations based on the binary mixing equation (see Langmuir et al., 1978). As mixing calculations between the analyzed crust-like target rocks (with an SiO<sub>2</sub> content of at maximum 58.96 wt.% which is lower than the SiO<sub>2</sub> content in IRG-2015/1 with 74.01 wt.% and Zh-6014 with 77.54 wt.%) and the ultrabasic target rock are not meaningful to exclude an ultrabasic component, an inconspicuous zhamanshinite and irghizite was chosen in place of a yet unsampled high silica target.

An amount of 0.1%, 1%, 10%, and 20% of an ultrabasic component (Zh-55/5) was added to the zhamanshinite Zh-30a and irghizite IRG 6200 (data from literature, see Abate et al., 1998). These calculations show that an admixture of an ultrabasic component of around 20% would generate major element compositions that are far off the trend defined by samples Zh-6014 and IRG2015/1 (the only impactites with excess PGE concentrations and, thus, the only candidates for a suspected meteoritic component; see section 3.3 and discussion below) based solely on major element, as well as Cr and Ni concentrations.

**Table 4.1:** Binary mixing calculations of a zhamanshinite (Zh-30a), inconspicuous of a meteoritic component, with proportions of 0.1%, 1%, 10%, and 20% of an ultrabasic component (Zh-55/5). Values are in wt.% and normalized so that sum equals to 100%.

	SiO <sub>2</sub>	Al <sub>2</sub> O <sub>3</sub>	Cr <sub>2</sub> O <sub>3</sub>	TiO <sub>2</sub>	K <sub>2</sub> O	CaO	FeO	MnO	Na <sub>2</sub> O	MgO	P <sub>2</sub> O <sub>5</sub>	NiO
Zh-30a	75.15	13.05	0.03	0.70	3.13	0.63	4.39	0.10	1.80	0.90	0.11	0.01
Zh-55/5	46.28	0.03	0.95	10.77	0.07	40.78	0.15	0.01	0.02	0.02	0.56	0.34
0.1%	75.12	13.04	0.03	0.71	3.13	0.67	4.39	0.10	1.80	0.90	0.11	0.01
1%	74.86	12.92	0.04	0.80	3.10	1.03	4.35	0.10	1.78	0.89	0.11	0.01
10%	72.26	11.75	0.12	1.71	2.82	4.64	3.97	0.09	1.62	0.81	0.16	0.04
20%	69.38	10.45	0.21	2.71	2.52	8.66	3.54	0.08	1.44	0.72	0.20	0.08
30%	66.49	9.15	0.31	3.72	2.21	12.67	3.12	0.07	1.27	0.64	0.25	0.11
Zh-6014	77.54	11.96	0.01	0.55	3.12	0.52	3.59	0.09	1.74	0.78	0.09	0.01

For Cr and Ni it can be stated that zhamanshinites as well as target rocks (regardless if ultrabasic or crust-like) are found to have a Ni/Cr ratio of ~0.45. Irghizites can be separated in two groups (shaded areas in Fig. 4.1), whereby low silica irghizites exhibit an average Ni/Cr ratio of ~1.6 and high silica irghizites an average of ~5.4. This observation is displayed in Figure 4.1. A possible explanation for this might be (i) the presence of different, maybe yet unsampled, target rocks, (ii) a possible meteoritic contamination, or (iii) syn- or post-impact alteration processes.

**Table 4.2:** Binary mixing calculations of an irghizite (IRG 6200), inconspicuous of a meteoritic component, with proportions of 0.1%, 1%, 10%, and 20% of an ultrabasic component (Zh-55/5). Data for IRG 6200 from Abate et al. (1998). Values are in wt.% and normalized so that sum equals to 100%.

	SiO <sub>2</sub>	Al <sub>2</sub> O <sub>3</sub>	Cr <sub>2</sub> O <sub>3</sub>	TiO <sub>2</sub>	K <sub>2</sub> O	CaO	FeO	MnO	Na <sub>2</sub> O	MgO	P <sub>2</sub> O <sub>5</sub>	NiO
IRG 6200	74.00	9.47	0.03	0.76	1.77	2.50	6.58	0.08	1.08	3.45	0.11	0.17
Zh-55/5	46.28	0.03	0.95	10.77	0.07	40.78	0.15	0.01	0.02	0.02	0.56	0.34
0.1%	73.97	9.46	0.03	0.77	1.77	2.54	6.57	0.08	1.08	3.45	0.11	0.17
1%	73.72	9.38	0.04	0.86	1.75	2.88	6.52	0.08	1.07	3.42	0.11	0.17
10%	71.23	8.53	0.12	1.76	1.60	6.33	5.94	0.07	0.97	3.11	0.16	0.19
20%	68.46	7.58	0.21	2.76	1.43	10.16	5.29	0.07	0.87	2.76	0.20	0.20
30%	65.68	6.64	0.31	3.76	1.26	13.98	4.65	0.06	0.76	2.42	0.25	0.22
IRG-2015/1	74.01	9.89	0.06	0.82	2.00	2.63	5.95	0.10	1.08	3.13	0.14	0.20

#### 4.2.2 Evidence from highly siderophile elements

In figure 4.2 CI chondrite normalized HSE patterns of the investigated target rocks are plotted. All crust-like target rock samples (DB-6, DB-9, ZSK-8, and Zh-2DBI) are found to have similar fractionated HSE patterns like the upper continental crust (composition of UCC from

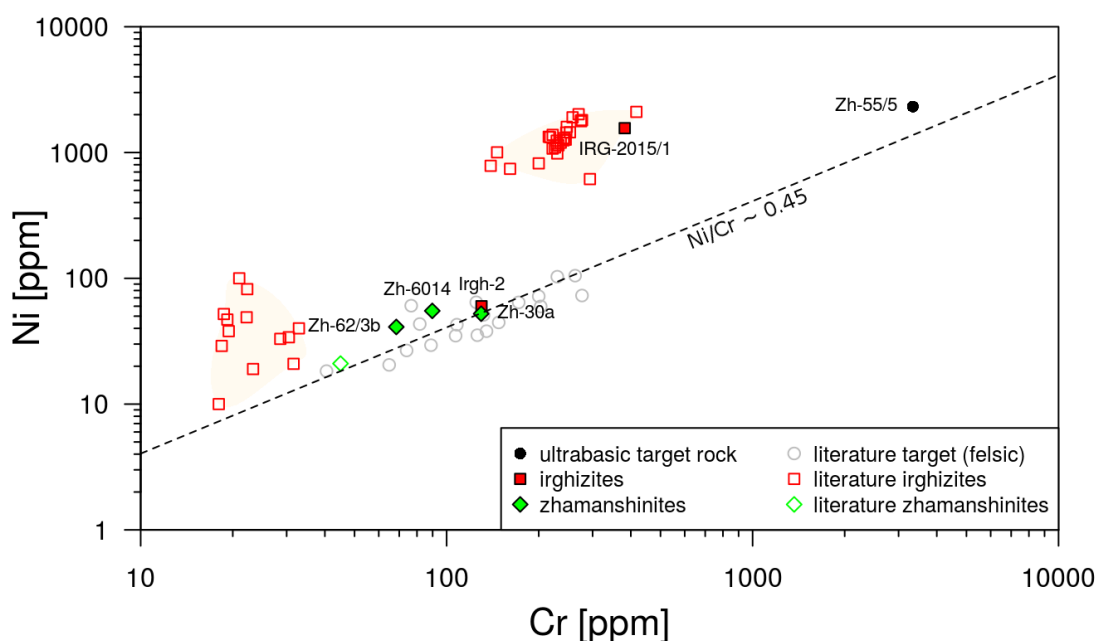


**Figure 4.1:** Plot of Ni versus Cr concentrations in ppm. Literature data from Ehmann et al. (1977); Palme et al. (1981) and C. Koeberl (pers. comm., 2015).

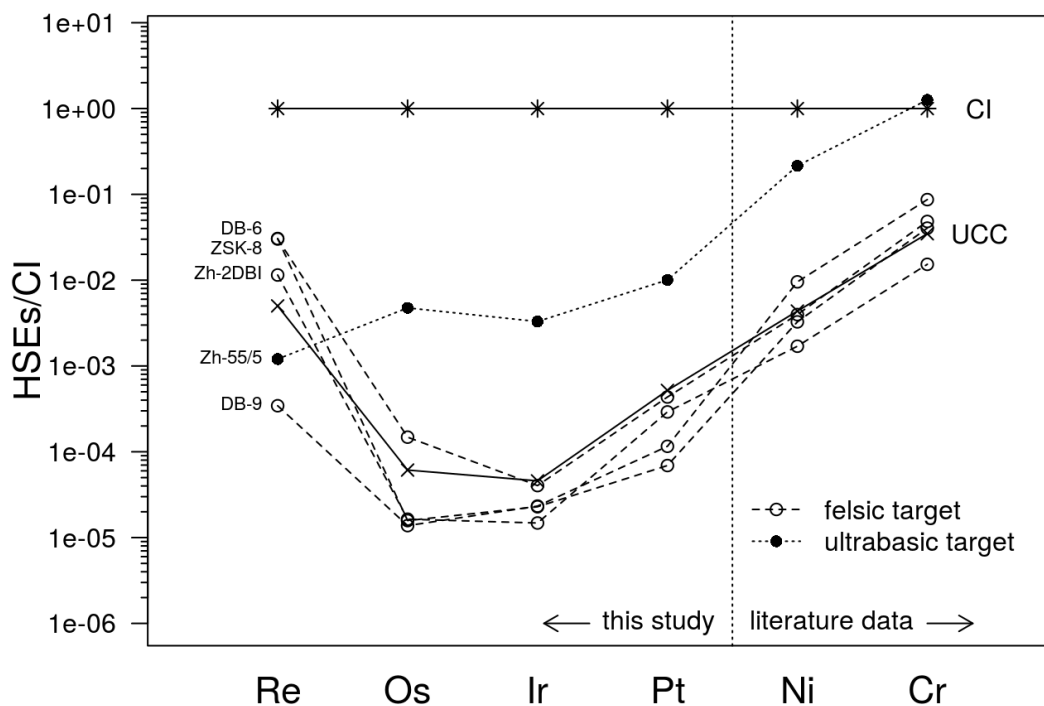


**Figure 4.2:** Highly siderophile element abundances of the Zhamanshin target rocks from this study normalized to CI chondrites. CI chondrite data from Horan et al. (2003). UCC composition from Peucker-Ehrenbrink and Jahn (2001). Errors smaller than symbol sizes.

Peucker-Ehrenbrink and Jahn, 2001). Hence the UCC represents a good proxy and can be taken as the average target composition. Furthermore the ultrabasic target sample exhibits a less fractionated HSE patterns which is characteristic for mantle rocks.

In Figure 4.3a, CI-chondrite-normalized patterns of the zhamanshinite samples, the ultrabasic target rocks, and the UCC are plotted. Two zhamanshinite samples (Zh-30a and Zh-62/3b) show HSE patterns similar to that of crust-like target rocks (shaded area as well as UCC for comparison). The analyzed zhamanshinite Zh-6014 show a less fractionated pattern, with Os concentrations elevated by two orders of magnitude and concentrations of Ir elevated by one order of magnitude. This elevated concentrations can be explained by (i) an ultrabasic contamination or (ii) a suspected meteoritic component. Figure 4.3b shows mixing calculations between the UCC and Zh-55/5 as end-members. To obtain a pattern similar to that of sample Zh-6014 a ultrabasic contamination of at least 10 % would be required. As stated previously with reverse mixing calculations performed with the major element composition between the ultrabasic target and sample Zh-6014 (see Table 4.1) such an amount of ultrabasic target rock is impossible and therefore such a consideration can be excluded. Figure 4.3c shows mixing calculations between the UCC and the average CI chondrite as end-members. An addition of  $\sim 0.12\%$  of a CI chondrite leads, except for Re and Pt to a composition similar to Zh-6014. The low concentrations of Re in Zh-6014

can easily be explained by Re loss during the impact process due to the volatile behavior of Re as an oxide during while high temperature events. For the lack of Pt in Zh-6014, the most likely options are (i) a yet unsampled precursor or (ii) syn- or post-impact fractionation processes or a combination of both.

In Figure 4.5a, CI-chondrite-normalized patterns of the irghizite samples, the ultrabasic target rock, and the UCC are plotted. The HSE pattern of the sample Irgh-2 is, except the unusual low concentration of Ir, crust-like and therefore inconspicuous. However, sample IRG-2015/1 shows the most unfractionated pattern of all investigated impactite samples and may zhamanshinite Zh-6014, either contain (i) an ultrabasic contamination or (ii) a meteoritic component. Abundances of Os, Ir, Pt, and Ni are elevated by at least one order of magnitude. Figure 4.5b shows mixing calculations performed between UCC and Zh-55/5 with amounts of 10, 25, 50 and 75% of an ultrabasic rock. It is easily understandable that a proportion of at least 25% of an ultrabasic contaminant is very unlikely due to (i) the under-represented ultrabasic lithologies in the zhamanshin area (see Figure 1.6) and (ii) the mixing calculations based on major element compositions (see Table 4.2). Figure 4.5c shows mixing calculations between the UCC and the average CI chondrite as end-members with proportions of 0.1, 0.5, 1 and 10% of a CI chondrite. It can be observed that a 0.1% meteoritic component leads to a HSE pattern, which is except for Pt, very similar to that of sample IRG-2015/1. The lack of Pt can be explained, as in the case of Zh-6014, by (i) a yet unsampled precursor rich in Pt or (ii) syn- or post-impact fractioning processes, or a combination of both.

In summary, it can be stated that two of the impactites analyzed in this study have enriched HSE concentrations that can be explained by a meteoritic admixture of about ~0.12 % for both samples.

Figure 4.4 shows selected CI normalized interelement ratios of the impactites. In Fig. 4.4a  $(\text{Re/Os})_n$  vs.  $(\text{Ir/Pt})_n$  and in Fig 4.4b  $(\text{Os/Pt})_n$  vs.  $(\text{Ir/Pt})_n$  is plotted. In both figures samples Zh-6014 and IRG-2015/1 (both of which contain a suspected meteoritic component) plot closest to the CI chondritic point (crossing of the dashed lines). Nevertheless, from these interelement ratios no unambiguous discrimination of the chemical nature of the projectile is possible.

### 4.2.3 Evidence from Os isotopes

Figure 4.6 shows the Re-Os isochron diagram for all investigated samples ( $^{187}\text{Os}/^{188}\text{Os}$  vs.  $^{187}\text{Re}/^{188}\text{Os}$  space). Due to strong interferences on mass 187 no data for the zhamanshinite sample Zh-6014 are available. As already mentioned in section 3.4, it can be seen that the analyzed samples do not exhibit an isochronous relationship. The huge variety of lithologies sampled and their varying ages are a primary reason for this. Additional Re-loss during the impact event, as postulated in section 4.2.2, would also jeopardize any preexisting isochron. However, whereas crust-like target rocks tend to be radiogenic (elevated  $^{187}\text{Os}/^{188}\text{Os}$  ratios) with higher  $^{187}\text{Re}/^{188}\text{Os}$  ratios, impactites (especially irghizite sample IRG-2015/1) tend to be less radiogenic and exhibit lower  $^{187}\text{Re}/^{188}\text{Os}$  ratios. Some impactites can, therefore, be interpreted to lie in a mixing field between the crust-like target rock cluster on the upper right hand corner of Fig. 4.6 and a chondritic end-member on the lower left-hand corner of the

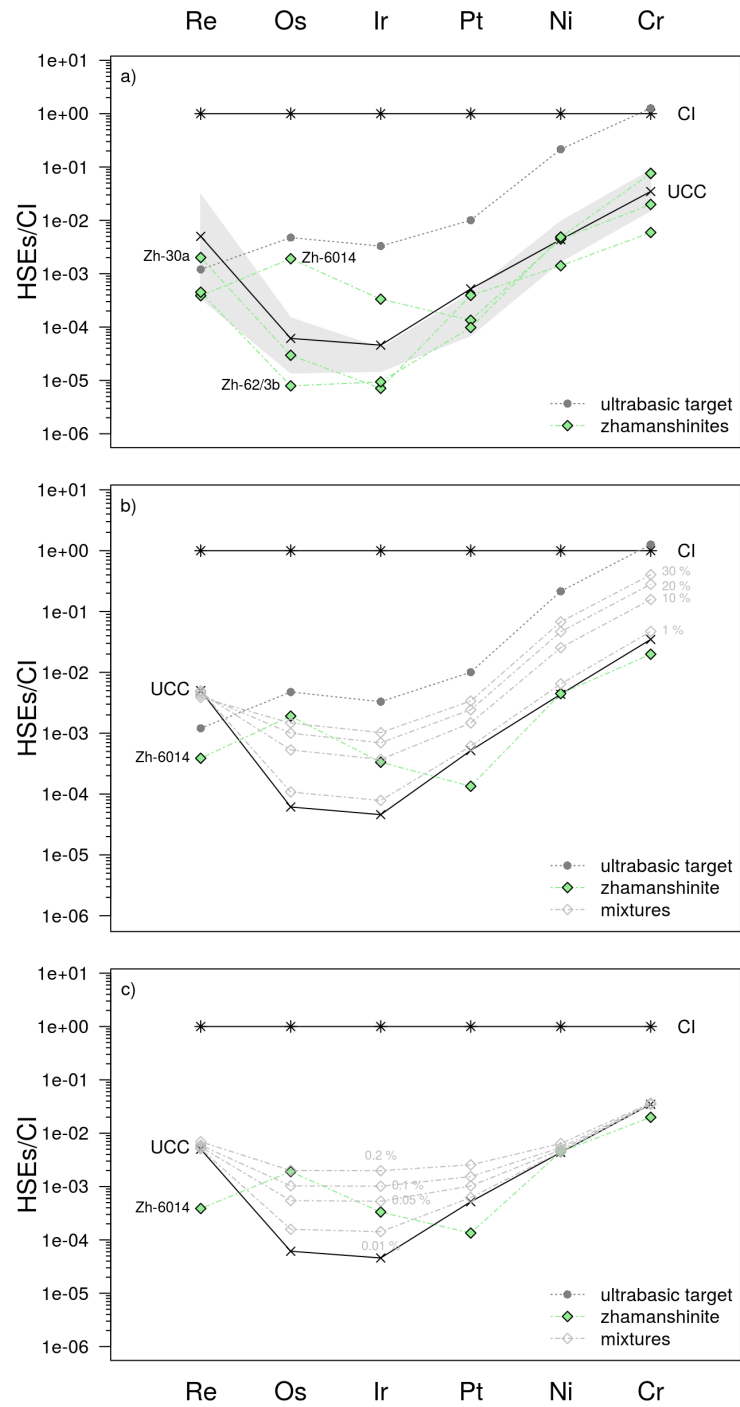


**Figure 4.3:** Highly siderophile element abundances of investigated zhamanshinites and the ultrabasic target rock Zh-55/5 normalized to CI chondrites. CI chondrite data from Horan et al. (2003). UCC composition from Peucker-Ehrenbrink and Jahn (2001). Errors smaller than symbol sizes.

diagram. Although the ultrabasic sample Zh-55/5 plots near to the chondrite point (with a slightly subchondritic  $^{187}\text{Re}/^{188}\text{Os}$  ratio), thus, serving as an alternative contaminant (instead of chondrites), a mixing relationship of the crust-like target material with this ultrabasic rock can now be explicitly ruled out based on the discussion in the previous sections (see section 4.2.1 and 4.2.2). Detailed mixing calculations based on the  $^{187}\text{Os}/^{188}\text{Os}$  vs.  $^{187}\text{Re}/^{188}\text{Os}$  space make little sense considering that the previously described selective Re-loss makes it impossible to properly connect target materials and impactites with binary mixing relations.

A reliable tool for identifying and also quantifying the mass input of a meteoritic component in impactites are mixing models between  $^{187}\text{Os}/^{188}\text{Os}$  ratios and Os concentrations (e.g., Lee et al., 2006). In Fig. 4.7 two crust-like target rock samples (DB-9 and Zh-2DBI, exhibiting the lowest and highest  $^{187}\text{Os}/^{188}\text{Os}$  signatures, at similar low Os concentration), serve as two possible end-member for a mixing with a chondritic component. Based on a CI chondritic endmember, a maximum meteoritic component of about 0.1% can be calculated for irghizite IRG-2015-1 (see also Table 4.3 for details of the mixing calculation). This value is similar to the amount of meteoritic component in that sample as was calculated from highly siderophile element concentrations (see section 4.2.2). The lack of a  $^{187}\text{Os}/^{188}\text{Os}$  ratio for the zhamanshinite Zh-6014 prevents the calculation of an extraterrestrial signature based on Fig. 4.7. All other impactites lie in the cluster defined by crust-like target rocks, thus, suggesting no meteoritic components in them. This is in accord with their inconspicuous PGE contents as mentioned above (see section 4.2.2). The meteoritic admixture quantified for IRG-2015/1 is not significantly affected by postulating any other chondritic endmember (ordinary or enstatite chondrites; see Table 4.3).

Moreover, Fig. 4.7 shows mixing calculations for a basic contaminant (Zh-55/5) of irghizite IRG-2015/1. Although already excluded as a possible component based on major element systematics and PGE contents (see section 4.2.1), it is interesting to note that the amount of basic contaminant needed to explain the Os isotope signature of IRG-2015/1

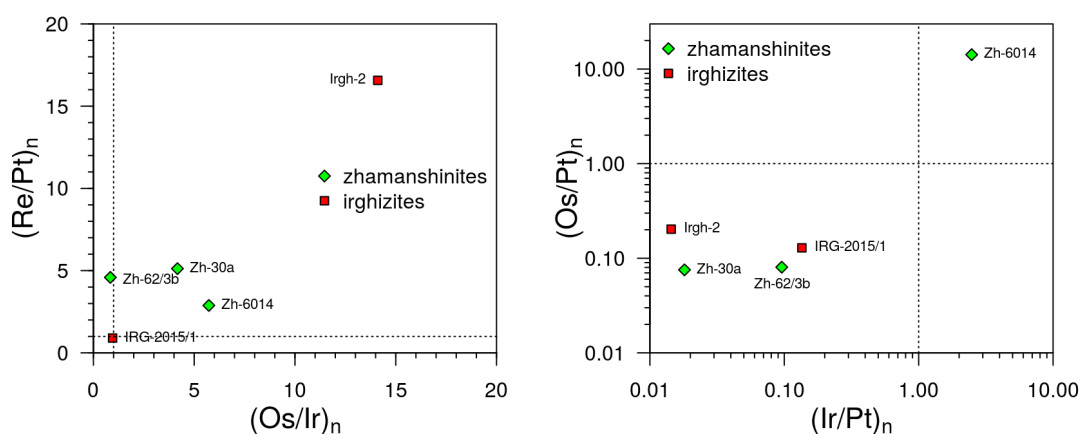


**Figure 4.4:** CI-chondrite-normalized interelement ratios of the investigated impactites. CI chondrite data (dashed lines) from Horan et al. (2003). Errors are smaller than symbol sizes.

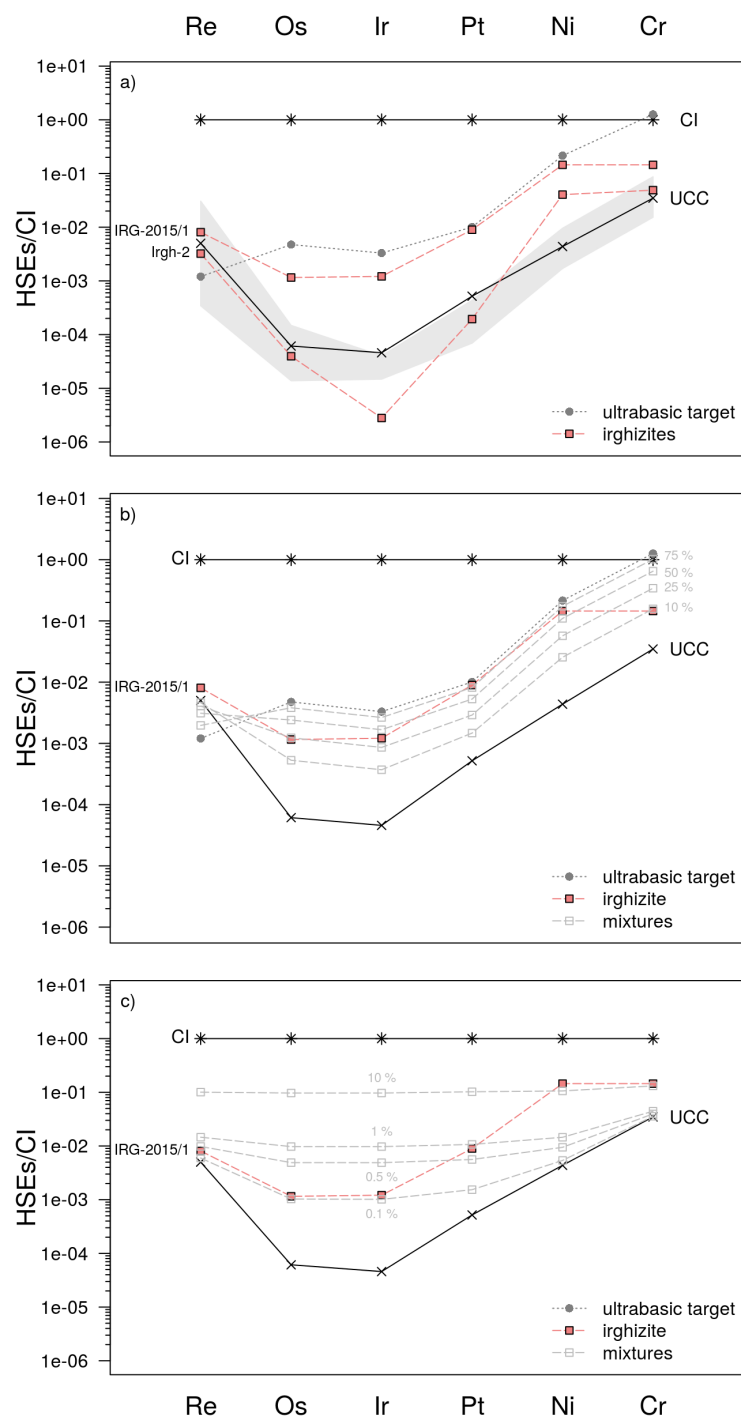


**Figure 4.5:** Highly siderophile element abundances of investigated irghizites and the ultrabasic target rock Zh-55/5 normalized to CI chondrites. CI chondrite data from Horan et al. (2003). UCC composition from Peucker-Ehrenbrink and Jahn (2001). Errors smaller than symbol sizes.



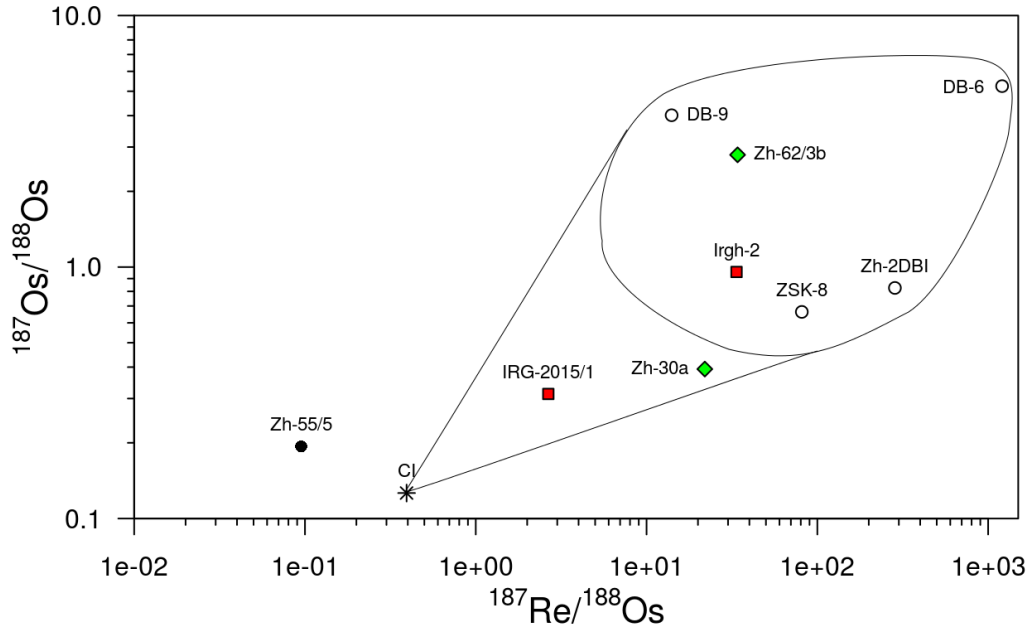


**Figure 4.6:** Plot of  $^{187}\text{Os}/^{188}\text{Os}$  vs.  $^{187}\text{Re}/^{188}\text{Os}$ . Isotopic composition of CI chondrite from Walker et al. (2002). Errors smaller than symbol sizes.

would be just as high (~25%) as what was calculated based on PGE abundances alone, a magnitude that would result in geochemically meaningless major element compositions (section 4.2.1 for details).

**Table 4.3:** End member used for  $^{187}\text{Os}/^{188}\text{Os}$  ratios vs. Os concentration mixing model. Values for carbonaceous-, ordinary- and enstatite chondrites from <sup>a</sup> Lodders and Fegley (1998) and <sup>b</sup> Walker et al. (2002).

	Contaminant				Target	
	CI	OC	EC	Zh-55/5	DB-6	Zh-2DBI
Os [ppt] <sup>a</sup>	$490 \cdot 10^3$	$835 \cdot 10^3$	$660 \cdot 10^3$	$2.4 \cdot 10^3$	8	8.3
$^{187}\text{Os}/^{188}\text{Os}$ <sup>b</sup>	0.126	0.128	0.128	0.194	5.241	0.826
Amount in IRG-2015/1	~0.10%	~0.06%	~0.08%	~21.94%	-	-

### 4.3 Strontium-neodymium isotopic composition

The previous sections provided a detailed discussion about the presence of a meteoritic component within two of the here analyzed impactite samples (zhamanshinite sample Zh-

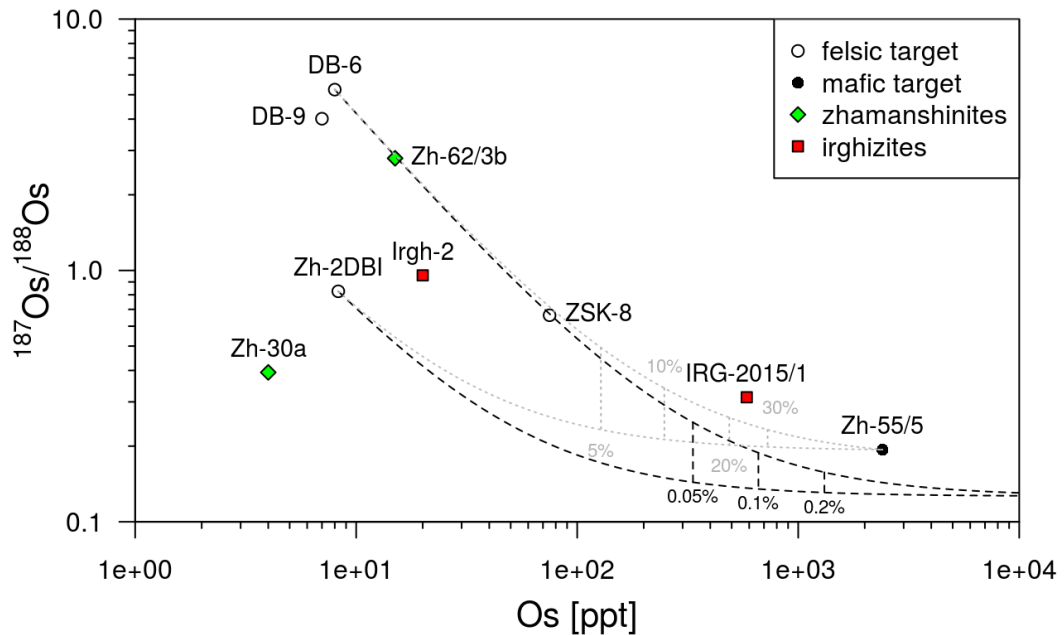


**Figure 4.7:**  $^{187}\text{Os}/^{188}\text{Os}$  vs. Os related mixing-calculations, suggesting about 0.1% of a chondritic component within irghizite sample IRG-2015/1. The mixing calculation based on end-member Zh-55/5 would require  $\sim 25\%$  of an ultrabasic contamination in IRG-2015/1 in order to explain its Os isotope signature, a value that was already mentioned in section 4.2.2 to be impossible. Black dashed lines shows mixing between selected targets and CI chondrite. Gray dotted line show mixing between selected targets and basic target rock. CI chondrite data from Horan et al. (2003) and Shirey and Walker (1998). Errors are smaller than symbol sizes.

6014 and irghizite sample IRG-2015/1). This discussion, based on major elements as well as PGE abundances and Os isotopes, also explicitly ruled-out any ultrabasic component within these samples, which could simulate the postulated chondritic admixture. Although unable to substantiate extraterrestrial components within impactites, Sr-Nd isotope data can serve as an additional tool to exclude ultrabasic contaminants. However, due to the huge variability of Sr-Nd isotope compositions of target rocks, no clear exclusion of an ultrabasic contamination can be made based on Sr and Nd isotope data, as was explicitly outlined for major element and PGE abundances as well as Os isotopes. Nevertheless, Fig. 3.5 and 4.8a clearly demonstrates the restricted range that irghizites exhibit in the  $\epsilon_{\text{Nd}}$  vs.  $^{87}\text{Sr}/^{86}\text{Sr}$  space (for both high- and low silica irghizites, respectively). The narrow scatter for the high silica irghizites also includes sample IRG-2015/1 (postulated to contain a chondritic admixture). The zhamanshinite sample Zh-6014 (also postulated to contain a chondritic admixture) plots within the trend defined by literature data for high silica zhamanshinites, but all samples for which literature data exist show a higher degree of scatter of isotopic composition compared to the irghizites.

Compared to Sr and Nd isotope compositions of tektites belonging to the four classic

strewn fields (each of which, beyond doubt, originated in one single impact event) our samples from the Zhamanshin area exhibit values, different from those of the intra-strewn field trends for the Ivory Coast, North American, Central European, and Australasian tektites (see Fig. 4.8b).

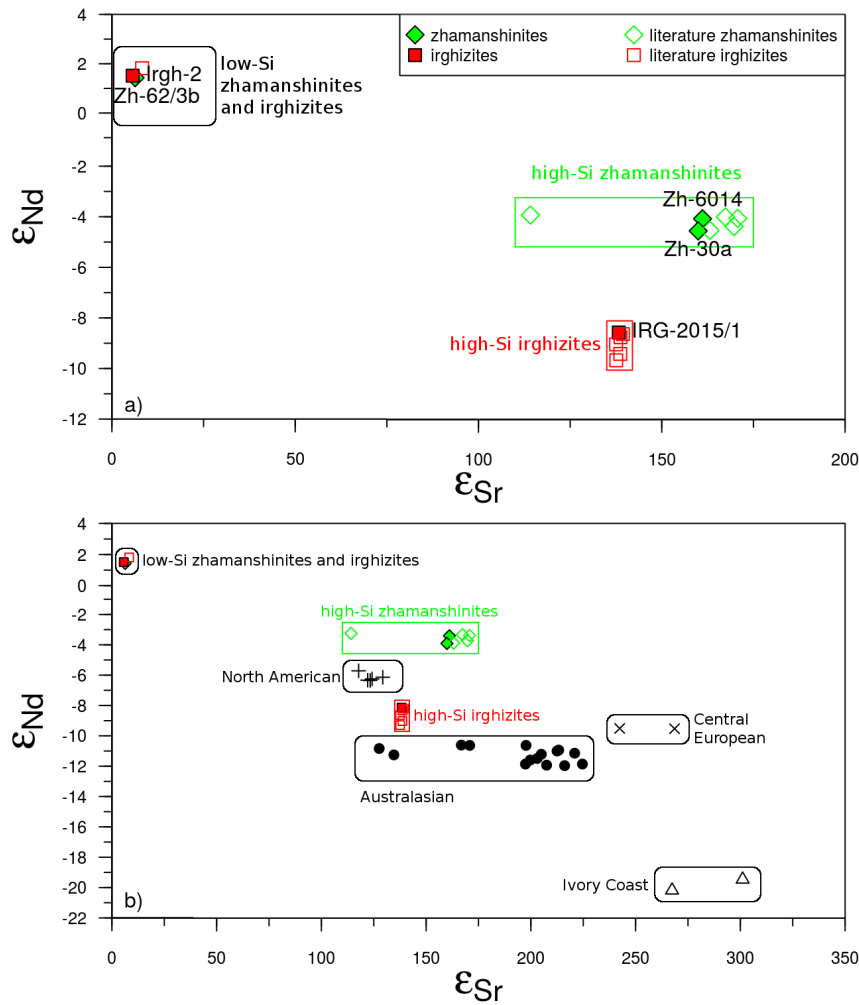


**Figure 4.8:** a) Plot of present day  $\epsilon_{Nd}$  vs.  $\epsilon_{Sr}$  isotope compositions for zhamanshinites and irghizites (literature data from Shaw and Wasserburg, 1982; Ostermann et al., 1996; Abate et al., 1998). b) Plot of present day  $\epsilon_{Nd}$  vs.  $\epsilon_{Sr}$  isotope compositions for impactites of the Zhamanshin crater and data from the four tektite strewn field of the world for comparison (data from Blum et al., 1992; Shaw and Wasserburg, 1982).

#### 4.4 Meteoritic components in impactites - a comparison of selected case studies

Tektites are natural glasses occurring on Earth in four distinct areas known as strewn fields (Australasian, Ivory Coast, Central European, and North American; see also introductory chapter). Obviously, the production of tektites require special conditions, because otherwise more than just four tektite strewn field would be known on earth, as there are about 150 known impact craters (see introductory chapter). Whenever craters are known to be associated with strewn fields, the craters are never in the center of them. Such an asymmetric distribution of tektites within a respective strewn field may point toward low-angle impacts, which seem to be a necessary (but alone not sufficient) prerequisite for the generation of tektites (Dressler and Sharpton, 1999).

Today, tektites production is widely accepted to have occurred before the main excavation phase of the crater formation and most likely involved predominantly target rock layer from close to the surface as precursor material (as evidenced by  $^{10}\text{Be}$  analyses; e.g. Serefidin et al., 2007). A loess-like precursor material from near to the surface was also proposed for the Irghizites (e.g. Verchovsky and Feldman, 1990). However, the restricted occurrence of the impact glasses (zhamanshinites) and of the aerodynamically shaped tektite-like irghizites, which are closely associated with their source crater, also prevents to refer to the irghizite-zhamanshinite area as a fifth tektite strewn field (Koeberl and Fredriksson, 1986).

But in the light of the here presented data it would be worth to compare the findings of this study with meteoritic signatures within tektites from the globally distributed strewn fields. Unfortunately such data sets are sparse. Koeberl and Shirey (1993) report on the presence of extraterrestrial Os in tektites from the Ivory Coast strewn field, which originated from the Bosumtwi impact crater, Ghana. Based on the  $^{187}\text{Re}-^{187}\text{Os}$  decay system they proposed a (most likely) chondritic admixture within the tektites of about 0.6% or less.

Koeberl (1993) provided data on microtektites associated with the Australasian tektite strewn field (the largest of the established tektite strewn fields and the one with a yet not identified source crater). Based on small but significant anomalies in the elemental abundances of Ir, Co and Ni in a microtektite-bearing layer (with Ir abundances of up to 160 ppt) an extraterrestrial component was proposed. However, based on this data, neither a suggestion of the projectile type, nor a quantification of the magnitude of the meteoritic admixture was drawn.

To the author's knowledge no data are available so far for possible extraterrestrial signatures in moldavites (tektites from the Central European strewn-field), as well as the tektites from the North-American strewn field.

Thus, compared to the only available quantitative data for the Ivory Coast tektites ( $\sim 0.6\%$  of a, most likely, chondritic component or less; Koeberl and Shirey, 1993), the postulated  $\sim 0.1\%$  of a chondritic component within one of the analyzed irghizites is only slightly lower.

## Summary and Conclusions

The Zhamanshin impact structure (with an age of 1 Ma and a diameter of 14 km) is situated in a semi-arid region of Kazakhstan and exhibits a heterogeneous suite of target rocks, of, predominantly upper continental crustal target lithologies (e.g. Silurian quartzites, Devonian shales, Carboniferous volcanoclastics, Cretaceous sandstones, shales, marls, limestones, and Cenozoic clays), as well as rare ultrabasic dykes. The Zhamanshin structure contains two types of impact glasses (zhamanshinites and irghizites).

The aim of this study was to perform geochemical analyses of target rocks and impact glasses in order to identify a possible meteoritic component in the impactites. This was achieved by performing (i) detailed petrographic descriptions of all samples, (ii) major element composition analyses of all impact glasses, (iii) highly siderophile element abundances (Re, Os, Ir, Pt), (iv) high precision Os isotope measurements and, finally, (v) determining Sr-Nd isotopic compositions.

The impact glasses from the Zhamanshin impact structure appear as chunky black rocks with pitted surfaces and bubbles (zhamanshinites) or as aerodynamically shaped splash forms with either a lustrous or dull surface (irghizites).

Both kinds of impact glasses were found to be quite homogeneous in their major element composition. Due to their silica content they can be subdivided in Si-poor and Si-rich specimens. According to their major element composition, the here analyzed zhamanshinites and irghizites perfectly match the typical trends as defined in the literature. A general fingerprint from the impact event can be found in the Re and Os elemental abundances of the impact glasses. Generally higher Re/Os in the target rocks compared to the here analyzed impact glasses can be interpreted as selective Re-loss of the zhamanshinites and irghizites during the high temperature impact event. Elevated platinum-group elemental abundances, near to chondritic interelement ratios as well as (always compared to the crust-like target rocks) less radiogenic  $^{187}\text{Os}/^{188}\text{Os}$  ratios within one zhamanshinite and one irghizite are interpreted in this study as resulting from a, most likely, chondritic admixture of about 0.12 %, a value that is comparable to those found in other impact glasses and tektites from around the world.

The meteoritic admixture postulated here is strongly supported by excluding any possible ultrabasic contribution to the impactites analyzed in this study. Sr-Nd isotopic compositions of the zhamanshinites and irghizites agree perfectly with trends as defined by the literature. For further research more target rocks and impact glasses should be analyzed to better constrain the contributions of impactor material to the two unique types of impact glasses and tektite-like objects found in the Zhamanshin area.

# Bibliography

- Abate B., Koeberl C., Kruger F., and Badjukov D. 1998, “Geochemistry of target rocks of the Zhamanshin crater, Kazakhstan, and their relationship to impact glasses”, *Unpublished Manuscript*.
- Acken, D. van, Brandon A., and Humayun M. 2011, “High-precision osmium isotopes in enstatite and Rumuruti chondrites”, *Geochimica et Cosmochimica Acta* 75, pp. 4020–4036.
- Ackerman L., Zák K., Jonášová S., Skála R., Magna T., and Deutsch A. 2015, “Highly siderophile element geochemistry of impact-related glasses and target rocks from the Zhamanshin impact structure, Kazakhstan”, *Lunar and Planetary Science*, vol. 46, abstract no. 1963.
- Bailer-Jones C. 2011, “Bayesian time series analysis of terrestrial impact cratering”, *Monthly Notices of the Royal Astronomical Society* 416, pp. 1163–1180.
- Birck J. L., Barman M. R., and Capmas F. 1997, “Re-Os Isotopic Measurements at the Femtomole Level in Natural Samples”, *Geostandards Newsletter* 21, pp. 19–27.
- Blum J., Papanastassiou D., Koeberl C., and Wasserburg G. 1992, “Neodymium and strontium isotopic study of Australasian tektites: New constraints on the provenance and age of target materials”, *Geochimica et Cosmochimica Acta* 56, pp. 483–492.
- Boiko Y. I., Mashchak M., and Raikhlin A. 1991, “Impact crater Zhamanshin”, (*abstract*), *All Union Geological Research Institute, West Kazakhstan*, p. 28, (In Russian).
- Bouška V., Povondra P., Florenskij P., and Řanda Z. 1981, “Irghizites and zhamanshinites: Zhamanshin crater, USSR”, *Meteoritics* 16, pp. 171–184.
- Brandon A., Humayun M., Puchtel I., Leya I., and Zolensky M. 2005, “Osmium isotope evidence for an s-process carrier in primitive chondrites”, *Science* 309, pp. 1233–1236.
- Burba G. and Meshcherskaya V. 1993, “Landscape and geomorphic survey of Zhamanshin area, Northern Kazakhstan: Preliminary report on 1992 field trip data”, (*abstract*), *Lunar and Planetary Science*, vol. 24, pp. 221–222.
- Coggon J., Luguët A., Nowell G., and Appel P. 2013, “Hadean mantle melting recorded by southwest Greenland chromitite  $^{186}\text{Os}$  signatures”, *Nature Geoscience* 6, pp. 871–874.
- Cohen A. and Waters F. 1996, “Separation of osmium from geological materials by solvent extraction for analysis by thermal ionisation mass spectrometry”, *Analytica Chimica Acta* 332, pp. 269–275.
- Day J. M., Pearson D. G., and Hulbert L. J. 2008, “Rhenium–osmium isotope and platinum-group element constraints on the origin and evolution of the 1.27 Ga Muskox layered intrusion”, *Journal of Petrology* 49, pp. 1255–1295.

- Deino A., Becker T., and Garvin J. 1990, "Laser-fusion  $^{40}\text{Ar}/^{39}\text{Ar}$  ages of acid Zhamanshinite", (*abstract*), *Lunar and Planetary Science 21 Houston*, pp. 271–272.
- Dressler B. and Sharpton V. 1999, *Large meteorite impacts and planetary evolution II*, Geological Society of America, Special Paper 339, 299–304 pp.
- Earth impact database. 2015, <http://www.passc.net/EarthImpactDatabase/>, [Online; accessed 14-November-2015].
- Ehmann W., Stroube Jr W., Ali M., and Hossain T. 1977, "Zhamanshin crater glasses: chemical composition and comparison with tektites", (*abstract*), *Meteoritics* 12, p. 212.
- Florensky P. 1977, "Der Meteoritenkrater Zhamanshin (nördliches Aralgebiet, UdSSR) und seine Tektite und Impaktite", *Chemie der Erde* 36, pp. 83–95.
- Florensky P. and Dabizha A. 1980, "The Zhamanshin meteorite crater", *Moscow Izdatel Nauka*, p. 127.
- Florensky P., Short N., Winzer S., and Fredriksson K. 1977, "The Zhamanshin structure: Geology and petrography", (*abstract*), *Meteoritics* 12, pp. 227–228.
- Glass B. P. and Simonson B. M. 2012, *Distal impact ejecta layers: A record of large impacts in sedimentary deposits*, Springer, Heidelberg, 707 pp.
- Grieve R. 1987, "Terrestrial impact structures", *Annual Review of Earth and Planetary Sciences* 15, pp. 245–270.
- Grieve R. and Shoemaker E. 1994, "The record of past impacts on Earth", *Hazards due to comets and asteroids*, vol. 1, University of Arizona Press (Tucson), pp. 462–417.
- Horan M., Walker R., Morgan J., Grossman J., and Rubin A. 2003, "Highly siderophile elements in chondrites", *Chemical Geology* 196, pp. 27–42.
- Ishikawa A., Senda R., Suzuki K., Dale C., and Meisel T. 2014, "Re-evaluating digestion methods for highly siderophile element and  $^{187}\text{Os}$  isotope analysis: Evidence from geological reference materials", *Chemical Geology* 384, pp. 27–46.
- Izokh E., Kashkarov L., and Korotkova N. 1993, *Age and chemical composition of the Zhamanshin crater impactites and tektites and comparison with Australasian tektites*, Russian Academy of Sciences, Siberian Branch, United Institute of Geology, Geophysics and Mineralogy, 94 pp.
- Jonášová Š., Ackerman L., Žák K., Skála R., Ďurišová J., Pack A., and Magna T. 2015, "Highly siderophile elements and triple-oxygen isotopes of tektite-like glasses from the Zhamanshin impact structure, Kazakhstan", *Goldschmidt Abstracts* 25, abstract no. 1472.
- Jourdan F., Renne P., and Reimold W. 2009, "An appraisal of the ages of terrestrial impact structures", *Earth and Planetary Science Letters* 286, pp. 1–13.
- Koeberl C. 1993, "Extraterrestrial component associated with Australasian microtektites in a core from ODP Site 758B", *Earth and Planetary Science Letters* 119, pp. 453–458.
- Koeberl C. 1998, "Identification of meteoritic components in impactites", *Meteorites: Flux with Time and Impact Effects*, ed. by Grady, M.M. and Hutchison, R. and McCall, G. and Rothery, D. Geological Society, London, Special Publications, vol. 140, pp. 133–153.
- Koeberl C. 2002, "Mineralogical and geochemical aspects of impact craters", *Mineralogical Magazine* 66, pp. 745–768.



- Koeberl C. 2006, "The record of impact processes on the early Earth: A review of the first 2.5 billion years", *Processes on the Early Earth*, ed. by Reimold, W.U. and Gibson, R.L. Geological Society of America Special Papers, vol. 405, pp. 1–22.
- Koeberl C. 2014, "2.5 - The geochemistry and cosmochemistry of impacts", *Treatise on Geochemistry*, ed. by Turekian, H.D. and Holland, K.K. Second Edition, Elsevier, Oxford, pp. 73–118.
- Koeberl C. and Fredriksson K. 1986, "Impact glasses from Zhamanshin crater (U.S.S.R.): chemical composition and discussion of origin", *Earth and Planetary Science Letters* 78, pp. 80–88.
- Koeberl C. and Schulz T. 2015, "Identifying extraterrestrial signatures in mafic impactites: An assessment based on the Lonar crater, India", *Lunar and Planetary Science*, vol. 46, abstract no. 1520.
- Koeberl C. and Shirey S. 1993, "Detection of a meteoritic component in Ivory Coast tektites with rhenium-osmium isotopes", *Science* 261, pp. 595–598.
- Koeberl C. and Shirey S. 1996, "Re-Os isotope study of rocks from the Manson impact structure", *The Manson Impact Structure, Iowa: Anatomy of an Impact Crater*, ed. by Koeberl, C. and Anderson, R.R. Geological Society of America Special Paper 302, pp. 331–339.
- Koeberl C. and Shirey S. 1997, "Re-Os isotope systematics as a diagnostic tool for the study of impact craters and distal ejecta", *Palaeogeography, Palaeoclimatology, Palaeoecology* 132, pp. 25–46.
- Koeberl C., Reimold W., and Shirey S. 1996, "Re-Os isotope and geochemical study of the Vredefort Granophyre: Clues to the origin of the Vredefort structure, South Africa", *Geology* 24, pp. 913–916.
- Koeberl C., Reimold W., and Shirey S. 1998, "The Aouelloul crater, Mauritania: On the problem of confirming the impact origin of a small crater", *Meteoritics & Planetary Science* 33.3, pp. 513–517.
- Koeberl C., Peucker-Ehrenbrink B., Reimold W., Shukolyukov A., and Lugmair G. 2002, "Comparison of the osmium and chromium isotopic methods for the detection of meteoritic components in impactites: Examples from the Morokweng and Vredefort impact structures, South Africa", *Catastrophic Events and Mass Extinctions: Impacts and Beyond*, ed. by Koeberl, C., and MacLeod, K.G., Geological Society of America, Special Papers 356, pp. 607–618.
- Koeberl C., Claeys P., Hecht L., and McDonald I. 2012, "Geochemistry of impactites", *Elements* 8, pp. 37–42.
- Krull-Davatzes A. E., Byerly G. R., and Lowe D. R. 2010, "Evidence for a low-O<sub>2</sub> Archean atmosphere from nickel-rich chrome spinels in 3.24 Ga impact spherules, Barberton greenstone belt, South Africa", *Earth and Planetary Science Letters* 296, pp. 319–328.
- Langmuir C. H., Vocke R. D., Hanson G. N., and Hart S. R. 1978, "A general mixing equation with applications to Icelandic basalts", *Earth and Planetary Science Letters* 37, pp. 380–392.
- Lassiter J. 2003, "Rhenium volatility in subaerial lavas: constraints from subaerial and submarine portions of the HSDP-2 Mauna Kea drillcore", *Earth and Planetary Science Letters* 214, pp. 311–325.

- Lee S. R., Horton J. W., and Walker R. J. 2006, "Confirmation of a meteoritic component in impact-melt rocks of the Chesapeake Bay impact structure, Virginia, USA—Evidence from osmium isotopic and PGE systematics", *Meteoritics & Planetary Science* 41, pp. 819–833.
- Lodders K. and Fegley B. 1998, *The planetary scientist's companion*, Oxford University Press, New York, 371 pp.
- Lowe D. R. and Byerly G. R. 1986, "Early Archean silicate spherules of probable impact origin, South Africa and Western Australia", *Geology* 14, pp. 83–86.
- Lugmair G. and Marti K. 1978, "Lunar initial  $^{143}\text{Nd}/^{144}\text{Nd}$ : differential evolution of the lunar crust and mantle", *Earth and Planetary Science Letters* 39, pp. 349–357.
- Luguet A., Nowell G. M., and Pearson D. G. 2008, " $^{184}\text{Os}/^{188}\text{Os}$  and  $^{186}\text{Os}/^{188}\text{Os}$  measurements by Negative Thermal Ionisation Mass Spectrometry (N-TIMS): Effects of interfering element and mass fractionation corrections on data accuracy and precision", *Chemical Geology* 248, pp. 342–362.
- Maier W., Andreoli M., McDonald I., Higgins M., Boyce A., Shukolyukov A., Lugmair G., Ashwal L., Graeser P., Ripley E., and Hart R. 2006, "Discovery of a 25-cm asteroid clast in the giant Morokweng impact crater, South Africa", *Nature* 441, pp. 203–206.
- McDonald I., Andreoli M., Hart R., and Tredoux M. 2001, "Platinum-group elements in the Morokweng impact structure, South Africa: Evidence for the impact of a large ordinary chondrite projectile at the Jurassic-Cretaceous boundary", *Geochimica et Cosmochimica Acta* 65, pp. 299–309.
- McHone J., Greeley R., Williams K., Blumberg D., and Kuzmin R. 2002, "Space shuttle observations of terrestrial impact structures using SIR-C and X-SAR radars", *Meteoritics & Planetary Science* 37, pp. 407–420.
- Meisel T., Burnham O., Kriete C., Bokhari S., and Schulz T. 2013, "Osmium isotope and PGE reference materials OKUM and MUH-1", *Mineralogical Magazine*, vol. 77, pp. 1734–1734.
- Meisel T. and Moser J. 2004a, "Platinum-group element and rhenium concentrations in low abundance reference materials", *Geostandards and Geoanalytical Research* 28, pp. 233–250.
- Meisel T. and Moser J. 2004b, "Reference materials for geochemical PGE analysis: new analytical data for Ru, Rh, Pd, Os, Ir, Pt and Re by isotope dilution ICP-MS in 11 geological reference materials", *Chemical Geology* 208, pp. 319–338.
- Meisel T., Moser J., Fellner N., Wegscheider W., and Schoenberg R. 2001, "Simplified method for the determination of Ru, Pd, Re, Os, Ir and Pt in chromitites and other geological materials by isotope dilution ICP-MS and acid digestion", *Analyst* 126, pp. 322–328.
- Melosh H. J. 1989, "Impact cratering: A geologic process", *New York, Oxford University Press (Oxford Monographs on Geology and Geophysics, No. 11)*, 253 p.
- Mizera J., Randa Z., and Tomandl I. 2012, "Geochemical characterization of impact glasses from the Zhamanshin crater by various modes of activation analysis. Remarks on genesis of irghizites", English, *Journal of Radioanalytical and Nuclear Chemistry* 293.1, pp. 359–376.
- Montanari A. and Koeberl C. 2006, *Impact Stratigraphy: The Italian Record*, Lecture Notes in Earth Sciences, Springer Berlin Heidelberg, 346 pp.
- Osinski G. and Pierazzo E. 2012, *Impact Cratering: Processes and Products*, Oxford: Wiley & Sons, 308 pp.

- Ostermann M., Deutsch A., and Masaitis V. 1996, "Geochemistry and Nd-Sr isotope signature of tektites (indochinites, urengoite) and impact melt glasses (zhmanshinites, irghizites)", *Lunar and Planetary Science*, vol. 27, pp. 987–988.
- Palme H., Grieve R., and Wolf R. 1981, "Identification of the projectile at the Brent crater, and further considerations of projectile types at terrestrial craters", *Geochimica et Cosmochimica Acta* 45, pp. 2417–2424.
- Palme H., Wolf R., and Grieve R. 1978, "New data on meteoritic material at terrestrial impact craters", (*abstract*), *Lunar and Planetary Science* 9, pp. 856–858.
- Peucker-Ehrenbrink B. and Jahn B. 2001, "Rhenium-osmium isotope systematics and platinum group element concentrations: Loess and the upper continental crust", *Geochemistry, Geophysics, Geosystems*, DOI: 10.1029/2001GC000172.
- Rehkämper M. and Halliday A. 1997, "Development and application of new ion-exchange techniques for the separation of the platinum group and other siderophile elements from geological samples", *Talanta* 44, pp. 663–672.
- Ryder G. 1990, "Lunar samples, lunar accretion and the early bombardment of the Moon", *Eos, Transactions American Geophysical Union* 71, No. 10, pp. 313–323.
- Ryder G., Koeberl C., and Mojzsis S. 2000, "Heavy bombardment on the Earth at 3.85 Ga: The search for petrographic and geochemical evidence", *Origin of the Earth and Moon*, ed. by Canup, R. and Righter, K. University of Arizona Press, Tucson, pp. 475–492.
- Savard D., Barnes S.-J., and Meisel T. 2010, "Comparison between nickel-sulfur fire assay Te co-precipitation and isotope dilution with high-pressure asher acid digestion for the determination of platinum-group elements, rhenium and gold", *Geostandards and Geoanalytical Research* 34, pp. 281–291.
- Serefiddin F., Herzog G., and Koeberl C. 2007, "Beryllium-10 concentrations of tektites from the Ivory Coast and from Central Europe: Evidence for near-surface residence of precursor materials", *Geochimica et Cosmochimica Acta* 71, pp. 1574–1582.
- Shaw H. and Wasserburg G. 1982, "Age and provenance of the target materials for tektites and possible impactites as inferred from Sm-Nd and Rb-Sr systematics", *Earth and Planetary Science Letters* 60, pp. 155–177.
- Shirey S. B. and Walker R. J. 1998, "The Re-Os isotope system in cosmochemistry and high-temperature geochemistry", *Annual Review of Earth and Planetary Sciences* 26, pp. 423–500.
- Shukolyukov A., Kyte F., Lugmair G., Lowe D., and Byerly G. 2000, "The oldest impact deposits on Earth—First confirmation of an extraterrestrial component", *Impacts and the early Earth*, ed. by Gilmour, I. and Koeberl, C. Springer, Heidelberg, pp. 99–115.
- Shukolyukov A. and Lugmair G. 1998, "Isotopic evidence for the Cretaceous-Tertiary impactor and its type", *Science* 282, pp. 927–930.
- Smoliar M., Walker R., and Morgan J. 1996, "Re-Os ages of group IIA, IIIA, IVA, and IVB iron meteorites", *Science* 271, p. 1099.
- Steiger R. H. and Jäger E. 1977, "Subcommission on geochronology: Convention on the use of decay constants in geo- and cosmochronology", *Earth and Planetary Science Letters* 36, pp. 359–362.

- Stöffler D. and Grieve R. 2007, "Impactites, Chapter 2.11", *Metamorphic rocks: a classification and glossary of terms, recommendations of the International Union of Geological Sciences*, ed. by Fettes, D. and Desmons, J. Cambridge University Press, Cambridge, pp. 82–92.
- Storzer D. and Koeberl C. 1989, "Fission track evidence for multiple source components of Zhamanshin impactites, and new fission track ages", (*abstract*), *Meteoritics* 24, p. 328.
- Taylor S. and McLennan S. 1979, "Chemical relationships among irghizites, zhamanshinites, Australasian tektites and Henbury impact glasses", *Geochimica et Cosmochimica Acta* 43, pp. 1551–1565.
- Trinquier A., Birck J.-L., and Allegre C. 2006, "The nature of the KT impactor. A  $^{54}\text{Cr}$  reappraisal", *Earth and Planetary Science Letters* 241, pp. 780–788.
- Verchovsky A. and Feldman V. 1990, "Noble gases in some impactites and tektites", *Meteoritics* 25, p. 416.
- Vetvicka I., Frank J., and Drtina J. 2010, "Electron microprobe analysis (WDS EPMA) of Zhamanshin glass reveals the impactor and a common role of accretion in the origin of splash-form impact glass", (*abstract*), *IOP Conference Series: Materials Science and Engineering*, vol. 7, IOP Publishing, pp. 12–29.
- Walker R., Horan M., Morgan J., Becker H., Grossman J., and Rubin A. 2002, "Comparative  $^{187}\text{Re}$ - $^{187}\text{Os}$  systematics of chondrites: Implications regarding early solar system processes", *Geochimica et Cosmochimica Acta* 66, pp. 4187–4201.
- Zolensky M. E. and Koeberl C. 1991, "Why are blue zhamanshinites blue? Liquid immiscibility in an impact melt", *Geochimica et Cosmochimica Acta* 55, pp. 1483–1486.

# List of Tables

2.1	Standard materials, used crystal, measuring times, and detection limits of EPMA analysis performed during this study with a Jeol JXA-8530F field emission electron microprobe. . . . .	17
2.2	Osmium isotope compositions for DROsS Os reference materials. Low sensitivity measurements in this study were performed in peak jumping mode using an electron multiplier in negative modus using the Triton Thermo Scientific TIMS at the University Vienna. Typical intensities for mass 240 ( $^{192}\text{OsO}_3^-$ ) ranged between $\sim 10.000$ and $\sim 100.000$ counts. Literature values are listed for comparison and represent high-precision measurements performed in multi-collector mode. . . . .	20
2.3	Concentrations (in $\text{ngg}^{-1}$ ) and relative standard deviations (RSD) for two standard reference materials. . . . .	20
2.4	Os isotopic composition for standard reference materials. . . . .	20
3.1	Petrographic description of target rocks and impactites. . . . .	23
3.2	Range of major element compositions of zhamanshinites and irghizites from the literature (Koeberl and Fredriksson, 1986; Izokh et al., 1993). Values are in wt%. . . . .	24
3.3	Rhenium and platinum-group element concentrations for target rocks and impact glasses (irghizites and zhamanshinites), measured via isotope dilution. Errors for element concentrations are $< 5\%$ ( $2\sigma$ RSD). . . . .	27
3.4	Major Element composition obtained by WDS-EPMA analysis. Averages from tables C.1–C.5 in the appendix. Concentrations in wt-%. Detection limits and $2\sigma$ -errors see Table 2.1 . . . . .	28
3.5	Concentration of HSEs (in ppt) and CI chondrite-normalized values for selected element ratios in target rocks and impactites. Errors for element concentrations are $< 5\%$ . of HSEs in CI chondrites used are from Horan et al. (2003). . . . .	28
3.6	Platinum-group element abundances for irghizites reported in Ackerman et al. (2015) and Jonášová et al. (2015). All values were estimated from HSE pattern plots. Samples IR-7 and IR-13 were interpreted to exhibit a meteoritic admixture. . . . .	30
3.7	Isotopic composition in target rocks and impactites (zhamanshinites and irghizites; this study). Initial ( $^{187}\text{Os}/^{188}\text{Os}$ ) ratios were calculated with a decay constant from Smoliar et al. (1996) and the age of the cratering event from Deino et al. (1990). . . . .	30
		57

3.8	Strontium-Nd isotope compositions and concentrations in target rocks and impactites (zhmanshinites and irghizites) from the Zhamanshin impact structure. Concentrations for SiO <sub>2</sub> are mentioned for comparison in wt.%, Sr and Nd in ppm. References: bold: this study; a: Abate et al. (1998); b: Shaw and Wasserburg (1982); c: Ostermann et al. (1996). . . . .	33
4.1	Binary mixing calculations of a zhamanshinite (Zh-30a), inconspicuous of a meteoritic component, with proportions of 0.1%, 1%, 10%, and 20% of an ultrabasic component (Zh-55/5). Values are in wt.% and normalized so that sum equals to 100%. 38	
4.2	Binary mixing calculations of an irghizite (IRG 6200), inconspicuous of a meteoritic component, with proportions of 0.1%, 1%, 10%, and 20% of an ultrabasic component (Zh-55/5). Data for IRG 6200 from Abate et al. (1998). Values are in wt.% and normalized so that sum equals to 100%. . . . .	39
4.3	End member used for <sup>187</sup> Os/ <sup>188</sup> Os ratios vs. Os concentration mixing model. Values for carbonaceous-, ordinary- and enstatite chondrites from <sup>a</sup> Lodders and Fegley (1998) and <sup>b</sup> Walker et al. (2002). . . . .	45
B.1	Chemical composition of impact glass and target rocks from the Zhamanshin impact feature from Abate et al. (1998). Major element contents in wt%. Trace element abundances in ppm. Average irghizite from Taylor and McLennan (1979). . . . .	72
C.1	EPMA point analysis data for impactite sample Zh-6014. Values in wt%. . . . .	74
C.2	EPMA point analysis data for impactite sample Zh-30a. Values in wt%. . . . .	75
C.3	EPMA point analysis data for impactite sample Zh-62/3b. Values in wt%. . . . .	76
C.4	EPMA point analysis data for impactite sample IRG-2015/1. Values in wt%. . . . .	77
C.5	EPMA point analysis data for impactite sample Irgh-2. Values in wt%. . . . .	78

# List of Figures

1.1	Histogram of ages of known terrestrial impact structures. Note that the scale is by far exceeded within the past 300 Ma. The dot-pattern indicates impact structures, whereas the hatched pattern signifies ejecta and/or spherule layers (from Koeberl, 2006). . . . .	2
1.2	Schematic cross section of the two main crater types (from Koeberl, 2014) . . . . .	3
1.3	Classification of impactites from single impacts according to geological setting, composition, texture and degree of shock metamorphism (from Stöffler and Grieve, 2007) . . . . .	5
1.4	Map showing the four tektite strewn fields on Earth. Formation ages of the tektites are shown in parentheses (from Glass and Simonson, 2012). . . . .	6
1.5	Osmium isotopic ratios vs. Os content showing the mixing relationship between a meteoritic and target rock endmember. Compositions of melt rocks plot along the hyperbolic mixing line, indicating extraterrestrial admixture (from Koeberl, 2014). . . . .	9
1.6	Approximated abundance of target rock lithologies in the Zhamanshin area. The calculation is based on target rock major element analyses from Izokh et al. (1993). . . . .	11
1.7	a) Zhamanshinite (photo by author) b) Irghizites (Figure from Ackerman et al., 2015). . . . .	12
2.1	Photomicrographs of thin sections for target rocks samples. DB6, and DB-9 are shales. ZSK-8 is a claystone. Zh-2DBI is a andesite. Zh-55/5 is an ultrabasic rock. Scale applies to all images. . . . .	15
2.2	Photomicrographs of thin sections for impactite samples. Zh-6014, Zh-30a, and Zh-62/3b are zhamanshinites. IRG-2015/1, and Irgh-2 are irghizites. Scale applies to all images. . . . .	16
3.1	Ternary plot of the relative abundances of SiO <sub>2</sub> , CaO, and MgO, showing the trend defined by literature data for zhamanshinites and irghizites. Also shown are the impactite samples analyzed in this work, which in plot the fields defined by the literature data. Literature data from Izokh et al. (1993). . . . .	25
3.2	Harker diagrams for major elements in impactite samples analyzed in this work. Values are in wt-%. . . . .	26
3.3	Selected interelement plots of platinum-group element (PGE) and rhenium abundances. Errors are smaller than symbol sizes. . . . .	29
		59

3.4	Isotope ratios measured in target rocks (subdivided into felsic or crust-like target rocks and basic target rocks, as represented by sample Zh-55/5) and impactites (subdivided into zhamanshinites and irghizites) of the Zhamanshin impact structure. The dotted line represents the average of the upper continental crust (UCC; ratios from Peucker-Ehrenbrink and Jahn, 2001). The dashed line represents the CI chondritic ratios from Shirey and Walker (1998). Errors are smaller than symbol sizes. . . . .	31
3.5	$\epsilon_{Nd}$ vs $^{87}Sr/^{86}Sr$ plot for comparison with literature data. Literature data from Abate et al. (1998), Ostermann et al. (1996), and Shaw and Wasserburg (1982) (see Tab. 3.8). Errors are smaller than symbol sizes. . . . .	32
4.1	Plot of Ni versus Cr concentrations in ppm. Literature data from Ehmann et al. (1977); Palme et al. (1981) and C. Koeberl (pers. comm., 2015). . . . .	39
4.2	Highly siderophile element abundances of the Zhamanshin target rocks from this study normalized to CI chondrites. CI chondrite data from Horan et al. (2003). UCC composition from Peucker-Ehrenbrink and Jahn (2001). Errors smaller than symbol sizes. . . . .	40
4.3	Highly siderophile element abundances of investigated zhamanshinites and the ultrabasic target rock Zh-55/5 normalized to CI chondrites. CI chondrite data from Horan et al. (2003). UCC composition from Peucker-Ehrenbrink and Jahn (2001). Errors smaller than symbol sizes. . . . .	42
4.4	CI-chondrite-normalized interelement ratios of the investigated impactites. CI chondrite data (dashed lines) from Horan et al. (2003). Errors are smaller than symbol sizes. . . . .	43
4.5	Highly siderophile element abundances of investigated irghizites and the ultrabasic target rock Zh-55/5 normalized to CI chondrites. CI chondrite data from Horan et al. (2003). UCC composition from Peucker-Ehrenbrink and Jahn (2001). Errors smaller than symbol sizes. . . . .	44
4.6	Plot of $^{187}Os/^{188}Os$ vs. $^{187}Re/^{188}Os$ . Isotopic composition of CI chondrite from Walker et al. (2002). Errors smaller than symbol sizes. . . . .	45
4.7	$^{187}Os/^{188}Os$ vs. Os related mixing-calculations, suggesting about 0.1% of a chondritic component within irghizite sample IRG-2015/1. The mixing calculation based on endmember Zh-55/5 would require ~25% of an ultrabasic contamination in IRG-2015/1 in order to explain its Os isotope signature, a value that was already mentioned in section 4.2.2 to be impossible. Black dashed lines shows mixing between selected targets and CI chondrite. Gray dotted line show mixing between selected targets and basic target rock. CI chondrite data from Horan et al. (2003) and Shirey and Walker (1998). Errors are smaller than symbol sizes. . . . .	46
4.8	a) Plot of present day $\epsilon_{Nd}$ vs. $\epsilon_{Sr}$ isotope compositions for zhamanshinites and irghizites (literature data from Shaw and Wasserburg, 1982; Ostermann et al., 1996; Abate et al., 1998). b) Plot of present day $\epsilon_{Nd}$ vs. $\epsilon_{Sr}$ isotope compositions for impactites of the Zhamanshin crater and data from the four tektite strewn field of the world for comparison (data from Blum et al., 1992; Shaw and Wasserburg, 1982).	47
A.1	Photographs of target rock samples. . . . .	64



A.2	Photographs of impactite samples. . . . .	65
A.3	Backscattered electron (BSE) image from thin section of impactite sample Zh-6014.	66
A.4	Backscattered electron (BSE) image from thin section of impactite sample Zh-30a.	67
A.5	Backscattered electron (BSE) image from thin section of impactite sample Zh-62/3b.	68
A.6	Backscattered electron (BSE) image from thin section of impactite sample IRG-2015/1. . . . .	69
A.7	Backscattered electron (BSE) image from thin section of impactite sample Irgh-2. .	70



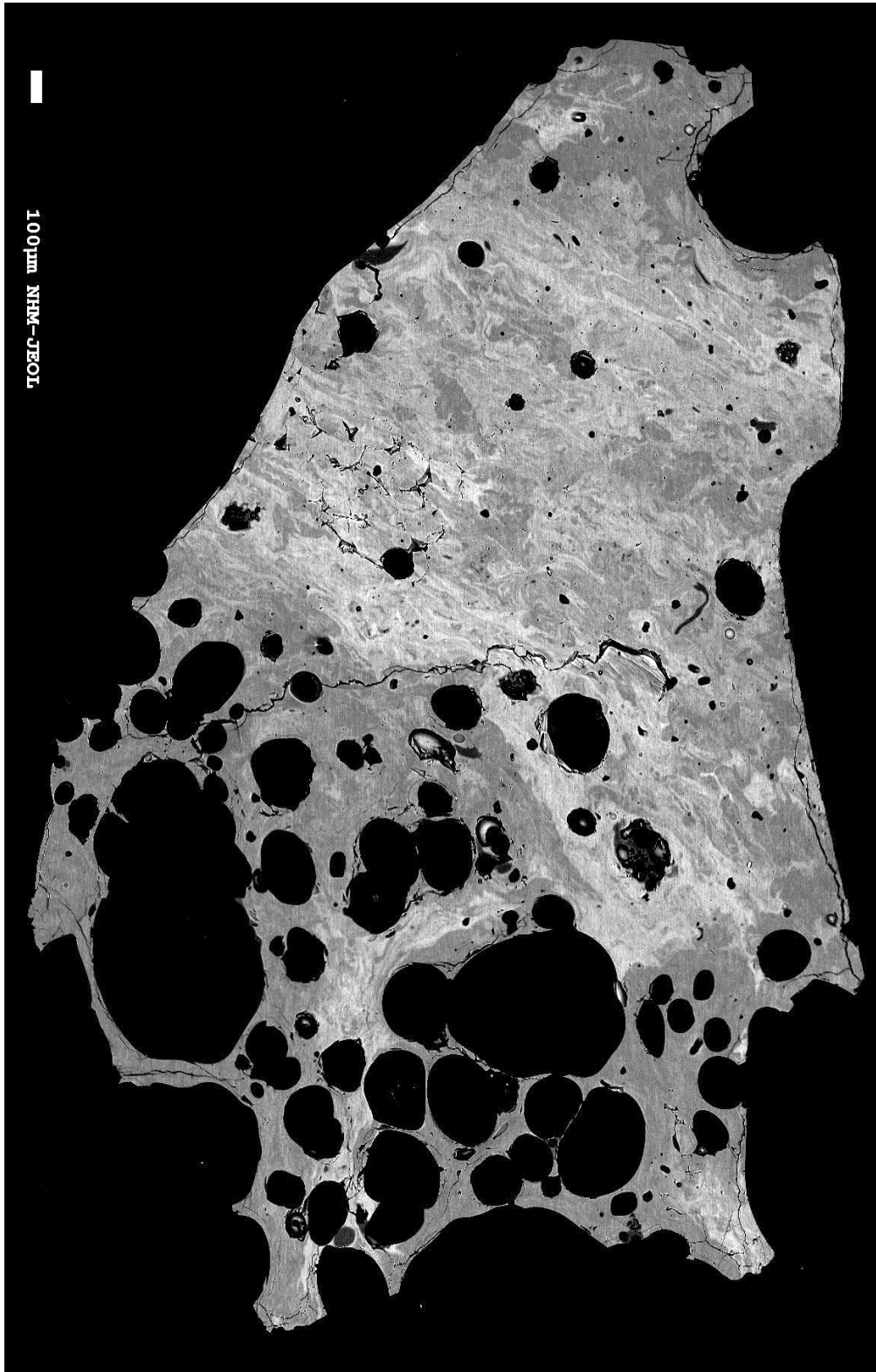
# Sample images



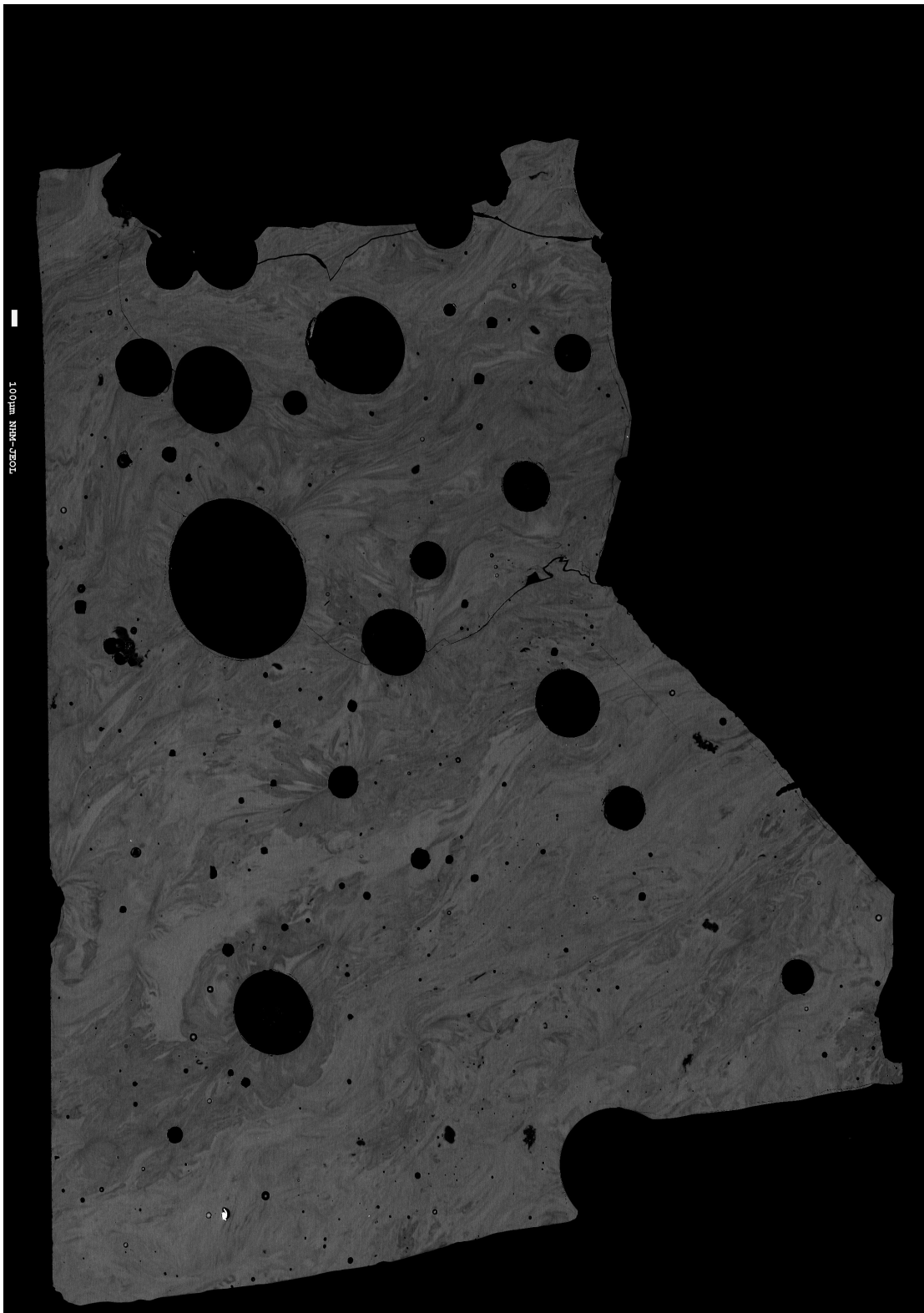
Figure A.1: Photographs of target rock samples.



Figure A.2: Photographs of impactite samples.



**Figure A.3:** Backscattered electron (BSE) image from thin section of impactite sample Zh-6014.



**Figure A.4:** Backscattered electron (BSE) image from thin section of impactite sample Zh-30a.

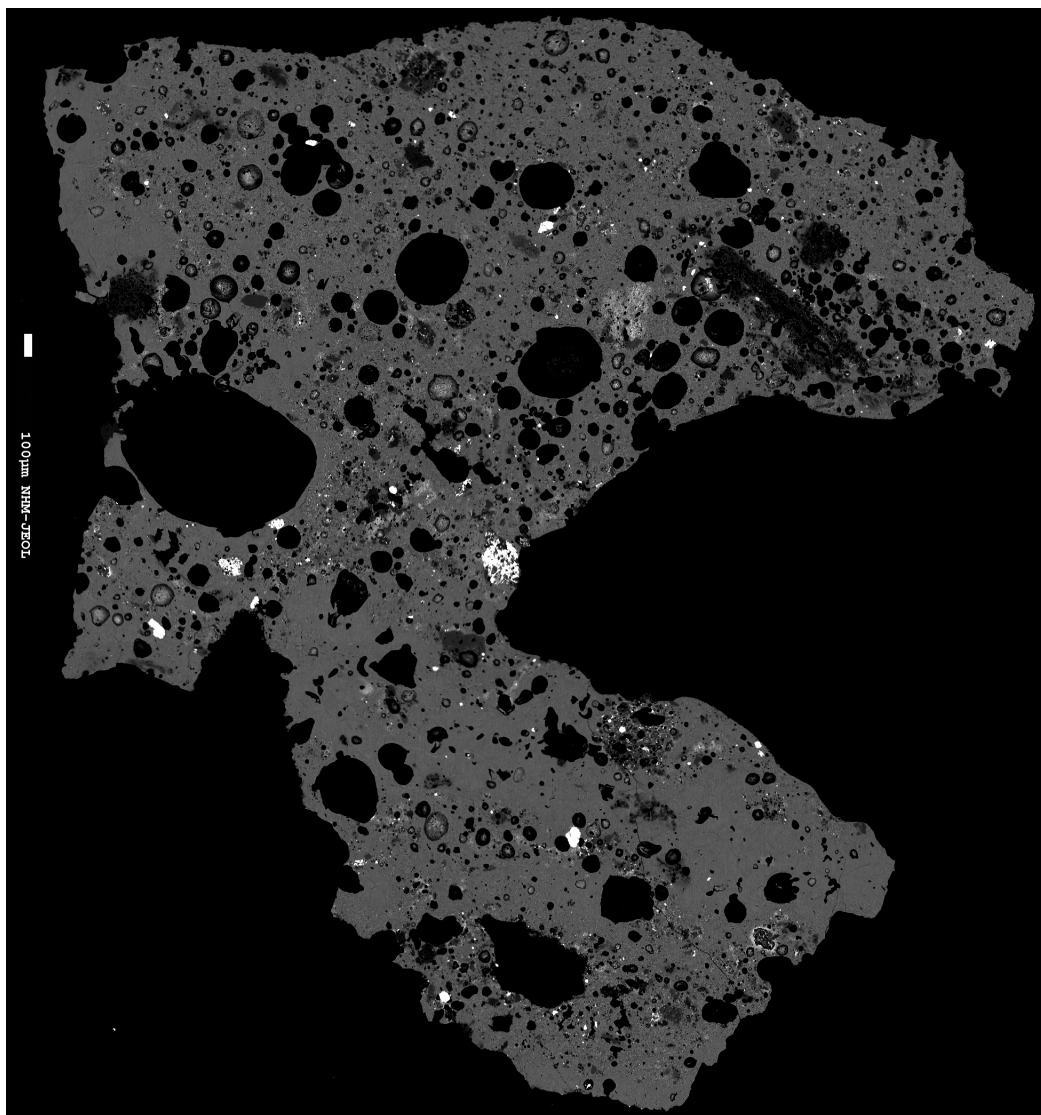


**Figure A.5:** Backscattered electron (BSE) image from thin section of impactite sample Zh-62/3b.



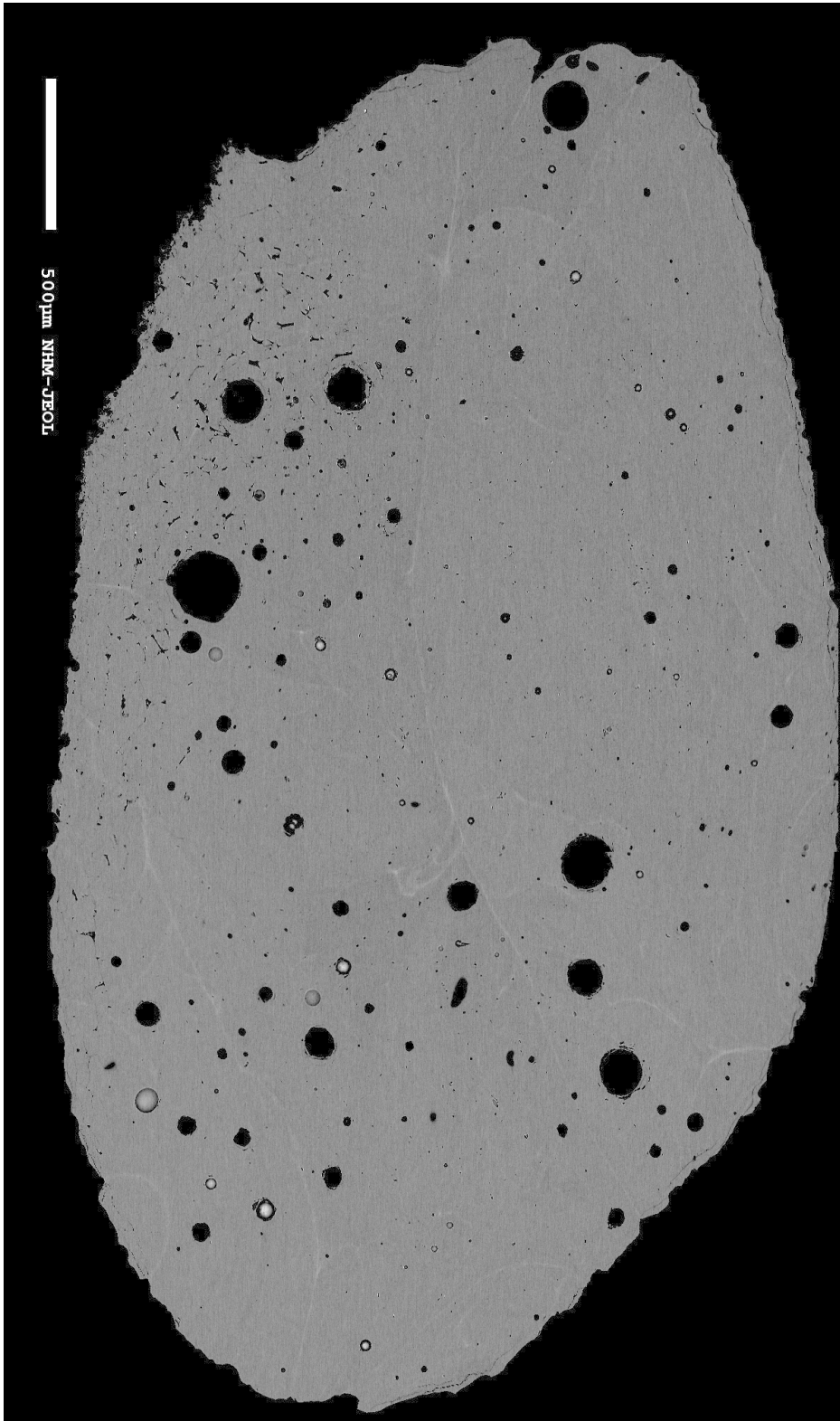


**Figure A.6:** Backscattered electron (BSE) image from thin section of impactite sample IRG-2015/1.

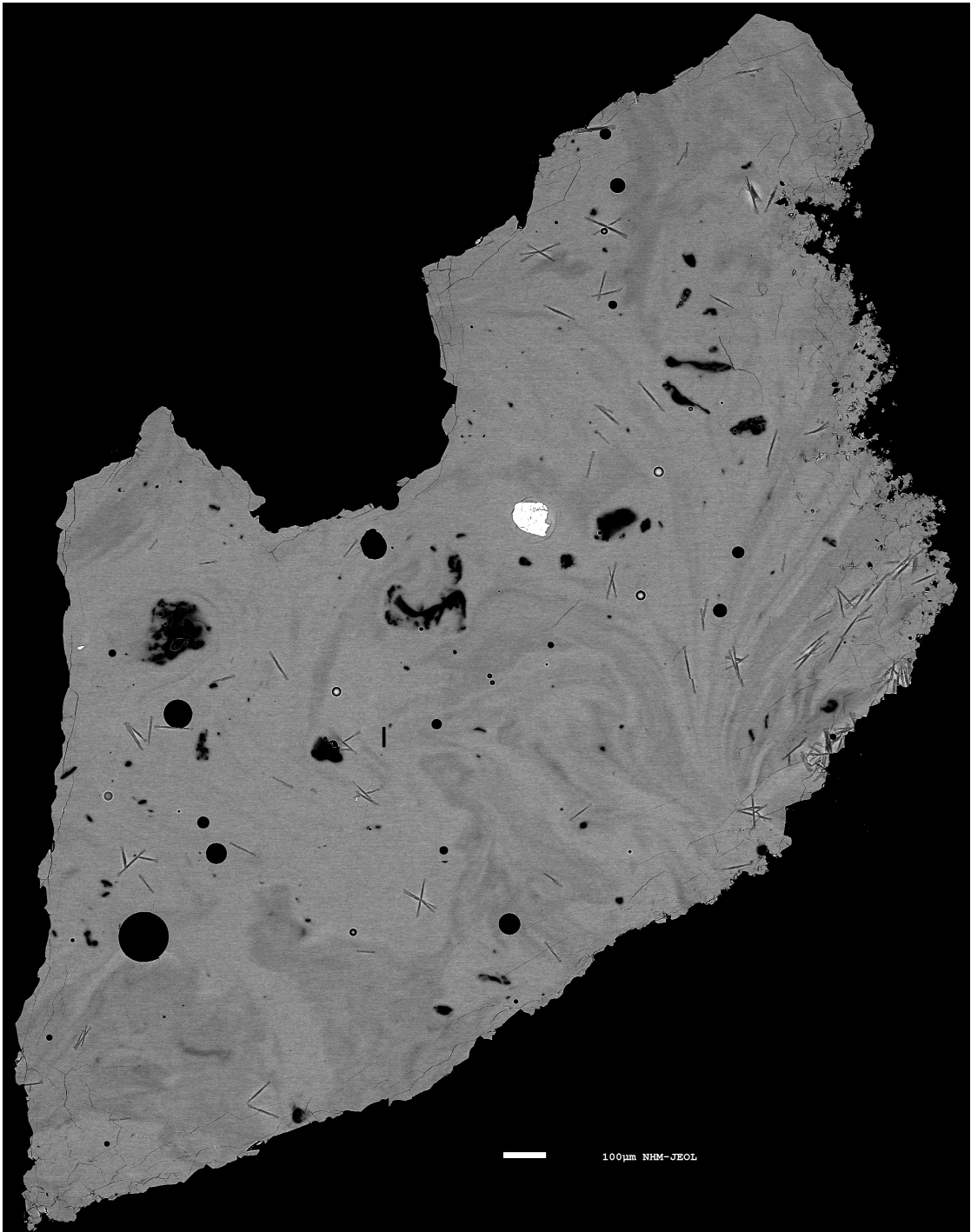


**Figure A.7:** Backscattered electron (BSE) image from thin section of impactite sample Irgh-2.

APPENDIX **B**

**Chemical Composition of  
Samples**

**Table B.1:** Chemical composition of impact glass and target rocks from the Zhamanshin impact feature from Abate et al. (1998). Major element contents in wt%. Trace element abundances in ppm. Average irghizite from Taylor and McLennan (1979).

	Target Rocks				Zhamanshinites		Average Irghizite	
	DB6	DB9	ZSK-8	2DB1	Zh-55/5	Zh-6014		Zh-62/3b
SiO <sub>2</sub>		45.11	58.96	55.9	40.29	75.3		74.28
Al <sub>2</sub> O <sub>3</sub>	16.1	17.7	17.16	18.6	0.83	11	19.7	10.16
TiO <sub>2</sub>		1.92	0.85	0.8	0.03			0.78
K <sub>2</sub> O	0.82	0.49	2.33	0.81	0.02	2.8	1.15	2
CaO	6.79	7.93	0.64	5.03	0.13	0.52	8.95	2.36
Fe <sub>2</sub> O <sub>3</sub>	12.4	12.58	7.61	9.61	9.38	4.08	9.24	5.6
MnO	0.14	0.16	0.05	0.14	0.06	0.09	0.15	
Na <sub>2</sub> O	4.45	3.43	0.93	4.85	0.01	1.73	3.04	0.97
MgO	5.74	7.26	2.09	2.43	35.5	0.21	2.69	2.93
P <sub>2</sub> O <sub>5</sub>		0.17	0.11	0.24	0.02			
L.O.I.		3.75	9.6	2.52	12.55			
Total		100.5	100.33	100.93	98.82			
Li	18	16	64	15	18	25	18	
Be	1.3	0.8	2	1	<0.3	1.6	0.9	
Sc	27.6	38	20.4	16.8	11	8.38	14.3	8.8
V	24620	232	215	259	43	72	232	6
Cr	107	259	128	40.5	3340	52.6	15.7	170
Co	34.7	38.5	20	18.7	92.5	9	17.4	73
Ni	35.2	103	42.8	18.3	2320	48.2	15.2	1200
Cu	44.5	68	17	18	1	14	21	24
Zn	123	105	92.8	79.4	77.8	49.1	93	
Ga	583	22.6	2.94	1.52	1.65	1.26	1.59	
As	2.42	1.86	14.8	17.8	3.34	7.93	17.1	
Br	<1	<0.6	4.87	0.18	0.3	9.12	<0.6	
Rb	13.3	11.5	104.7	18.4	3.2	98	27.7	
Sr	160	422	164.7	697	5	114	642	
Y	49	39	46	27	<5	n.d.	n.d.	33.8
Zr	214	201	202	67	13	199	147	351
Nb	0.1	<0.1	15	<0.1	<0.1	0.2	0.2	12.5
Mo	0.6	<0.5	0.7	0.8	<0.5	<0.5	<0.5	0.4
Cd	0.1	<0.1	0.1	<0.1	<0.1	0.2	0.2	
Sb	5.38	4.33	1.56	1.09	4.29	0.9	2.14	
Cs	0.3	0.19	7.05	1.26	0.04	5.49	8.74	44.2
Ba	167	52	274	356	9.5	423	581	
La	13.8	10.4	35.3	12	0.2	24.2	9.9	
Ce	31.9	24.5	68.7	26.8	0.56	49.5	20.6	
Nd	20.5	15.9	31.0	14.9	0.49	24	12.3	18.7
Sm	5.89	4.29	6.18	3.06	0.07	5.19	2.97	3.78
Eu	2.06	1.84	1.61	1.05	0.03	1.02	0.89	0.8
Gd	5.1	2.73	6.26	3	<1	5.81	3.8	3.46
Tb	1.07	0.57	0.83	0.44	0.09	0.81	0.87	0.6
Tm	0.51	0.31	0.44	0.24	0.03	0.45	0.24	
Yb	2.24	2.03	2.88	1.7	0.1	2.73	1.54	
Lu	0.32	0.32	0.74	0.29	0.012	0.36	0.22	1.9
Hf	4.10	2.93	4.50	1.97	0.03	5.6	1.58	8.66
Ta	1.41	0.72	1.05	0.2	<0.1	0.8	0.15	
W	<6	0.32	1.44	<1	<0.3	1.06	1.11	0.17
Ir	<2	<1	<2	<1	<2	0.23	<1	
Au	4.26	7.39	1.94	2.54	<2	3.6	2.09	
Tl	<0.1	<0.1	0.3	<0.1	<0.1	0.4	<0.1	
Pb	2	1	18	7	<1	37	10	2.9
Bi	<0.5	<0.5	<0.5	<0.5	<0.5	<0.5	<0.5	0.04
Th	1.78	0.93	12.0	2.96	0.03	8.61	2.33	
U	0.49	0.56	3.09	0.59	0.98	2.72	0.58	
K/U	13891	7263	6259	11396	169	8545	16459	
Zr/Hf	52.2	68.6	44.9	33.9	446	35.5	93	40.5
Zr/U	437	359	65.4	113	13.7	73.2	253	
Co/Ni	0.99	0.37	0.47	1.02	0.04	0.19	1.14	0.06
La/Sc	0.99	0.27	1.73	0.71	0.02	2.89	0.69	
La/Th	0.5	11.2	2.94	4.05	6.67	2.81	4.25	
Th/U	7.75	1.66	3.88	5.02	0.03	3.17	4.02	
(La/Sm)N	3.63	1.53	3.6	2.47	1.8	2.93	2.1	
(La/Yb)N	4.16	3.46	8.28	4.77	1.35	5.99	4.34	
Eu/Eu*	1.05	1.64	0.79	1.06	0.34	0.57	0.81	0.52

APPENDIX

C 

# EPMA data

**Table C.1:** EPMA point analysis data for impactite sample Zh-6014. Values in wt%.

No.	SiO <sub>2</sub>	Al <sub>2</sub> O <sub>3</sub>	Cr <sub>2</sub> O <sub>3</sub>	TiO <sub>2</sub>	K <sub>2</sub> O	CaO	FeO	MnO	Na <sub>2</sub> O	MgO	P <sub>2</sub> O <sub>5</sub>	NiO	Total
1	81.56	9.21	n.d.	0.53	3.19	0.42	2.48	0.04	1.61	0.52	0.04	n.d.	99.59
2	81.31	9.48	0.02	0.41	3.17	0.42	2.22	0.07	1.73	0.49	0.08	n.d.	99.40
3	80.90	9.87	0.02	0.36	3.28	0.49	2.53	0.11	1.54	0.57	0.07	0.01	99.75
4	82.22	9.22	n.d.	0.26	3.19	0.39	2.31	0.06	1.67	0.50	0.05	0.02	99.91
5	81.96	9.36	n.d.	0.25	3.22	0.41	2.29	0.07	1.74	0.50	0.05	0.02	99.85
6	82.19	9.04	0.03	0.21	3.16	0.40	2.45	0.05	1.57	0.50	0.07	n.d.	99.68
7	81.90	9.08	n.d.	0.37	3.15	0.37	2.32	0.03	1.73	0.46	0.06	n.d.	99.49
8	73.15	13.96	0.03	0.84	3.07	0.63	4.63	0.16	1.93	1.02	0.13	n.d.	99.57
9	73.22	14.02	n.d.	0.72	3.06	0.63	4.76	0.14	1.84	1.04	0.14	n.d.	99.57
10	73.19	14.08	0.01	0.65	3.04	0.65	4.91	0.12	1.87	1.11	0.12	n.d.	99.74
11	73.87	14.07	n.d.	0.59	3.08	0.62	4.49	0.14	1.94	1.02	0.08	0.03	99.94
12	73.66	13.80	0.03	0.77	3.09	0.64	4.50	0.14	1.86	1.01	0.11	n.d.	99.60
13	73.16	14.12	n.d.	0.68	3.02	0.62	4.76	0.15	1.88	1.14	0.15	0.03	99.70
14	74.83	13.52	n.d.	0.52	3.13	0.57	4.32	0.08	1.95	0.95	0.12	0.01	99.99
15	75.30	13.48	0.05	0.72	3.07	0.55	4.18	0.07	1.69	0.87	0.10	n.d.	100.08
16	71.08	15.80	0.04	0.79	3.02	0.73	5.34	0.10	1.65	1.18	0.13	n.d.	99.85
17	70.93	16.14	n.d.	0.90	3.07	0.67	5.27	0.14	1.82	1.19	0.13	n.d.	100.25
18	82.65	9.29	n.d.	0.47	3.04	0.36	2.18	0.08	1.57	0.43	0.04	n.d.	100.12
19	83.06	9.30	n.d.	0.34	3.08	0.33	2.12	0.06	1.47	0.41	0.03	n.d.	100.20
AVG	77.38	11.94	0.01	0.55	3.11	0.52	3.58	0.09	1.74	0.78	0.09	0.01	99.80

For n.d. value is below detection limit.

**Table C.2: EPMA point analysis data for impactite sample Zh-30a. Values in wt%.**

No.	SiO <sub>2</sub>	Al <sub>2</sub> O <sub>3</sub>	Cr <sub>2</sub> O <sub>3</sub>	TiO <sub>2</sub>	K <sub>2</sub> O	CaO	FeO	MnO	Na <sub>2</sub> O	MgO	P <sub>2</sub> O <sub>5</sub>	NiO	Total
1	71.01	15.49	0.056	0.75	2.99	0.64	5.49	0.17	1.87	1.17	0.12	0.034	99.79
2	71.26	15.35	0.048	0.85	2.99	0.61	5.28	0.08	1.83	1.14	0.14	0.009	99.60
3	71.60	15.28	n.d.	0.69	3.05	0.62	5.39	0.12	1.89	1.08	0.13	n.d.	99.85
4	71.93	15.12	0.040	0.70	3.07	0.67	5.01	0.13	1.90	1.12	0.13	n.d.	99.81
5	77.60	11.12	0.021	0.60	3.17	0.70	3.78	0.08	1.71	0.77	0.09	0.006	99.65
6	78.13	11.33	0.003	0.38	3.28	0.69	3.29	0.07	1.81	0.69	0.10	n.d.	99.78
7	80.29	9.97	n.d.	0.61	3.24	0.59	2.59	0.05	1.70	0.49	0.06	n.d.	99.59
8	78.75	10.22	0.049	0.73	3.12	0.62	3.54	0.07	1.61	0.65	0.09	0.008	99.47
9	71.06	15.46	n.d.	0.83	3.04	0.62	5.55	0.11	1.89	1.16	0.12	0.011	99.86
10	70.95	15.54	0.051	0.79	3.03	0.63	5.65	0.17	1.85	1.15	0.11	0.013	99.94
11	70.35	15.45	0.064	0.92	3.00	0.62	5.71	0.13	1.85	1.18	0.13	0.020	99.44
12	71.55	15.26	0.058	0.86	3.05	0.62	5.29	0.11	1.84	1.15	0.12	n.d.	99.90
13	77.71	11.29	0.009	0.63	3.20	0.71	3.78	0.10	1.81	0.75	0.08	n.d.	100.06
14	79.55	10.00	0.047	0.51	3.15	0.61	3.43	0.05	1.68	0.68	0.09	n.d.	99.79
15	78.92	10.62	0.025	0.67	3.27	0.66	3.21	0.07	1.80	0.63	0.10	0.005	99.98
16	79.23	10.86	n.d.	0.67	3.26	0.53	3.11	0.07	1.75	0.61	0.08	n.d.	100.17
AVG	74.99	13.02	0.03	0.70	3.12	0.63	4.38	0.10	1.80	0.90	0.11	0.01	99.79

For n.d. value is below detection limit.

**Table C.3: EPMA point analysis data for impacite sample Zh-62/3b. Values in wt%.**

No.	SiO <sub>2</sub>	Al <sub>2</sub> O <sub>3</sub>	Cr <sub>2</sub> O <sub>3</sub>	TiO <sub>2</sub>	K <sub>2</sub> O	CaO	FeO	MnO	Na <sub>2</sub> O	MgO	P <sub>2</sub> O <sub>5</sub>	NiO	Total
1	82.39	9.99	n.d.	0.23	1.22	1.92	2.37	0.04	0.97	0.55	0.05	n.d.	99.74
2	87.70	4.22	n.d.	0.10	2.26	2.75	1.52	0.05	0.54	0.39	0.04	n.d.	99.55
3	89.46	2.85	n.d.	n.d.	1.58	4.34	0.98	0.06	0.32	0.10	0.03	n.d.	99.70
4	86.63	2.89	n.d.	n.d.	2.33	4.80	1.97	0.08	0.43	0.19	0.02	n.d.	99.33
5	65.40	13.03	n.d.	0.54	5.03	6.85	5.01	0.12	1.39	1.74	0.12	n.d.	99.23
6	71.03	10.36	0.02	0.28	5.18	6.01	4.16	0.09	1.22	1.37	0.07	n.d.	99.79
7	66.47	13.72	0.02	0.32	4.86	7.90	3.61	0.15	1.24	1.24	0.09	n.d.	99.62
8	72.76	8.02	n.d.	0.39	4.42	8.34	3.42	0.11	0.94	1.04	0.06	0.01	99.51
9	56.99	18.13	0.01	0.69	1.34	8.83	6.88	0.15	4.26	2.47	0.18	0.01	99.92
10	56.21	18.42	n.d.	0.60	1.38	8.52	7.42	0.20	3.99	2.66	0.21	n.d.	99.61
11	53.92	19.39	n.d.	0.78	1.36	8.61	8.50	0.24	3.66	2.99	0.22	n.d.	99.66
12	56.54	18.46	0.05	0.87	1.27	8.82	6.94	0.16	4.18	2.50	0.20	0.03	100.03
13	56.50	18.45	n.d.	0.76	1.31	8.90	6.65	0.12	4.21	2.47	0.21	0.02	99.60
14	54.41	20.13	0.03	0.86	0.96	9.05	7.38	0.13	4.16	2.67	0.19	0.01	99.97
15	53.97	19.56	n.d.	0.76	1.01	9.15	7.43	0.11	4.15	2.75	0.19	n.d.	99.08
16	54.29	20.24	0.03	0.62	0.97	9.17	7.48	0.09	4.32	2.41	0.22	n.d.	99.84
17	54.09	20.00	0.01	0.97	1.05	9.03	7.37	0.11	4.06	2.80	0.20	0.01	99.70
AVG	65.810	13.991	0.010	0.516	2.207	7.234	5.240	0.118	2.590	1.785	0.134	0.005	99.64

For n.d. value is below detection limit.



**Table C.4:** EPMA point analysis data for impactite sample IRG-2015/1. Values in wt%.

No.	SiO <sub>2</sub>	Al <sub>2</sub> O <sub>3</sub>	Cr <sub>2</sub> O <sub>3</sub>	TiO <sub>2</sub>	K <sub>2</sub> O	CaO	FeO	MnO	Na <sub>2</sub> O	MgO	P <sub>2</sub> O <sub>5</sub>	NiO	Total
1	75.30	10.12	n.d.	0.71	1.99	2.52	5.16	0.10	1.12	2.79	0.03	0.15	99.99
2	74.96	10.09	0.01	0.85	2.08	2.59	5.07	0.10	1.07	2.81	0.02	0.15	99.80
3	74.82	10.02	n.d.	0.90	2.02	2.58	5.00	0.10	1.10	2.86	0.01	0.14	99.55
4	74.71	10.08	0.04	0.88	2.06	2.57	5.10	0.10	1.11	2.77	0.04	0.16	99.61
5	74.95	9.96	0.05	1.12	1.99	2.53	5.24	0.07	1.07	2.73	0.01	0.13	99.85
6	75.15	10.11	0.06	0.84	2.03	2.56	4.96	0.11	1.08	2.79	0.03	0.15	99.88
7	74.79	9.78	0.03	0.73	2.01	2.42	5.80	0.09	1.08	3.03	n.d.	0.22	99.99
8	74.39	9.72	0.07	0.72	1.97	2.38	5.89	0.09	1.09	3.16	0.02	0.18	99.67
9	74.58	9.64	0.06	0.76	2.03	2.45	5.62	0.12	1.12	3.06	0.02	0.21	99.66
10	74.67	9.63	0.03	0.89	2.00	2.44	5.68	0.10	1.04	3.17	0.01	0.16	99.83
11	74.65	9.63	0.05	0.67	2.01	2.44	5.73	0.07	1.12	3.02	0.04	0.19	99.64
12	74.96	9.57	0.03	0.73	1.98	2.38	5.71	0.09	1.07	3.06	0.04	0.18	99.80
13	72.04	9.82	0.07	0.94	1.92	2.82	6.90	0.11	1.13	3.40	0.27	0.24	99.66
14	72.27	9.83	0.05	0.79	1.94	2.81	6.98	0.14	1.12	3.44	0.22	0.25	99.83
15	72.43	9.70	0.14	0.72	1.93	2.78	6.79	0.10	1.08	3.32	0.25	0.22	99.45
16	70.16	10.00	0.12	0.88	1.91	3.26	7.49	0.10	0.95	3.85	0.76	0.29	99.77
17	71.13	10.12	0.12	0.91	1.94	2.95	6.93	0.11	1.06	3.51	0.63	0.25	99.65
18	72.82	9.71	0.08	0.79	2.06	2.69	6.79	0.10	1.07	3.38	0.12	0.30	99.92
AVG	73.82	9.86	0.06	0.82	1.99	2.62	5.93	0.10	1.08	3.12	0.14	0.20	99.75

For n.d. value is below detection limit.

**Table C.5:** EPMA point analysis data for impactive sample Irgh-2. Values in wt%.

No.	SiO <sub>2</sub>	Al <sub>2</sub> O <sub>3</sub>	Cr <sub>2</sub> O <sub>3</sub>	TiO <sub>2</sub>	K <sub>2</sub> O	CaO	FeO	MnO	Na <sub>2</sub> O	MgO	P <sub>2</sub> O <sub>5</sub>	NiO	Total
1	55.30	20.11	0.01	0.89	1.42	8.31	7.33	0.15	3.48	2.60	0.20	n.d.	99.79
2	55.76	19.97	n.d.	0.79	1.45	8.00	7.27	0.12	3.58	2.48	0.19	n.d.	99.60
3	55.38	20.12	0.05	0.87	1.51	8.02	7.32	0.16	3.63	2.52	0.22	0.05	99.85
4	56.06	20.10	0.05	0.87	1.56	7.56	7.21	0.13	3.61	2.46	0.20	n.d.	99.81
5	56.01	20.11	n.d.	0.88	1.53	7.59	7.26	0.14	3.56	2.46	0.16	0.03	99.74
6	55.84	20.07	0.03	1.02	1.56	7.70	7.34	0.11	3.47	2.35	0.19	n.d.	99.68
7	56.05	20.17	0.06	0.87	1.51	7.40	7.30	0.13	3.64	2.43	0.24	n.d.	99.80
8	56.09	20.18	0.02	0.78	1.53	7.40	7.35	0.13	3.60	2.51	0.22	0.01	99.82
9	56.05	20.19	n.d.	0.79	1.52	7.65	7.28	0.13	3.61	2.49	0.18	n.d.	99.90
10	57.39	20.07	n.d.	0.78	1.63	7.28	6.53	0.13	3.73	2.21	0.19	n.d.	99.94
11	56.97	20.16	0.04	0.81	1.54	7.54	6.61	0.12	3.65	2.33	0.20	0.02	99.99
12	57.04	19.91	0.02	0.75	1.62	7.43	6.47	0.12	3.70	2.24	0.19	n.d.	99.49
13	54.71	20.09	0.02	0.73	1.31	9.16	7.28	0.18	3.37	2.75	0.20	n.d.	99.79
14	54.93	19.99	0.02	0.84	1.31	9.05	7.30	0.11	3.28	2.69	0.23	n.d.	99.75
15	54.46	20.09	n.d.	0.83	1.32	9.18	7.53	0.12	3.31	2.61	0.21	n.d.	99.66
16	54.68	19.94	n.d.	0.85	1.30	9.07	7.59	0.19	3.16	2.94	0.20	n.d.	99.95
17	54.89	20.12	n.d.	0.82	1.30	8.90	7.36	0.14	3.20	2.87	0.21	n.d.	99.81
18	54.64	19.99	0.02	0.83	1.36	8.72	7.40	0.18	3.16	2.85	0.18	n.d.	99.32
19	54.62	19.96	0.04	0.78	1.39	8.80	7.52	0.18	3.36	2.76	0.19	n.d.	99.60
20	54.48	19.90	0.02	0.98	1.32	8.88	7.41	0.17	3.20	2.87	0.17	0.02	99.42
21	54.32	19.81	0.03	1.09	1.30	9.27	7.23	0.14	3.33	2.94	0.19	0.03	99.68
AVG	55.51	20.05	0.02	0.85	1.44	8.23	7.23	0.14	3.46	2.59	0.20	0.01	99.73

For n.d. value is below detection limit.